Methods for modeling of soft-tissue speech articulators

Reiner Wilhelms-Tricarico

1993. 12. 13

Methods for modeling of soft-tissue speech articulators Technical Report

Reiner Wilhelms-Tricarico

Dec 1993

Abstract

The soft tissues of tongue and lips can be approximated as continua. This gives a foundation for applying the finite element method to simulate these structures in a biomechanical speech production model. Movements and deformations of these organs can then be computed as the solutions of a non-linear second order system of ordinary differential equations which is obtained from a finite element approximation of an energy rate equation. The muscle fibers in the organs are represented as direction specifying fields. In each muscle type pure tensil active stress contributions are produced. Three types of boundaries are considered: boundaries where impact and sliding can take place, such as the hard palate; boundaries of where a body surface can only move on another fixed surface; and attachments to moving rigid structures. A method for maintaining an incompressibility condition as a geometric constraint during the simulation is presented in detail. The implementation of the simulation procedures as a C++ class library is in progress. A partial model of a tongue with eight muscles was completed and tested.

Introduction

The mandible, lip, tongue, velum, and pharyngeal constrictors are the primary articulators which determine the vocal tract shape and thus the acoustical transfer function. The larynx, traditionally modeled as the source of speech production, influences in addition the vocal tract shape mainly by varying its length. The larynx is a complicated system that can in principle be modeled with fluid mechanics and with body-fluid interaction methods, which is not covered in this article. The focus here is on the "slow" articulators, slow compared to

1

the vibratory cycle of the vocal folds, and in particular on the soft tissue components, such as the lips and the tongue. Much of the methods discussed below apply in principle to other articulatory organs made of soft tissue.

More difficult to observe, and less understood than lip movements are the movements of the tongue. Oberservations during speech production or swallowing are difficult and only partial. Various technical methods have been devised for this, such as the observation of the tongue surface with ultra-sound methods (c.f. Watkin and Rubin [WR89], and Stone [Sto90]) and the tracking of pellets or coils glued to the tongue surface using x-ray micro-beam (see Nadler et al. [NAF87]) or magnetic methods (see Perkell et al. [PCS+92]). Recently another method was developed, called Tagging Snapshot MRI, which can be utilized to visualize the deformation of the internal structures of the tongue, see Kumada et al. [KNNH92], and Niitsu et al. [NKNI92]. A critical discussion of various techniques can be found in Fujimura [Fuj90].

So far only few computer simulations of tongue deformations using finite element methods or related approaches have been undertaken. Perkell's dissertation [Per74] was the first work dedicated to the construction of a physiological model of the human tongue, albeit a two-dimensional projection in the sagittal plane. His model of the tongue as a lumped-parameter lumped force system has some resemblance to finite element modeling (FEM) (Zienkiewicz, [Zie71] and Oden [Ode72]). Kiritani et. al. [KMFM76] based their model on a finite element approximation of the continuum, employing essentially an incremental load method. Using a similar method, Kakita et al. [KFH85] demonstrated similarities between measured EMG activity in lingual muscles and the computed amount of stress required for static vowel articulations. Hashimoto and Suga [HS86] used a larger number of elements, and approximated mid-sagittal tongue shapes from x-ray data by least-square methods to find optimal muscle stress parameters.

The formentioned models [KMFM76] [HS86] of the tongue are essentially based on infinitesimal elasticity methods, and describe the deformation process as a sequence of quasistatic equilibrium configurations, i.e. inertia is neglected. As yet there is no dynamic three-dimensional model for the tongue. This article gives the foundations of modeling the tongue and lips as a dynamic systems that is capable of large deformations.

1 Continuum representation

Soft tissue in speech articulators are virtually incompressible because it contains a high percentage of water. The tongue and lips have no internal skeleton, but they are mounted on bone structures. The tongue is a composite muscle system which can generate protrusion and deflection only through active contraction in one or more directions, causing extension in directions where little or no active stress is generated. Smith and Kier [SK89] describe

$\mathcal{C}, \mathcal{C}^d$	Bound region in reference/deformed configuration
$\boldsymbol{X}$	Body or material coordinates in $\mathcal{C}$
$\boldsymbol{x}$	Spatial coordinates of particle $\boldsymbol{X}$ in $\mathcal{C}^d$: $\boldsymbol{x} = \chi(\boldsymbol{X})$.
$\boldsymbol{\xi}$	Coordinate in a master element
$\mathcal{TC}(\boldsymbol{X}), \mathcal{TC}^d(\boldsymbol{x})$	Tangent space at $\boldsymbol{X}$, $\boldsymbol{x}$
$d\boldsymbol{X}, d\boldsymbol{x},$	Vectors in tangent spaces
$\boldsymbol{u}, \dot{\boldsymbol{u}}, \ddot{\boldsymbol{u}}$	Displacement, velocity, acceleration field
$\boldsymbol{F}$	Deformation gradient
∇	Gradient in the reference configuration
$\boldsymbol{C}$	Right Cauchy deformation tensor: $\boldsymbol{F}^T \boldsymbol{F}$
$\boldsymbol{E}$	Green-Venant or Lagrange deformation tensor: $\frac{1}{2}(\boldsymbol{C} - \boldsymbol{I})$
$\boldsymbol{I}$	Second order unity tensor
ρ	Mass density
$\boldsymbol{T}$	Cauchy stress tensor
$\boldsymbol{P}$	First Piola-Kirchhoff tensor: $\det(\boldsymbol{F})\boldsymbol{T}\boldsymbol{F}^{-T}$
$\boldsymbol{S}$	Second Piola-Kirchhoff tensor: $\det(\boldsymbol{F})\boldsymbol{F}^{-1}\boldsymbol{T}\boldsymbol{F}^{-T}$
$\boldsymbol{n}$	(Surface-) normal vector in deformed configuration
$\boldsymbol{N}$	(Surface-) normal vector in undeformed configuration
$\Psi, \mathcal{N}$	Shape functions
Ω	Volume in reference configuration
$\partial\Omega$	Surface in reference configuration
N_E	Number of nodes of an element

Table 1: Frequently used symbols

this behavior as that of a "muscular hydrostat".

The human tongue consists of at least 12 different muscles which are partially interwoven. It also contains glands, blood vessels, layers of fatty tissue, and skin. Each component has different physical properties, and most tissues are nonhomogeneous. Detailed displays of fiber distribution in the tongue can be found in a study by Miyawaki [Miy74]. As a descriptive approximation, the tongue is treated as a continuum to obtain a physical foundation for applying the finite element method. In the continuum mechanical approximation, the general structure of the tongue is retained, while the fine details of tissue structures are not included in the model.

For the description of motion, two representations, an arbitrary state called the reference configuration, and the deformed configuration will be used. When the body is in the (static) reference configuration it occupies a domain $\mathcal{C}$ of an euclidean point space $\mathcal{E}$. When it is in a (time variant) deformed configuration, it occupies a domain $\mathcal{C}^d$. Material points are identified with their coordinates, $\boldsymbol{X} = (X_1, X_2, X_3)$, when the system is in the reference configuration. These are called the material coordinates. The coordinates of particle $\boldsymbol{X}$ in

the deformed configuration are denoted $\boldsymbol{x} = \boldsymbol{x}(\boldsymbol{X}, t)$, and are called spatial coordinates.

Motion and deformation are described as a time variant one-to-one mapping from the reference to the deformed configuration: $\boldsymbol{X} \to \boldsymbol{x}(\boldsymbol{X}, t)$. Associated with each material point in $\mathcal{C}$ and $\mathcal{C}^d$ are tangent vector spaces, $\mathcal{TC}(\boldsymbol{X})$ and $\mathcal{TC}^d(\boldsymbol{x})$, respectively. The tangent space $\mathcal{TC}(\boldsymbol{X})$ contains all infinitesimal difference vectors $d\boldsymbol{X}$ between $\boldsymbol{X}$ and neighbored particles. The following kinematic entities are useful.

1.1   Basic definitions

Following general continuum mechanics (see Truesdell [Tru91] and Gurtin [Gur81]), some definitions of used variables describing deformation processes are given below.

The vector field $\boldsymbol{u} = \boldsymbol{x} - \boldsymbol{X}$ is the *displacement field*. Its rate of change is a *velocity field* $\dot{\boldsymbol{u}}$. The *deformation gradient* $\boldsymbol{F}$, which is the differential of the mapping $\boldsymbol{X} \to \boldsymbol{x}$, describes the mapping between the associated tangent spaces $\mathcal{TC}(\boldsymbol{X}) \to \mathcal{TC}^d(\boldsymbol{x})$, that is, it maps a vector $d\boldsymbol{X}$ in $\mathcal{TC}(\boldsymbol{X})$ onto a corresponding $d\boldsymbol{x}$ in $\mathcal{TC}^d(\boldsymbol{x})$: $d\boldsymbol{x} = \boldsymbol{F}\, d\boldsymbol{X}$.

$$F = \nabla x = \frac{\partial x}{\partial X} = I + \frac{\partial u}{\partial X} \qquad \text{(in components:} \quad \left[\delta_{ij} + \frac{\partial u_i}{\partial X_j}\right]) \tag{1}$$

An infinitesimal plane area element through a point $\boldsymbol{X}$ in $\mathcal{C}$ can be represented by the cross product of two vectors $d\boldsymbol{X}$ and $d\boldsymbol{Y}$ in $\mathcal{TC}(\boldsymbol{X})$. $d\boldsymbol{N} = d\boldsymbol{X} \wedge d\boldsymbol{Y}$. $d\boldsymbol{N}$ is understood as a vector perpendicular to the area element and has a magnitude equal to the area. Using the mapping between the tangent spaces. The area element in the deformed configuration is represented by

$$d\boldsymbol{n} = d\boldsymbol{x} \wedge d\boldsymbol{y} = (\boldsymbol{F}d\boldsymbol{X}) \wedge (\boldsymbol{F}d\boldsymbol{Y}) = \det(\boldsymbol{F})\boldsymbol{F}^{-T}d\boldsymbol{N} \quad , \tag{2}$$

where $(.)^{-T}$ means inverse and transposed. The *right Cauchy tensor* $\boldsymbol{C}$ and the *Green-Venant strain tensor* $\boldsymbol{E}$ are:

$$C = F^T F \quad \text{and} \quad E = \tfrac{1}{2}(C - I) = \tfrac{1}{2}(F^T F - I) \quad \text{where } I \text{ is the unit tensor } [\delta_{ij}] \quad . \tag{3}$$

The rates of these tensors are:

$$\dot{C} = 2\,\dot{E} = 2F^T D F \quad \text{with} \quad D = \operatorname{sym} \operatorname{grad}_{x} \dot{u} \quad . \tag{4}$$

where $\boldsymbol{D}$ is the symmetric part of the gradient of the velocity field $\dot{\boldsymbol{u}}$. Its trace is the divergence of the velocity field.

1.2 Surfaces, films, and skin

For modeling of skin, films or other thin surfaces, a two dimensional approximation may be sufficient in many cases. For skin in particular, constitutive equations can be found in the literature. Following Green [GZ60], a description of a surface in the reference and deformed configurations is given below.

It is convenient to describe the surface, represented as a two-dimensional manifold, in both the reference and the deformed configuration by curvilinear coordinate systems. Let $(\mathbf{i}_1, \mathbf{i}_2, \mathbf{i}_3)$ form an orthonormal basis in the Euclidean space. In the reference configuration, the surface points have 3-dimensional coordinates $\mathbf{X}(\xi_\alpha, \xi_\beta)$, and in the deformed configuration $\mathbf{x}(\xi_\alpha, \xi_\beta)$. The variables ξ_α and ξ_β are varying usually over the surface of some master element, that is, over a square or a triangle. The Greek indices indicate that two numbers from the index set (1,2,3) are used. We can create new basis vectors which are tangential to the surface:

$$\mathbf{g}_j := \frac{\partial X_i}{\partial \xi_j} \mathbf{i}_i \tag{5}$$

in the reference configuration, and

$$\mathbf{G}_j := \frac{\partial X_i}{\partial \xi_j} \mathbf{i}_i \tag{6}$$

in the deformed configuration. Usually the $\mathbf{g}_j$ and $\mathbf{G}_j$ are not orthogonal and not normal. Two different surface metric tensors are defined in the reference and deformed configuration ('.' denoting inner product):

$$\mathbf{a}_{\alpha\beta} = \mathbf{g}_\alpha \cdot \mathbf{g}_\beta \tag{7}$$

and in the deformed surface:

$$\mathbf{A}_{\alpha\beta} = \mathbf{G}_\alpha \cdot \mathbf{G}_\beta \tag{8}$$

The thickness of a thin surface may change under deformation of the whole body. This can be described by a ratio h of the thickness in the deformed configuration divided by the thickness in the deformed configuration. The Green -St. Venant strain tensor is then obtained as a function of the surface coordinates:

$$\mathbf{E}_{\alpha\beta} = \frac{1}{2}(\mathbf{A}_{\alpha\beta} - \mathbf{a}_{\alpha\beta}) \quad , \quad \mathbf{E}_{\gamma\gamma} = \frac{1}{2}(h^2 - 1) \quad \text{and} \quad \mathbf{E}_{\gamma\alpha} = \mathbf{E}_{\gamma\beta} = 0 \quad (\text{sym.}) \tag{9}$$

The index γ represents the third direction, perpendicular to the surface. Constitutive equations of skins can often be approximated by a hyperelastic law, so that the stress is obtained as a 2nd Piola-Kirchhoff tensor which is the derivative of a strain energy function W with respect to the components of $\boldsymbol{E}$.

$$S^{\alpha\beta} = \frac{\partial W}{\partial \boldsymbol{E}_{\alpha\beta}} \tag{10}$$

A special example is surface tension, which can be approximated by a law that relates the surface energy simply to the area of the surface. An area element of the surface is the squareroot of the determinant of the surface metric tensor:

$$W = c\,A^{1/2} = c\,(\mathbf{A}_{\alpha\alpha}\mathbf{A}_{\beta\beta} - \mathbf{A}_{\alpha\beta}^2)^{1/2} \tag{11}$$

c is a surface-tension coefficient. In this case, the second Piola Kirchhoff tensor in the surface, which represents the surface tension, is obtained as:

$$S^{\alpha\beta} = c\,A^{1/2}\mathbf{A}^{\alpha\beta} \quad , \tag{12}$$

where $\mathbf{A}^{\alpha\beta}$ is the inverted metric tensor. After computing the rate of the Green-St. Venant tensor:

$$\dot{\boldsymbol{E}}_{\alpha\beta} = \frac{1}{2}(\mathsf{G}_\alpha \cdot \dot{\mathsf{G}}_\beta + \dot{\mathsf{G}}_\alpha \cdot \mathsf{G}_\beta) \quad , \tag{13}$$

A useful expression for the rate of strain energy (stress power) in the surface is obtained:

$$\dot{W} = S^{\alpha\beta}\dot{\boldsymbol{E}}_{\alpha\beta} = S^{\alpha\beta}\frac{1}{2}(\mathsf{G}_\alpha \cdot \dot{\mathsf{G}}_\beta + \dot{\mathsf{G}}_\alpha \cdot \mathsf{G}_\beta) = S^{\alpha\beta}\dot{\mathsf{G}}_\alpha \cdot \mathsf{G}_\beta \quad , \tag{14}$$

because S is symmetric.

1.3 Finite element formulation

The reference configuration is subdivided into finite elements. Let $\mathcal{B}_0$ be one of these, and $\mathcal{B}$ the corresponding element in the deformed configuration. Material coordinates in $\mathcal{B}_0$ are described by mapping a natural coordinate system in a master element $\mathcal{M}$ onto $\mathcal{B}_0$.

In $\mathcal{B}_0$, fields are approximated with the help of isoparametric shape functions: Three invertible one-to-one mappings are defined between $\mathcal{M}$, $\mathcal{B}_0$, and $\mathcal{B}$, namely φ, φ_0, and χ, see
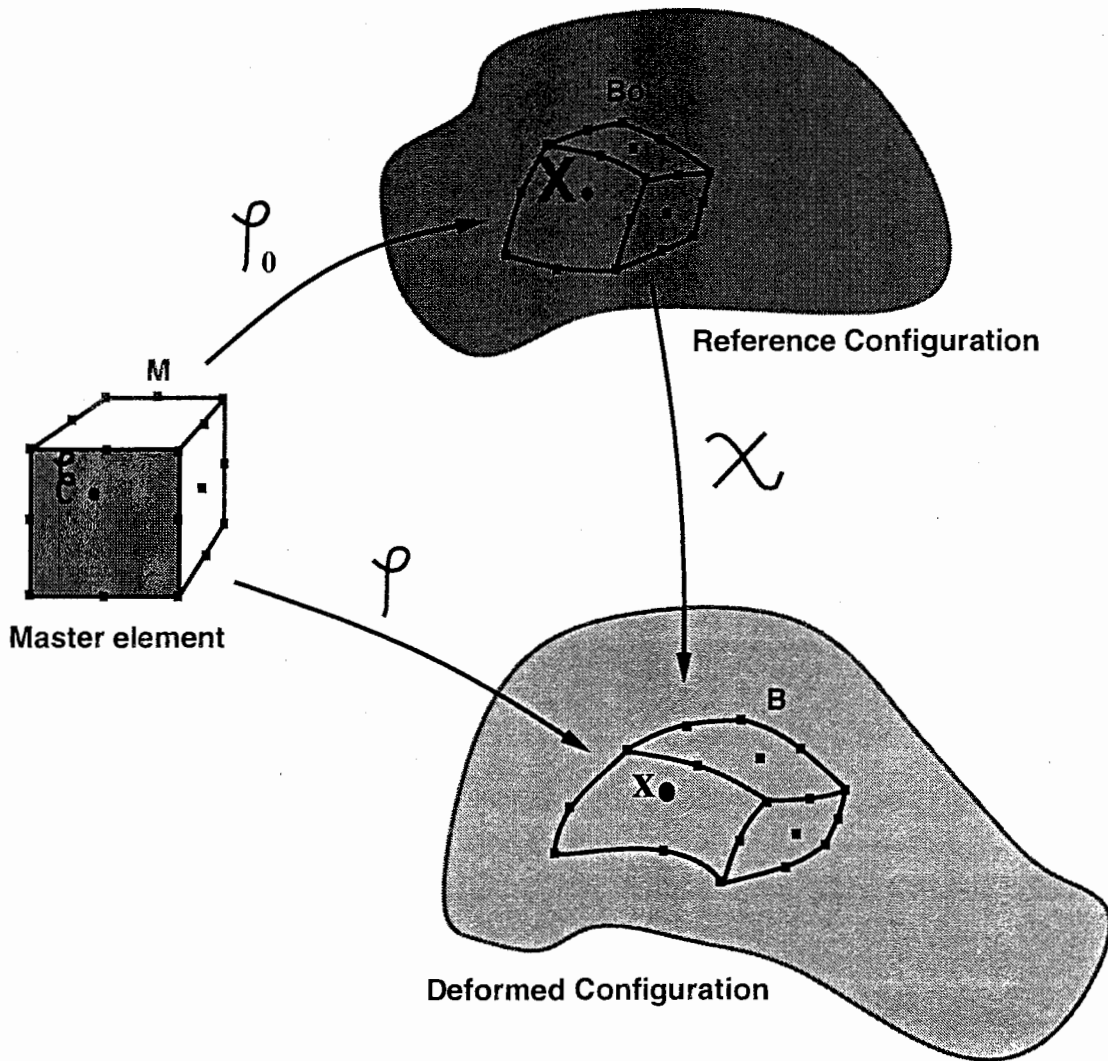
Figure 1: Mappings for deformation and the representation of a solid.

figure 1. In $\mathcal{M}$, a set of N_E interpolation (shape) functions $\{\Psi_K\,,\ K = 1,\ldots,N_E\}$ is defined. They have the property:

$$\Psi_K(\boldsymbol{\xi}_J) = \delta_{KJ}\quad, \tag{15}$$

where $\boldsymbol{\xi}_J$ is the coordinate of the J-th node in the master element $\mathcal{M}$.

The material coordinates within $\mathcal{B}_0$ are generated by the mapping $\varphi_0 : \boldsymbol{\xi} \rightarrow \boldsymbol{X}$ as:

$$\boldsymbol{X} = \boldsymbol{X}(\boldsymbol{\xi}) = \sum_{K=1}^{N_E} \boldsymbol{X}^K \Psi_K(\boldsymbol{\xi})\quad, \tag{16}$$

where $\boldsymbol{X}^K$ are the coordinates of the element nodes in $\mathcal{C}$.

Isoparametric shape functions on the domain of a typical element $\mathcal{B}_0$ are defined by:

$$\mathcal{N}_K(\boldsymbol{X}) = \mathcal{N}_K(\boldsymbol{X}(\boldsymbol{\xi})) = \Psi_K \circ \varphi_0^{-1} = \Psi_K(\boldsymbol{\xi})\quad. \tag{17}$$

All fields in the reference configuration are interpolated with the same shape functions. Therefore, they can be expressed as either functions of the coordinates in the master element $\mathcal{M}$ or as functions of material coordinates $\boldsymbol{X}$ in the reference element $\mathcal{B}_0$. For example, the deformation field and velocity field are represented as

$$\boldsymbol{u} = \sum_{K=1}^{N_E} \boldsymbol{u}^K \Psi_K = \sum_{K=1}^{N_E} \boldsymbol{u}^K \mathcal{N}_K(\boldsymbol{X}) \quad\text{and}\quad \dot{\boldsymbol{u}} = \sum_{K=1}^{N_E} \dot{\boldsymbol{u}}^K \Psi_K = \sum_{K=1}^{N_E} \dot{\boldsymbol{u}}^K \mathcal{N}_K(\boldsymbol{X}) \tag{18}$$

where $\boldsymbol{u}^K$ and $\dot{\boldsymbol{u}}^K$ are the displacement vector and displacement velocity vector relative to node K in the reference configuration.

The shape functions are differentiable and their gradients are

$$\nabla\mathcal{N}_K(\boldsymbol{X}) = \nabla\mathcal{N}_K(\boldsymbol{X}(\boldsymbol{\xi})) = \mathrm{grad}_{\boldsymbol{\xi}}\left(\Psi_K(\boldsymbol{\xi})\right)\boldsymbol{J}^{-1}\quad, \tag{19}$$

where $\boldsymbol{J}$ is defined as:

$$\boldsymbol{J} = \sum_{k=1}^{N_E} \boldsymbol{X}^K \mathrm{grad}_{\boldsymbol{\xi}}(\Psi_K)\quad, \tag{20}$$

The deformation gradient and its rate can now be approximated as:

$$\boldsymbol{F} \;=\; \boldsymbol{I} + \sum_{K=1}^{N_E} \boldsymbol{u}^K \nabla \mathcal{N}_K(\boldsymbol{X}) \quad \text{with components} \quad \left[\delta_{ij} + \mathcal{N}_{K,j} u_i^K \right] \tag{21}$$

$$\dot{\boldsymbol{F}} \;=\; \nabla \dot{\boldsymbol{u}} = \sum_{K=1}^{N_E} \dot{\boldsymbol{u}}^K \, \nabla \mathcal{N}_K(\boldsymbol{X}) \quad \text{with components} \quad \left[\mathcal{N}_{K,j} \, \dot{u}_i^K \right] \;, \tag{22}$$

where $\mathcal{N}_{K,i}$ is the K-th shape function differentiated with respect to the i-th spatial direction.

2 The equations of motion

The equations of motion for a continuous body can be expressed in the reference configuration $\mathcal{C}$ whereby all field variables are functions of time and the material coordinates (see Gurtin [Gur81], pp. 178):

$$\text{Div} \boldsymbol{P} + \boldsymbol{B}^0 = \rho_0 \ddot{\boldsymbol{u}} \;, \tag{23}$$

where $\boldsymbol{P}$ represents the first Piola-Kirchhoff tensor, which is related to the Cauchy stress tensor $\boldsymbol{T}$ by $\boldsymbol{P} = \det(\boldsymbol{F}) \boldsymbol{T} \boldsymbol{F}^{-T}$. The force density $\boldsymbol{B}^0$ is a field of external body forces (caused for instance by gravity). It is related to the real force density, $\boldsymbol{b}$ expressed in the spatial description $\mathcal{C}^d$, by $\boldsymbol{B}^0 = \det(\boldsymbol{F}) \boldsymbol{b}$. ρ_0 represents the mass density in the reference configuration. All variables are functions of the material coordinates.

The starting point for an analysis with the finite element method can be obtained from an energy rate equation. It can be derived by taking the inner product of equation (23) with the velocity field $\dot{\boldsymbol{u}}$, and integrating over an arbitrary volume $\Omega \subseteq \mathcal{C}$. By making use of the equivalence:

$$\text{Div}(\boldsymbol{P}^T \dot{\boldsymbol{u}}) \;=\; \text{Div}(\boldsymbol{P}) \bullet \dot{\boldsymbol{u}} + \boldsymbol{P} : \text{Grad} \dot{\boldsymbol{u}} \;, \tag{24}$$

and Gauss' divergence theorem, the following rate equation can be obtained:

$$\int_{\partial\Omega} \boldsymbol{P} \boldsymbol{N} \bullet \dot{\boldsymbol{u}} \, d(\partial\Omega) + \int_{\Omega} \boldsymbol{B}^0 \bullet \dot{\boldsymbol{u}} \, d\Omega \;=\; \underbrace{\int_{\Omega} \boldsymbol{P} : \dot{\boldsymbol{F}} \, d\Omega}_{(\star)} + \frac{d}{dt} \int_{\Omega} \rho_0 \frac{1}{2} \dot{\boldsymbol{u}} \bullet \dot{\boldsymbol{u}} \, d\Omega \;. \tag{25}$$

This equation can be stated in words as: *The rate of work of the surface forces plus the rate of work done by the body forces equals the stress power plus the rate of kinetic energy change.*

The term $(\star)$ in (25) is called stress power. It can be rewritten as:

$$\int_\Omega \boldsymbol{P} : \dot{\boldsymbol{F}} \, d\Omega = \int_\Omega \mathrm{Tr}\left(\boldsymbol{P}^T \dot{\boldsymbol{F}}\right) d\Omega = \int_\Omega \mathrm{Tr}\left((\boldsymbol{P}^T \boldsymbol{F}^{-T})(\boldsymbol{F}^T \dot{\boldsymbol{F}})\right) d\Omega = \int_\Omega \boldsymbol{S} : (\boldsymbol{F}^T \dot{\boldsymbol{F}}) d\Omega \quad .(26)$$

$\boldsymbol{S}$ is the 2nd Piola-Kirchhoff stress tensor [Ogd84] defined as:

$$\boldsymbol{S} = \det(\boldsymbol{F}) \boldsymbol{F}^{-1} \boldsymbol{T} \boldsymbol{F}^{-T} \quad . \tag{27}$$

By interpreting the product $\boldsymbol{PN}$ as the surface traction, the energy balance law (25) can be rewritten as:

$$\int_{\partial\Omega} \boldsymbol{Z} \bullet \dot{\boldsymbol{u}} \, d(\partial\Omega) + \int_\Omega \boldsymbol{B}^0 \bullet \dot{\boldsymbol{u}} \, d\Omega - \int_\Omega \boldsymbol{P} : \dot{\boldsymbol{F}} \, d\Omega = \int_\Omega \rho_0 \ddot{\boldsymbol{u}} \bullet \dot{\boldsymbol{u}} \, d\Omega \tag{28}$$

The expression $\boldsymbol{PN}$ in (25) was replaced in (28) by an equivalent surface force field $\boldsymbol{Z}$ acting on the body surface in the reference configuration.

2.1 Tissue modelling and stress computation

The total stress is computed as the sum $\boldsymbol{S}_p + \boldsymbol{S}_a$ of the 2nd Piola-Kirchhoff tensors representing passive and active stress. Much can be learned from the research on cardiac musculature, c.f. Humphrey and Yin [HY89], Pinto [Pin87], Yin [Yin85], Horowitz et al. [HLY+88], [HSL+88b], and [HSL88a], and Bovendeerd et al. [BAH+92].

Following the continuum physics approach, the main fiber directions and distributions for each muscle type must be represented as continuous functions in $\mathcal{C}$. Several muscle types can overlap, e.g., the Transversalis and the Verticalis intrinsic muscles in the human tongue. For each muscle type m, an activation parameter π_m is defined, which varies with time. In the FEM approximation, the direction fields are represented by direction angles specified at each node, and the activation levels by scalars specified at each node.

As is done for cardiac tissue in Bovendeerd et al. [BAH+92], the passive stress can be modeled approximately according to the assumption of hyper-elasticity, where it is expressed by means of a strain energy density function $W(\boldsymbol{E})$:

$$\boldsymbol{S}_p = \frac{\partial W(\boldsymbol{E})}{\partial \boldsymbol{E}} \tag{29}$$

The function W depends only upon the principal invariants of $\boldsymbol{E}$ if the tissue is isotropic. Transversely isotropic materials can be modeled by extending the function W to one that

depends upon a term E_{33} representing the third diagonal component of $\boldsymbol{E}$ when it is written in a rotated system, where the fiber direction is the z-axes.

Strain energy functions for various tissues can be found in the biomechanical literature, e.g. Fung [Fun81], and [Fun90]; for tongue tissue in particular, such functions are not well known.

The active muscle stress is represented as pure tensile stress in the direction of the muscle fibers. It depends on the local strain and strain rate in the direction of the muscle fibers which can be computed for muscle type m as

$$\lambda_m = (\boldsymbol{N}_m^T \boldsymbol{C} \boldsymbol{N}_m)^{\frac{1}{2}} \quad , \quad \text{and} \quad \dot{\lambda}_m = \frac{1}{2} \frac{\boldsymbol{N}_m^T \dot{\boldsymbol{C}} \, \boldsymbol{N}_m}{\lambda_m} \quad , \tag{30}$$

where $\boldsymbol{N}_m$ represents a unit vector in the m-th fiber direction in $\mathcal{C}$. If the constitutive law for muscle fiber is given as scalar functions $\tau_m(\lambda_m, \dot{\lambda}_m, \pi_m)$ describing the force due to a dimensionless activation parameter π_m per unit area perpendicular to the fiber direction in the deformed configuration, the corresponding pure tensile Cauchy stress can be represented as

$$\boldsymbol{T}_m = \tau_m(\lambda_m, \dot{\lambda}_m, \pi_m) \, \boldsymbol{n}_m \otimes \boldsymbol{n}_m \quad , \tag{31}$$

where $\otimes$ represents the tensor product, and $\boldsymbol{n}_m$ a unit vector in the direction of the fibers in $\mathcal{C}^d$. Since the unit vector $\boldsymbol{n}_m$ can be obtained as:

$$\boldsymbol{n}_m = \frac{1}{\lambda_m} \boldsymbol{F} \boldsymbol{N}_m \quad , \tag{32}$$

the tensile stress (31) can also be expressed as:

$$\boldsymbol{T}_m = \frac{1}{\lambda_m^2} \tau_m(\lambda_m, \dot{\lambda}_m, \pi_m) \, \boldsymbol{F} \, (\boldsymbol{N}_m \otimes \boldsymbol{N}_m) \, \boldsymbol{F}^T \quad . \tag{33}$$

From this the corresponding second Piola-Kirchhoff tensor can be obtained via (27):

$$\boldsymbol{S}_m = \tau_m(\lambda_m, \dot{\lambda}_m, \pi_m) \, \frac{\det \boldsymbol{F}}{\lambda_m^2} \boldsymbol{N}_m \otimes \boldsymbol{N}_m \quad . \tag{34}$$

The expression (34) represents an active contribution to the total stress tensor field. The total stress tensor is thus computed as the sum

$$\boldsymbol{S} = \boldsymbol{S}_p + \sum_m \boldsymbol{S}_m \tag{35}$$

To maintain isochoric motion of the incompressible tissue, only the deviatoric part of the total stress tensor enters the equations of motion. If T is the Cauchy stress corresponding to the total stress S, its deviatoric part is $T - \frac{1}{3} \operatorname{Tr}(T) I$. The deviatoric part of S is obtained via (27) as:

$$\hat{S} = S - \frac{1}{3} \operatorname{Tr}\left(FSF^T\right) C^{-1} \quad . \tag{36}$$

3 Finite element approximation

A FEM discrete approximation is obtained by using the piecewise smooth approximation of the field variables $\dot{u}$, $\ddot{u}$, F and $\dot{F}$, see (18), (21), and (22). In the FE representation, these fields depend only upon the node displacement, velocity, and acceleration vectors. The integrations are carried out over each element. Since the velocity field $\dot{u}$ was chosen arbitrarily, it can be dropped from the equations, and a system of second order equations is the final result (see also Oden [Ode72], section 13.4). The following expressions are obtained in the approximation, using appropriate abreviations for the numerically evaluated integrals:

$$\int_{\partial \mathcal{B}_0} Z \bullet \dot{u} \, d(\partial \mathcal{B}_0) = \int_{\partial \mathcal{B}_0} Z_i \mathcal{N}_K \, d(\partial \mathcal{B}_0) \ \dot{u}_i^K = \tau_{Ki} \dot{u}_i^K \tag{37}$$

$$\int_{\mathcal{B}_0} B^0 \bullet \dot{u} \, d\mathcal{B}_0 = \int_{\mathcal{B}_0} B^0{}_i \mathcal{N}_K \, d\mathcal{B}_0 \ \dot{u}_i^K = \beta_{Ki} \dot{u}_i^K \tag{38}$$

$$\int_{\mathcal{B}_0} P : \dot{F} = \int_{\mathcal{B}_0} P^{il} \mathcal{N}_{K,l} d\mathcal{B}_0 \, \dot{u}_i^K = \iota_{Ki} \dot{u}_i^K \tag{39}$$

$$\int_{\mathcal{B}_0} \rho_0 \ddot{u} \bullet \dot{u} \, d\mathcal{B}_0 = \int_{\mathcal{B}_0} \rho_0 \mathcal{N}_K \mathcal{N}_L \, d\mathcal{B}_0 \, \ddot{u}_i^L \dot{u}_i^K = m_{KL} \ddot{u}_i^L \dot{u}_i^K \tag{40}$$

After dropping the arbitrary velocity field $\dot{u}_i^K$, the equation (28) can then be approximated as the force equation for node K:

$$m_{KL} \ddot{u}_i^L = -\iota_{Ki} + \beta_{Ki} + \tau_{Ki} \quad , \tag{41}$$

In this equation, the symbols represent entities which are in general different for each element: m: mass matrix, ι: vector of inner forces, β: vector of outer body forces, and τ: vector of surface traction forces.

By assembling the element matrices and forces to global matrices and forces, one arrives at a system of equations that can be written as follows:

$$\mathbf{M}\ddot{\mathbf{U}} + \mathbf{I}(\mathbf{U}, \dot{\mathbf{U}}; \Pi) = \mathbf{B} + \mathbf{T}(\mathbf{U}, \dot{\mathbf{U}}) \quad . \tag{42}$$

In (42) $\mathbf{M}$ represents the global mass matrix, $\mathbf{I}$ represents inner forces, $\mathbf{B}$ is a node force vector representing body forces, $\mathbf{T}$ is a global surface force vector, which contains only non-zero elements for nodes on the surface where traction is applied, depending on the dynamic state of the model. $\mathbf{U}$ is the global node displacements vector.

Due to the computation of the stress tensor $\boldsymbol{S}$, the inner force vector $\mathbf{I}$ depends in non-linear manner on the global node displacement vector $\mathbf{U}$, the global node velocity vector $\dot{\mathbf{U}}$, and further upon a multi-tuple of parameters Π which influence the constitutive behavior of the matter (strain–stress relation). For the tongue and lips, whose internal stress field is influenced by various muscular activities, these parameters are controls (activation levels) of the different muscles.

3.0.1 Surface tension

Some of the elements have outer surfaces which model thin film or skin. For these surfaces the surface tension has to be lumped into forces acting on the nodes that lay on the surface of the assembly. The surfaces are approximated by isoparametric shape functions $\boldsymbol{\Upsilon}$ which depend on only two parameters.

$$\boldsymbol{X}(\xi, \eta) = \boldsymbol{\Upsilon}(\xi, \eta)_K \boldsymbol{X}^K \quad \boldsymbol{x}(\xi, \eta) = \boldsymbol{\Upsilon}(\xi, \eta)_K (\boldsymbol{X}^K + \boldsymbol{U}^K) \tag{43}$$

Again $\boldsymbol{X}^K$ are the (3-dimensional) node positions in the reference configuration. By integrating the rate of the surface strain energy density, $\dot{W}$, over the element surface, one obtains a total surface strain energy rate which must be equal to the total power formed by multiplying the node velocities with the lumped forces representing the surface tension in the finite element approximation.

From (14) we have:

$$\int_{\partial \mathcal{B}_0} \dot{W} \, d(\partial \mathcal{B}_0) = \int_{\partial \mathcal{B}_0} \boldsymbol{S}^{\alpha\beta} \dot{\mathsf{G}}_\alpha \cdot \mathsf{G}_\beta \, d(\partial \mathcal{B}_0) \tag{44}$$

Using the FEM representation of the surface base vectors:

$$\mathsf{G}_\alpha = \boldsymbol{\Upsilon}_{K,\alpha}(\boldsymbol{X}^K + \boldsymbol{U}^K) \quad \text{and} \quad \dot{\mathsf{G}}_\alpha = \boldsymbol{\Upsilon}_{K,\alpha}\dot{\boldsymbol{U}}^K \quad , \tag{45}$$

One obtains for the surface strain energy rate:

$$\int_{\partial \mathcal{B}_0} \dot{W} \, d(\partial \mathcal{B}_0) = \int_{\partial \mathcal{B}_0} \sum_{K=1}^{M} \sum_{L=1}^{M} S^{\alpha\beta} \Upsilon_{L,\beta} \Upsilon_{K,\alpha} (\boldsymbol{X}^L + \boldsymbol{U}^L) \cdot \dot{\boldsymbol{U}}^K d(\partial \mathcal{B}_0) \quad . \tag{46}$$

This gives rise to node force contributions:

$$f^K = \int_{\partial \mathcal{B}_0} \sum_{L=1}^{M} S^{\alpha\beta} \Upsilon_{K,\alpha} \Upsilon_{L,\beta} \, d(\partial \mathcal{B}_0) \, (\boldsymbol{X}^L + \boldsymbol{U}^L) \tag{47}$$

acting upon the K-th node.

3.1 Accounting for geometric boundaries I

In this part the case is investigated where some parts of the surface of the tongue body are in sliding contact with structures while being not attached to them. This is modeled as a geometric constraint that some surface nodes can only move on a surface, and here friction is neglected.

To obtain a method for handling this type of boundary, let the vectors $\boldsymbol{y}$ and $\boldsymbol{v}$ represent the generalized coordinates and velocities of an unconstraint dynamic system $\boldsymbol{G}(\boldsymbol{y}, \boldsymbol{v})$:

$$\begin{aligned} \dot{y} &= v & \text{(a)} \\ \dot{v} &= \boldsymbol{G}(\boldsymbol{y}, \boldsymbol{v}) & \text{(b)} \end{aligned} \tag{48}$$

Here $\boldsymbol{y}$ is a column vector containing the instantaneous coordinates of all nodes: $\boldsymbol{y} = \mathbf{X} + \mathbf{U}$, where $\mathbf{X}$ and $\mathbf{U}$ are the global node position and displacement vectors, respectively, and $\boldsymbol{v}$ is the same as $\dot{\mathbf{U}}$ in (42). Some of the nodes are movement constrained to a surface represented by the equation

$$g(\boldsymbol{y}) = 0 \quad . \tag{49}$$

To account for these constraints, the above system can be extended, by introducing forces perpendicular to the constraint surface, and scaled by Lagrange multipliers:

$$\begin{aligned} \dot{y} &= v \\ \dot{v} &= \boldsymbol{G}(\boldsymbol{y}, \boldsymbol{v}) + \sum_{\nu=1}^{M} \Lambda_\nu c_\nu \\ c_\nu^T v &= 0 \quad \text{for} \quad \nu = 1, \dots, M \end{aligned} \tag{50}$$

where c_ν referes to the gradient of the constraint function $g(\boldsymbol{y})$ taken at the ν-th node that has to satisfy the constraint.

The Lagrange multipliers can be obtained by differentiating the last of the above equations with respect to the time parameter, substituting $\dot{\boldsymbol{y}}$ and $\dot{\boldsymbol{v}}$ from (50), and making use of the fact that $c_\mu^T c_\nu = 0$ if $\mu \neq \nu$:

$$\Lambda_\nu = -\frac{1}{c_\nu^T c_\nu} \left(\boldsymbol{v}^T \mathbf{H}_\nu \boldsymbol{v} + c_\nu^T G(\boldsymbol{y}, \boldsymbol{v}) \right) \quad , \tag{51}$$

and are inserted into the extended system equations (50).

In (51) $\mathbf{H}_\nu$ represents the matrix of second derivatives (Hesse matrix) of the constraint function for constraint node ν:

$$\mathbf{H}_\nu = [H_{ij}]_\nu = \left[\frac{\partial^2 g(\boldsymbol{y})}{\partial y_i \partial y_j} \right]_\nu \quad . \tag{52}$$

3.2 Isochoric motion constraint.

Biological tissues are in physiological pressure ranges absolutely incompressible. This is a geometrical constraint on the deformation. It is impossible to fulfill the requirement for each point of the body because in a discretization by the finite element method. The incompressibility condition is approximated by requiring that each finite element has precisely constant volume during the movement. This results in an additional system of equations that have to be fulfilled during the computation of the movement.

The volume of an isoparametric finite element depends on the location of the nodes. In general, constraints like the volume constraint can be stated as implicite scalar equations:

$$A(\boldsymbol{U}^1, ..., \boldsymbol{U}^{N_N}) = 0 : \tag{53}$$

where $\boldsymbol{U}^K$ are the node displacements of node K of one element.

Let A_μ be the μ-th geometrical constraint function. A_μ has to remain constant and, without loss of generality, equal to zero.

The global equations of motion of the finite element system can be written in short as a first order ordinary differential equation system.

$$\begin{aligned}
\dot{U}_i^K &= V_i^K \\
\dot{V}_i^K &= \Gamma_{KN} F_i^N
\end{aligned} \tag{54}$$

where Γ_{KN} represents the inverse global mass matrix. Since we demand that $A = 0$ always, any linear combination of A and its time derivatives must be equal to zero. The combination of the system equations and the geometric constraint equations is obtained as the following system with Lagrange multipliers:

$$
\begin{aligned}
\dot{U}_i^K &= V_i^K \\
\dot{V}_i^K &= \Gamma_{KN} F_i^N + \lambda_\mu \frac{\partial A_\mu}{\partial U_i^K} \\
0 &= \ddot{A}_\nu + \frac{2}{\tau} \dot{A}_\nu + \frac{1}{\tau^2} A_\nu \quad \text{for } \nu = 1, \cdots, \text{Number of constraints}
\end{aligned}
\tag{55}
$$

(Summation over equal indices is implied here and in the following; in particular summation over μ is assumed in the above formula. The index K runs over the entire number of nodes, and the index i over the 3 dimensions.)

The constraint equation is a second order critically damped system which has a stable point if the constraints are exactly fulfilled. τ is a parameter which specifies how fast the system snaps back to its constraint if it drifts away.

The Lagrange multipliers λ_μ need to be found to combine all constraints appropriately, by solving a linear system of equations. Starting from the above ansatz, the system is obtained as:

$$
D_{\nu\mu} \lambda_\mu = r_\nu
\tag{56}
$$

with (V^L velocity vector of L-th node)

$$
D_{\nu\mu} = \frac{\partial A_\nu}{\partial U_i^K} \frac{\partial A_\mu}{\partial U_i^K} \quad \text{and} \quad r_\nu = -\frac{\partial^2 A_\nu}{\partial U_j^L \partial U_i^K} V_j^L V_i^K - \frac{\partial A_\nu}{\partial U_i^K} \Gamma_{KN} F_i^N - \frac{2}{\tau} \dot{A}_\nu - \frac{1}{\tau^2} A_\nu
\tag{57}
$$

3.3   Accounting for geometric boundaries II

The tongue is in varying contact with the hard palate and the teeth. This is essential for the articulation of consonants but also plays a crucial role in the production of front vowels. The force laws that are underlying the contact between tongue and hard palate are not well known. In comparison to the tongue, the hard palate can be seen as undeformable. A method is needed that prevents the model tongue from penetrating the palate during the simulation. The hard palate is modeled as the set of points y which fulfill the equation $g(y) = 0$. A surface traction is introduced which depends on the width of a gap between the tongue surface and the hard palate.

If $\boldsymbol{x}$ is a point on the tongue surface and $\boldsymbol{y}$ is a point on the palate surface, the function

$$h(\boldsymbol{x},t) = min\{|\boldsymbol{x}-\boldsymbol{y}|, g(\boldsymbol{y}) = 0\} \tag{58}$$

can be called the gap width function. The rate of change of the width is:

$$\dot{h}(\boldsymbol{x},t) = \frac{\boldsymbol{x}-\boldsymbol{y}}{|\boldsymbol{x}-\boldsymbol{y}|} \bullet \dot{\boldsymbol{u}} \quad , \tag{59}$$

where $\dot{\boldsymbol{u}}$ is the velocity of the point $\boldsymbol{x}$.

A force law may be introduced which computes a surface traction τ_n acting perpendicularly upon the tongue surface if the tongue is moving close to the hard palate. The impact of the tongue onto the hard palate is mostly inelastic. A simple model is given by the following:

$$\tau_n = \begin{cases} a_1 \, (h-h_\epsilon)^{a_2} \left(1-\text{sign}\dot{h}\right) \dot{h}^{a_3} & \text{if} \quad h < h_\epsilon \\ 0 & \text{if} \quad h \geq h_\epsilon \end{cases} \tag{60}$$

The coefficients a_1, $a_2 \geq 1$, and $a_3 \geq 1$ have to be specified and optimized in experiments. h_ϵ is a threshold gap width at which a force begins to be active. The term $(1-\text{sign}\dot{h})$ sets the traction to zero if the surface point $\boldsymbol{x}$ is moving away from the hard palate.

3.4   Geometric boundaries III - fixed connections

Needs revision. Lips and tongue are mounted on bony structures. Some parts of the surface of the soft tissue components act as interfaces with rigid structures, namely the skull and jaw. The mechanical principle for handling the interactions, for instance between the tongue and jaw, is that of the balance of forces and moments at the interface. For example, mandible movement can be described sufficiently in terms of two translational and one rotational degrees of freedom. Corresponding to the translational degree of freedom, a total force acting upon the jaw by the tongue is obtained by summing the forces at all nodes of the tongue that are attached to or in contact with the mandible. The total moment is obtained by summation of all partial moments of the same nodes. The moment at each node is the vector product of the node's distance vector relative to the mandible's pivot point, and the force at the node.

The mandible can be described by a second order dynamic system, which receives several general muscle forces as input.

$$\begin{aligned} M\ddot{y} &= F(y,\dot{y},\theta,\dot{\theta},\nu) + f \tag{61} \\ I\ddot{\theta} &= N(y,\dot{y},\theta,\dot{\theta},\nu) + n \tag{62} \end{aligned}$$
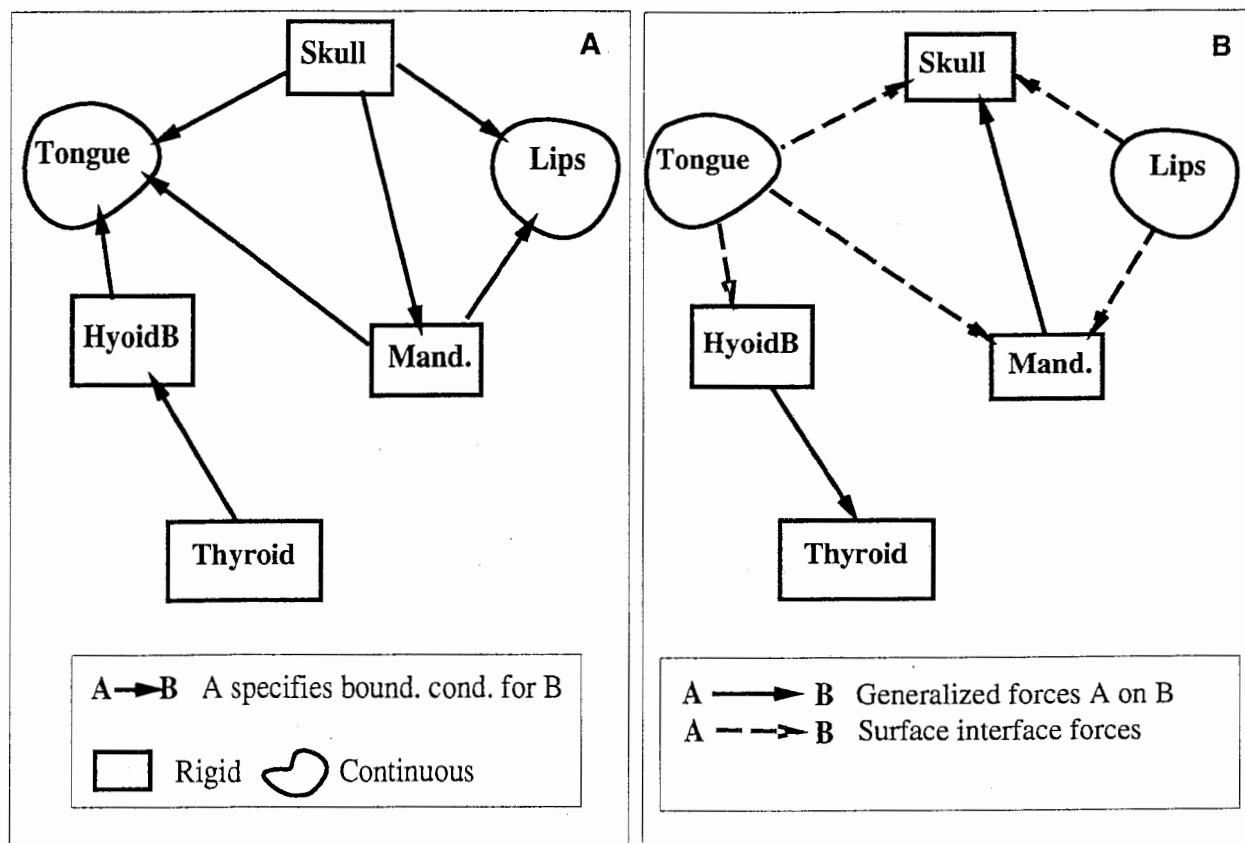
Figure 2: This pair of figures shows two kinds of relationships. A: Chosen geometrical dependence. B: Force relationships. The dashed lines indicate that the source of the arrow integrates forces over a surface. The figure neglects several existing interactions.

In this system, M represents the total mass of the rigid structure of the jaw, I is a moment of inertia, y represents the (2-dimensional) position of a point of reference in the midsagittal plane (relative to a reference point that is fixed in the skull) θ is an angle of rotation (relative to a reference direction fixed in the skull). F represents the sum of translational forces, and N represents the sum of torques that are generated in the mandible system. The terms f and n are the net forces and torques that which are results of the action of the tongue (and lips) onto the mandible.

The mandible dynamic system and that describing the movements of the tongue and the lips have to be integrated simultaneously. The sums of forces and moments at the nodes that are connected to the mandible appear as external forces in the mandible system (f and n above). In the tongue simulation, the trajectories of the nodes connected to the mandible are computed from the instantaneous state of the mandible model, and the equations of motion for these nodes are removed from the dynamic system of the tongue.

Treating tongue-mandible and lip-mandible interaction in the way outlined above gives free-

dom in defining the boundary between these organs. It is only assumed that all tissue components that are considered to be part of the "mandible" are moving in a rigid manner with the mandible system, and their masses must be taken into account in the computation of the constants M and I in (61) and (62). The mass of the attached soft tissue of tongue and lips is modeled properly in the finite element simulation of those systems. Fig. 2 shows the relations between geometrical dependencies and force dependencies. In the figure, skull, mandible and hyoid bone are assumed to be the masters which determine the boundary conditions of the tongue and the lips. The forces that act on the boundaries have to be calculated in the dependent subsystems, namely in the tongue and lips models. The location and velocity of the nodes which form the interface between, e.g., tongue and mandible, are completely determined by the movements of the mandible. The interaction with the hyoid bone is modeled in the same way. It can be noticed that there is an arbitrariness in this decision. Would the geometrical dependency relation be inverted (see the arrow in Fig. 2-A between hyoid bone and tongue), the computation of the nodes on the hyoid bone surface would be complicated. The fact that these nodes are in fixed geometrical relations to each other (via the geometry of the hyoid bone) would enter the system of equations for the tongue as a geometrical constraint for each (tongue-model) node connected to the hyoid. From the view of physics, though, both possible dependencies are equivalent.

4 Implementation issues

A finite element code that is specialized for modeling soft tissues is being implemented. As an alternative to most existing complete libraries, an object oriented approach was adopted, and all components of the library are implemented as C++ objects. Figure 3 shows some of the structure of the class library. Currently only a Runge-Kutta algorithm is being used, in the future faster algorithms are considered. To make the implementation independent from the particular integration method that is used, only the higher level base classes communicate. (a superclass named *vector3Dsolver* and a class *vector3Drightside*, representing the right side of a system of ordinary differential equations.) The class *Assembly* which holds a list of elements and nodes, is derived from the class *vector3Drightside*. From within the class *Assembly* all classes representing elements are treated the same. The elements are derived from an abstract class *Element3D* which contains many virtual functions, that have to be defined in the derived classes. So far the class *Brick8Element* has been completed, and the classes *Tetrahedron* and *Prism* are in work.

The methods for maintaining incompressibility, which are implemented in the element classes and the assembly class have been tested on examples of drop formation and later with a simple tongue model. The volume deviation from the initial condition volumes was only of magnitude 10^{-5} per unit volume.
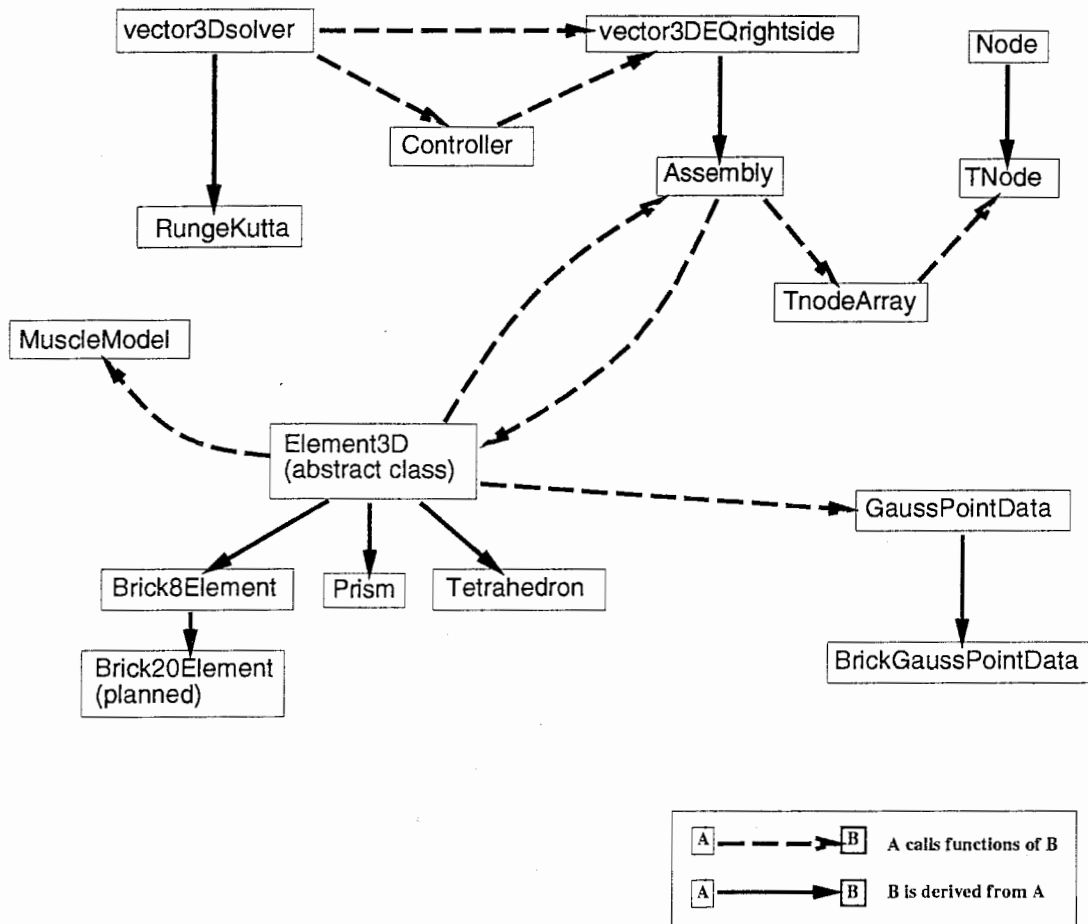
Figure 3: Some of the main classes of a class library written in C++ for modeling tissue. Solid arrows represent class dependencies - the end of the arrow points to the derived class, and dashed arrows denote "making use of" relations.

5 An experimental tongue model

The main purpose of the tongue model described below was to obtain some reasonable and nevertheless simplified simulation of a tongue suited to test the computational algorithms. The model has only 42 elements which allows a computation speed of about 1000 times real time (e.g. for one second of computed movement, 1000 seconds of CPU are needed on a sparc 10). Even though the subdivision of the tongue into only 42 elements alows only a poor representation of the anatomy, some typical movements of the tongue can be simulated with the model.

5.1 Methods of construction

For the preliminary tongue model some methods of geometric design were tried out by implementing a specialized simple CAD modeler as a **Matlab** program. The topology of the model tongue was specified manually, resulting in the initial block in figure 16. The coordinates of the nodes are specified within a unit-cube. This cube, with coordinates r,s,t is then deformed using trivariate Bezier polynomials:

An n-set of univariate Bézièrpolynomals is given by

$$B_i^n(t) = \binom{n}{i} t^i (1-t)^{n-i} \quad \text{where} \quad \binom{n}{i} = \frac{n!}{i!(n-i)!} \tag{63}$$

A Bézièrcube can be described by the cartesian product of three sets (l,m,n):

$$B_{ijk}^{lmn}(r,s,t) = B_i^l(r) B_j^m(s) B_k^n(t) \tag{64}$$

The $(l \times m \times n)$ trivariate polynomials $B_{ijk}^{lmn}(r,s,t)$ constitute a basis which can be used to map the unit cube onto deformed versions of the unit cube. For this purpose a grid of control points (control vertices), b_{ijk}, is defined which have the same number as base polynomials. A mapping of the unit cube onto a curvilinear cube is then given by the following:

$$\boldsymbol{b}(r,s,t) = \sum_{i=0}^{l} \sum_{j=0}^{m} \sum_{k=0}^{n} \boldsymbol{b}_{ijk} B_{ijk}^{lmn}(r,s,t) \tag{65}$$

Changing the positions of the control points $\boldsymbol{b}_{ijk}$ results in a deformation of the image of the mapping.

To use this mapping for modeling purposes, the nodes of an initial simple geometric structure are specified in the unit cube. Be moving the Bézièrcontrol vertices with a mouse, the model thus embedded in in the unit cube is deformed and rescaled. The fiber directions of the muscles are also defined in the unit cube in such a way that they do not need to be re-defined when the control vertices are changed in order to design the shape of the tongue. For simplicity, for this model it is assumed that the fiber directions are constant throughout each element and are specified at the center of the element, see figure 17 for an example. If the Bézièrcontrol vertices are moved, also the mappings of the tangent spaces change at each (r,s,t) point, induced by the mapping (65). Muscle fiber directions are represented as elements of the tangent space at the center of each finite element. Let (r,s,t) be the coordinates of such an element center. The basis of the tangent space at that position is obtained as the three vectors: $\frac{\partial \boldsymbol{b}(r,s,t)}{\partial (r,s,t)}$. This basis can be computed by making use of the properties of Bézièrpolynomials. E.g., differentiation with respect to the first coordinate r results in:

$$\frac{d}{dr}\boldsymbol{b}(r,s,t) = l \sum_{i=0}^{l-1} \sum_{j=0}^{m} \sum_{k=0}^{n} (\boldsymbol{b}_{ijk} - \boldsymbol{b}_{i+1,j,k}) B_{ijk}^{l-1,mn}(r,s,t) \tag{66}$$

The muscle fiber directions that were used in computational experiments are shown in the figures 24 - 31.

Besides modifying the Bézièr control vertices to form a tongue model, it is also possible to modify interactively the positions of individual nodes in the (r,s,t) coordinates. This is exemplified in the sequence of figures 22 and 23.

5.2   A muscle model for the preliminary tongue

The passive tissue model of cardiac tissue was used and modified by dropping the non-isotropic components. The modified passive cardiac tissue model [BAH+92] is specified by the following strain energy function:

$$W = a_0(exp(a_1 J_1^2 + a_2 J_2) - 1) \quad , \tag{67}$$

where J_1 and J_2 are the strain invariants when computed from the Euler tensor $\boldsymbol{E}$. The constants in this strain energy function are: $a_1 = 3.0$, $a_2 = 6.0$ and $a_0 = 0.5$ kPa. Restated in terms of invariants of the Cauchy tensor, this gives:

$$W = a_0 exp\Big(\frac{a_1}{4}(I_1 - 3)^2 + \frac{a_2}{4}(2I_1 + I_2 - 3) - 1\Big) \tag{68}$$

To obtain a second Piola-Kirchhoff stress tensor from this strain energy function we need the differentials:

$$\frac{\partial W}{\partial I_1} = \left(\frac{a_1}{2}(I_1 - 3) + \frac{a_2}{2}\right) W \quad \text{and} \quad \frac{\partial W}{\partial I_2} = \frac{a_2}{4} W \quad . \tag{69}$$

$$\frac{\partial I1}{\partial E_{ij}} = \delta_{ij} \quad \text{and} \quad (\frac{\partial I_2}{\partial \boldsymbol{E}})_{ij} = \frac{\partial I_2}{\partial E_{ij}} = \begin{pmatrix} -E_{22} - E_{33} & E_{12} & E_{13} \\ E_{12} & -E_{11} - E_{33} & E_{23} \\ E_{13} & E_{23} & -E_{11} - E_{22} \end{pmatrix} \quad . \tag{70}$$

The resulting passive stress tensor is then:

$$\boldsymbol{S}_{ij} = 2\frac{\partial W}{\partial I_1}\delta_{ij} + 2\frac{\partial W}{\partial I_2}\frac{\partial I_2}{\partial E_{ij}} \quad . \tag{71}$$

The above definition of the passive tissue is true if the deformation of the tissue is isochoric. This is approximately realized by imposing the geometric constraint that each element in the finite element simulation stays at a constant volume.

In figure 4 the stress components $\boldsymbol{S}_{11}$ and $\boldsymbol{S}_{12}$ are plotted as a function of a planar strain and shear. In this case the Cauchy tensor is that of an isochoric planar stretch and shear:

$$C = \begin{pmatrix} \lambda^2 & \lambda s & 0 \\ \lambda s & \frac{1}{\lambda} + s^2 & 0 \\ 0 & 0 & \frac{1}{\lambda} \end{pmatrix} \quad , \tag{72}$$

where λ represents an extension ratio and s a shear. The deformation is ischoric since the determinante of C is one.

5.2.1 The active component of the muscle model

The active muscle stress function has the general form

$$t(\lambda, \dot{\lambda}, \alpha) = g(\dot{\lambda}) f(\lambda, \alpha) \quad , \tag{73}$$

where λ is the relative elongation, $\dot{\lambda}$ its rate, and α an activation parameter that varies usually between 0 and 1. One of the possible stress mobilisation functions which relate the active stress to the fiber length (extension ratio) is:

$$f(\lambda, \alpha) = \alpha\, c\, \frac{\exp\left(-a(\lambda - 1 + s)\right)}{1 + \exp\left(-a\, b\,(\lambda - 1 + s)\right)} \tag{74}$$
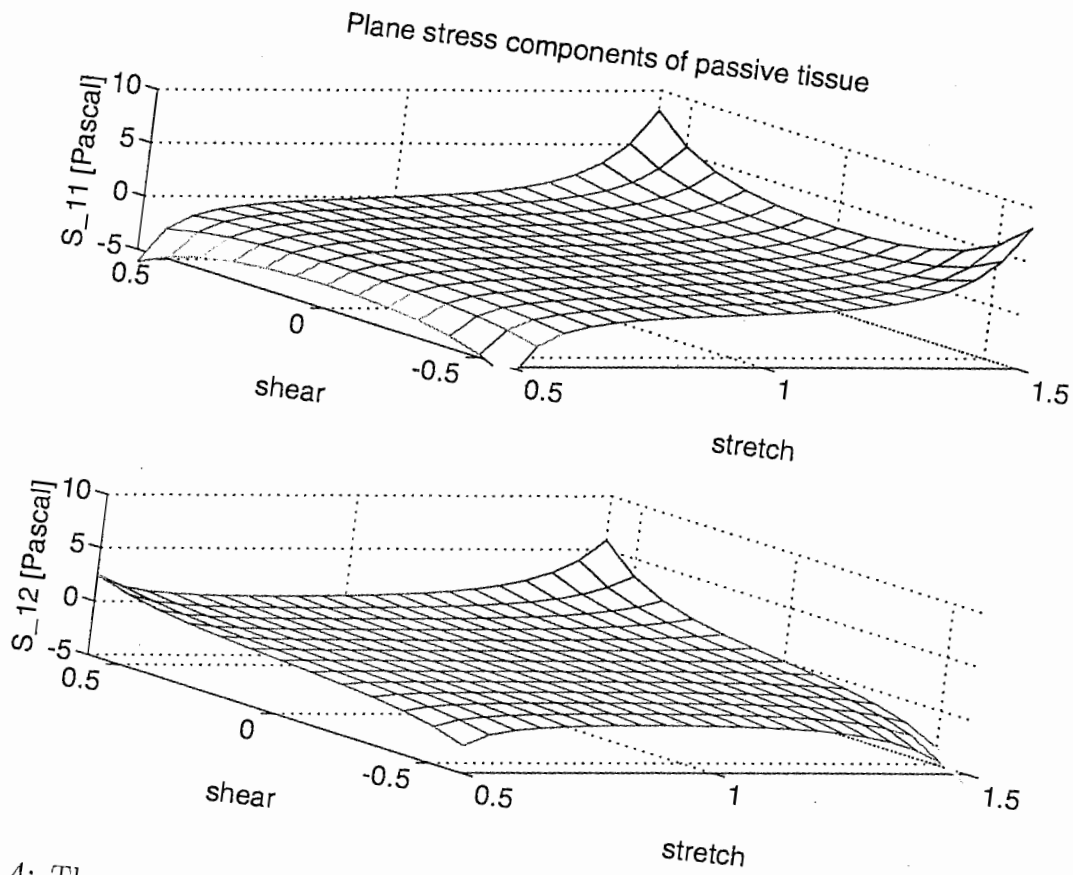
Figure 4: The components of stress for isochoric tissue deformation in the plane, using the passive cardiac model
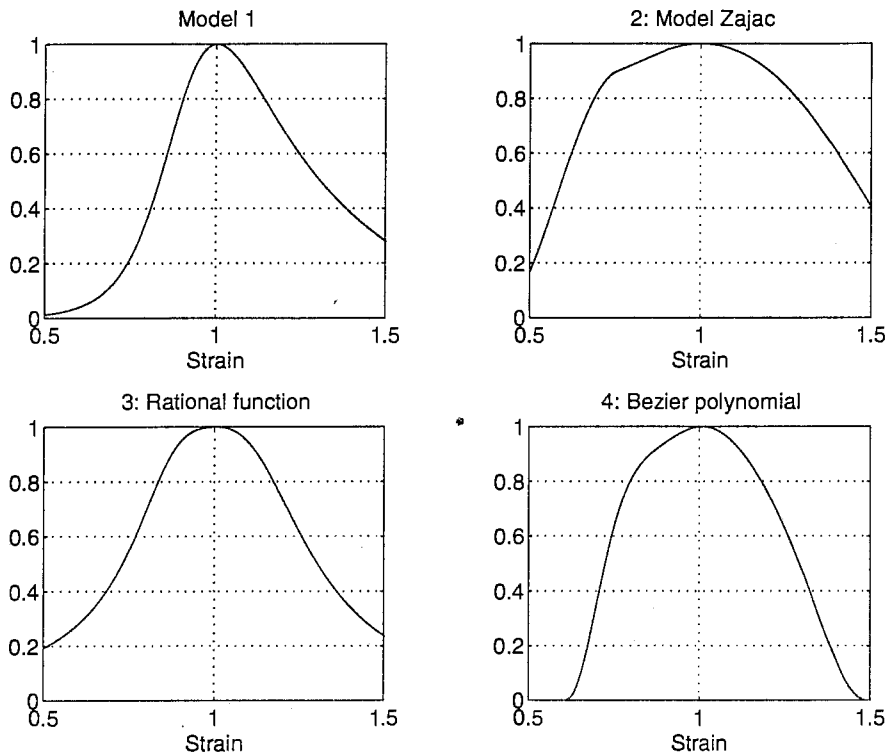
Figure 5: *Four stress mobilisation functions $f(\lambda, 1)$ as a function of the muscle fiber extension ratio (strain).*

This function (Model 1 in fig 5) has a maximum at $\lambda = 1$ if the coefficients are choosen as:

$$s = \frac{\ln(b-1)}{a\,b} \quad , \quad c = b\,(b-1)^{-(1-\frac{1}{b})} \tag{75}$$

The values for a and b were chosen as: $a = 3$, $b = 5$ in the modeling. Another extrem was an assumption of stress mobilization function which resembes the ones found in Zajac [Zaj89]. The simulation results came out rather similarly for the different curves except when this curve was chosen. Deformations were larger for this curve because the activity range is bigger.

The force-velocity characteristic of muscles is such that for fast contraction the active stress is reduced. The active stress is greater while the muscle is expanding (due to external load). This behavior was modeled with a sigmoid function as follows:

$$g(\dot\lambda) = \frac{1}{2}\left(1 + \frac{1 - e^{-b-a\,\dot\lambda}}{1 + e^{-b-a\,\dot\lambda}}\right) \tag{76}$$

The value for b in the above formula is chosen such that $g(0) = y_0$ where y_0 was chosen as 0.7. This results in:

$$b = \ln \frac{y_0}{1 - y_0} \tag{77}$$

The coefficent a is determined from the requirement that at a contraction rate (negative strain rate) $\dot{\lambda}_1$, the value of the function is given as $g(-\dot{\lambda}_1) = y_1$. The pair y_1, and $\dot{\lambda}_1$ were chosen as: $y_1 = 0.2$ and $\dot{\lambda}_1 = 25 sec^{-1}$. This condition delivers the other coefficient:

$$a = \frac{1}{\dot{\lambda}_1} \ln \frac{y_1(1 - y_0)}{y_0(1 - y_1)} \tag{78}$$

The resulting function $g(\dot{\lambda})$ is shown in figure 6.

The active stress is the product of the two functions, one that is only depending on the extension ratio of the fibers and one that depends on the rate of change of the extension ratio. The active stress function is shown in figure 7 for two different levels (0.25 and 1.0) of activation. The total tensil stress in the direction of a muscle fiber is the sum of the passive tissue stress component and the active stress. This is shown for a low value of activation (0.1) in figure 8. For the current tongue muscle model, it turned out to be necessary that the active stress far exceeds the passive stress for reasonable ranges of deformation (extension ratio between 0.7 to 1.3). Only for high shortening (extension ratio < 0.6) and for high lengthening (extension ratio > 1.5) the passive stress begins to be really noticable. Therefore, in future work the improvement of the active stress model ia more important than obtaining a better passive tissue model of tongue from data.

5.3   Experiments with the preliminary tongue model

In order to get an impression of the behavior of the current tongue model, an attempt was made to run simulations based on realistic tongue muscle activation levels. For this purpose a set of EMG measurements of tongue and laryngeal muscles was used. The set is from work at Haskins laboratories. Of the tongue, needle insertions had been made in the styloglossus, the posterior and anterior parts of the genioglossus and in the hyoglossus. In order to use them as activation levels, the data were normalized by dividing each data set through the maximum EMG level in the data. It was assumed that the measurements had been done with the same instrument settings, including amplification. Since the intrinsic muscles of the tongue (for the current model relevant: verticalis, transversalis, inferior and superior longitudinalis) had not been measured, their activation levels were assumed to be constant at a low level. This assumption is quite questionable but no other evidence for correlations which would result in estimates of the intrinsic muscle activation was available.
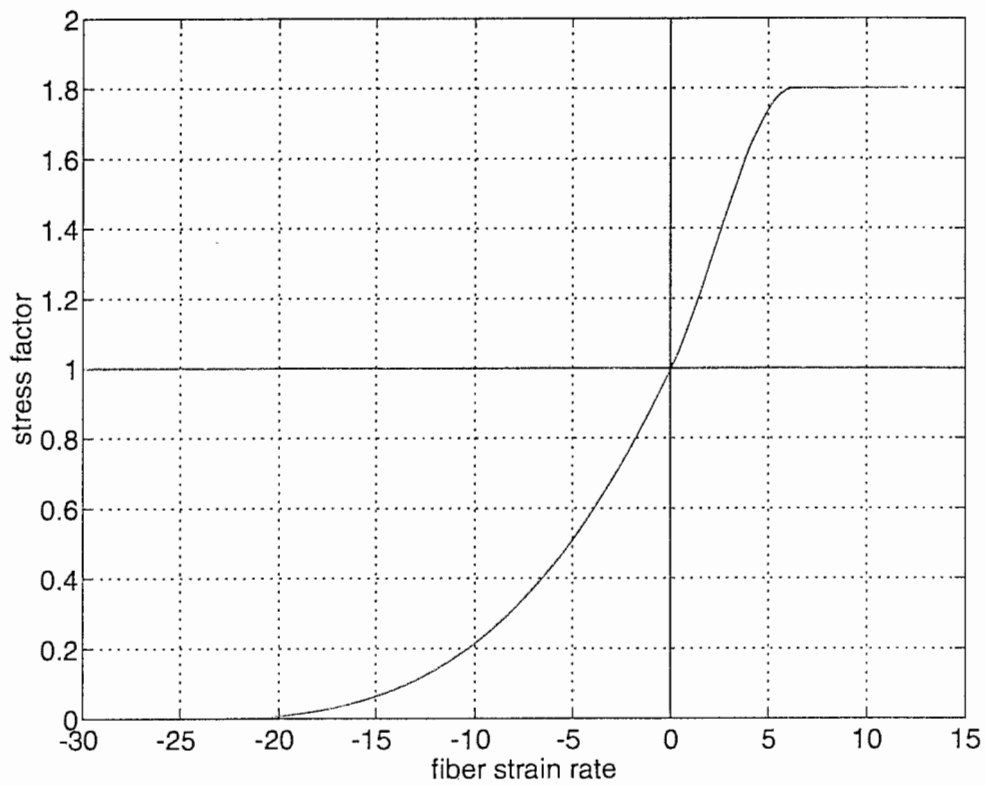
Figure 6: The dependency of the active stress from the rate of contraction for constant length. A negative fiber strain rate represents the contraction of the muscle fibers. The strain rate is positive if the muscle fibers are elongated by external fources.
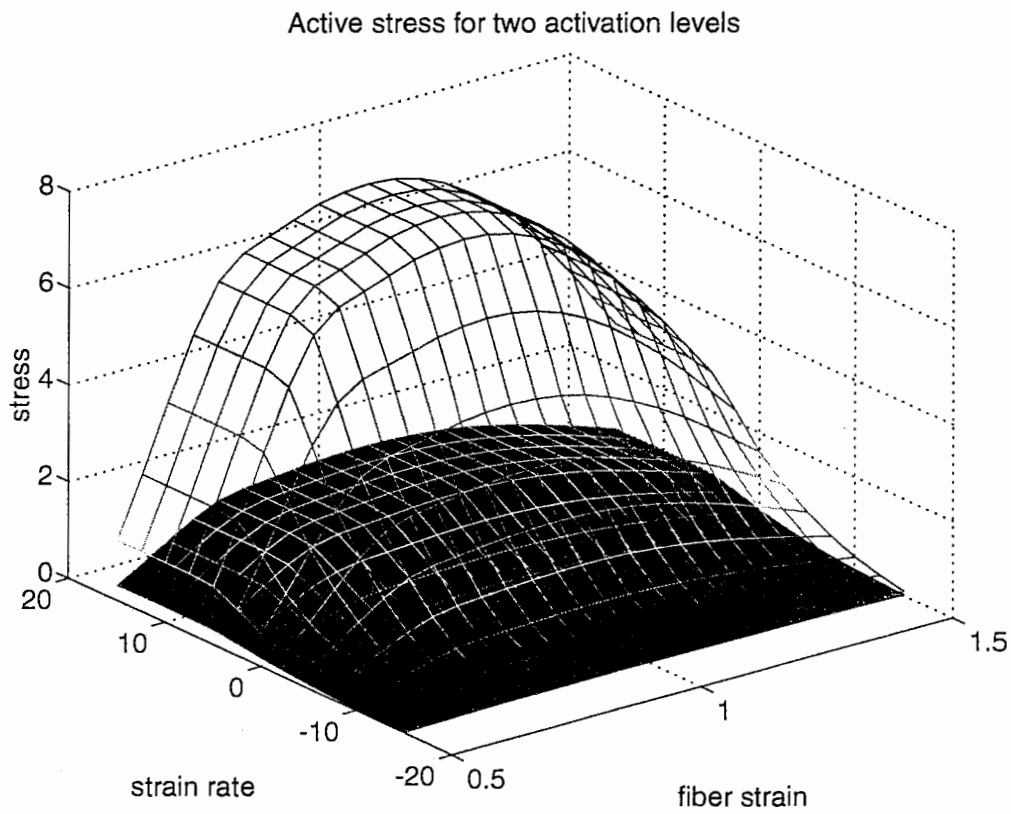
Figure 7: The active stress as a function of the contraction and rate of contraction of the muscle fibers, shown for the activation levels 0.25 and 1.0.
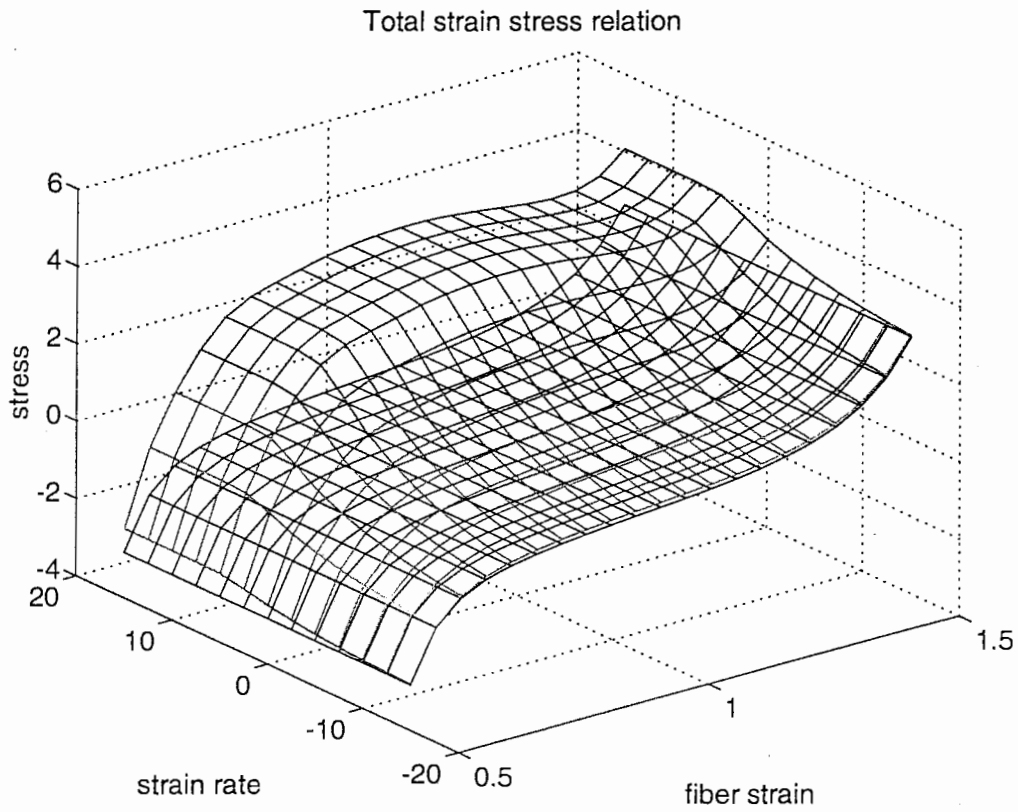
Figure 8: In this figure the lower surface represents the passive stress component for a simple stretch whereby isochoric deformation is assumed. The upper surface is the total stress (active plus passive) in the muscle fibers for small activation of the muscle fibers.

fs= 625 Hz

Cutoff = 40 Hz. .

N_FIR= 125

Tng Back versus Tng Blade

'rest' distance: 1.647 cm

Hypothesis: rest at end
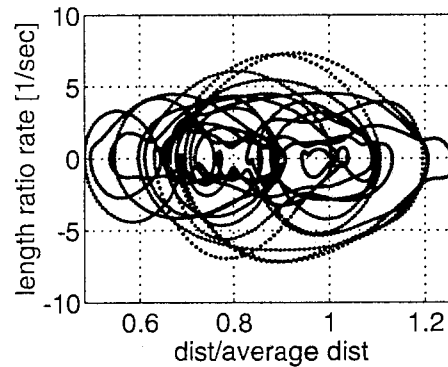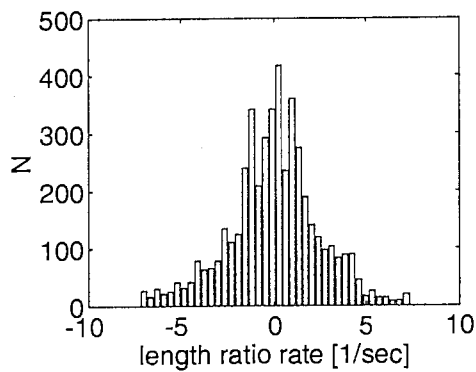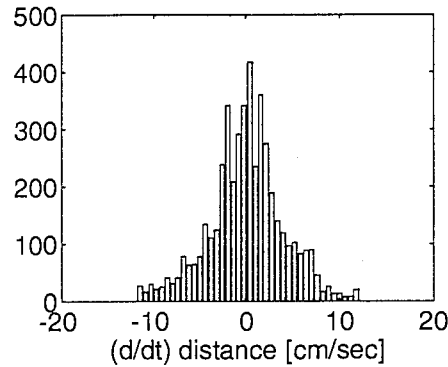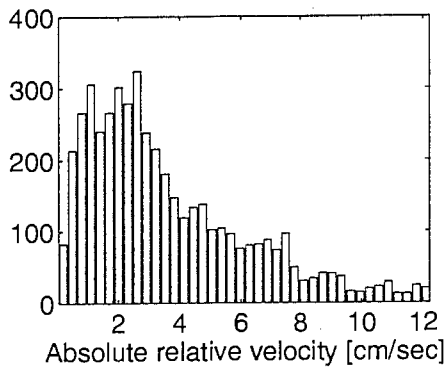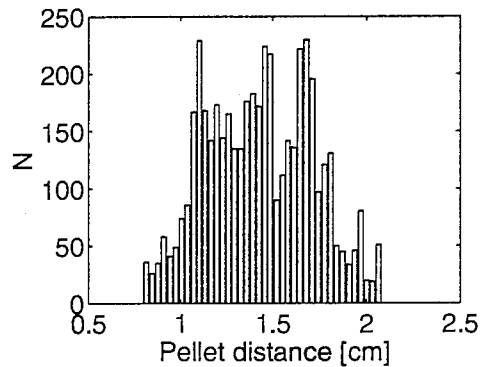
Figure 9: *Estimation of tongue deformation and rate of deformation. The pellet tracings (articulometer) of an utterance of about 7 seconds speech followed by silence of about 1 sec was analysed. Two neighboring pellets were compared. The assumption was made that during the silent portion at the end of the utterance the tongue was in a 'relaxed' state. The average distance between the pellets during that interval was used as the reference distance between the pellets. Data borrowed from Eric Bateson. It was a single sentence of recited speech, not read.*

The results of the simulation were displayed in computer animation sequences and captured on video. Without jaw movement, the interpretation of the resulting animations is difficult. However, several obvious mistakes in the specification of muscle fibers and muscle strength could be corrected by this study. The general limitations of the model became clearer. For example, without modeling the mouth floor properly, at least with some elements, the effect of the posterior genioglossus are wrong. It is known from observation of tongue pellet movements that the contraction of genioglossus posterior results mostly in a movement of the back of the tongue while the tongue body is lifted, bulged up. In the current model however, the whole tongue body moves towards the mouth opening. The interim solution to limit the modeling effort by attaching the tongue model at about the plane of the hyoid bone to some fixed surface, interferred considerably with the activity in particular of the genioglossus posterior.

The described initial tongue model can not be considered a realistic simulation of the tongue, it's main purpose was to investigate the feasibility of the modeling approach by testing some assumed hypothesis about possible tongue muscle activation patterns. However, several conclusions could be drawn from implementing and testing the preliminary tongue model with 42 elements and 8 muscle types.

1) The anatomy of the tongue calls for considerable refinement of the current model. Several artifacts of the too coarse discretization in too few elements could be observed. It seems more reasonable to have on average one element for each cubic centimeter of the tongue which leads to about 150 elements to model the whole tongue body, in order to obtain sufficient accuracy in representing properly the cross sectional areas of the different muscles. The insuffient accuracy in representing the cross sectional areas of each muscle could in the current model in part be cured by specifying scaling parameters for each element and muscle. These parameters represent a normalized fiber density and have in most cases the value 1. The tensile stress in muscle fiber direction is multiplied with these parameters. The specification of these parameters was done in evaluation of simulation results for individual muscle contractions. In the next modeling attempt non-uniformity of the muscle fiber density will only be introduced based on evidence in the anatomy. Proper modeling of muscle cross sections according to the anatomy is more reliable than additional assumptions that are needed in a coarse model to compensate discretization artifacts.

2) In the experiments with real EMG data driving the extrinsic muscles of the tongue model it became clear that the scope of modeling was too restrictive. The hyoid bone was not modeled as a moving structure and the floor of the mouth was not represented. This leads to a mechanical structure that has only limited resemblance with the real tongue. For example, the contraction of the genioglossus posterior should result in a forward movement of the back of the tongue and should not cause a large movements of the tip of the tongue. The observed model behavior was that the tongue body moves upwards and far forward, and seemed to indicate that also the genioglossus anterior

was contracting. This behavior can be explained from the missing of the moving hyoid bone. The fact that the mouth floor was not modeled resulted sometimes in instability of the model when all muscles have very low activity.

3) Even though the methods have been worked out, so far no interaction between tongue surface and the hard palate and teeth were implemented. This is required to make more realistic studies of articulatory gestures containing non vocalic configurations with the model. In real speech it is also generally assumed that the tongue is always in some supporting contact with molars and the hard palate, whereas the region close to the midsagittal plane has no contact with the hard palate most of the time, especially in vowels. As is planned for the next version of the model, including these interactions will probably change the model behavior towards increased stability and naturalness of simulation results.

4) For the preliminary model, the simplifying assumption was made that within a reference finite element the direction of the fibers of each muscle does not vary. Thus, within one element in its reference configuration all fibers of one muscle type are parallel (one element has usually several muscle fiber directions, e.g. Transversalis and Verticalis muscle fibers. The fiber directions are calculated for 8 integration points by evaluating the mapping between the reference configuration and the deformed configuration. Thus, the fiber directions vary according to the local deformation in the element, even if only one uniform fiber direction is specified in the reference configuration.) To obtain a more accurate representation of the muscles, in the new model the fiber directions in the reference elements will be specified at each integration point, The necessary information can be obtained from anatomical drawings.

5) In the preliminary model all muscles behave completely equal. Fiber density, maximal stress per cross sectional area in the reference, and the relation between rate of contraction and stress generation are held the same for all muscles. With increased spatial resolution by using more elements, diverting properties of tongue tissue, e.g. glants versus muscle, can be specified. As far as specific information on histochemistry of tongue muscles can be found, it will be implemented. However, without further knowledge of such variations, only the muscle cross sections can be modeled more accurately, and reasonable assumptions have to be made about the force velocity relation. If no information is available a crude estimation technique can be applied and was used already for the first model: For a long tracing of pellet data the distribution of the rate of change of relative pellet positions on the tongue surface was investigated to obtain an approximation of maximal contraction rate.

6) The muscle properties of the model, which sofar followed more available engineering models of muscle, lack physiological realism. As it is attempted to go as far as building anatomically correct biomechanical model of the tongue, it would be stopping half way if the physiology of muscles were not modeled to represent known properties of musculature, as far as these can be represented in a continuum mechanical model.

The modified muscle model will be implemented in the new model. It includes a computational mechanism of recruitment, graded force development, and proprioceptive feedback.

6   Miscellaneous

This section was added to report some new ideas and methods for the planned design of a new tongue model which will have an enlarged scope of the modeling and more accurate representation of the anatomy.

6.1   Methods for building a refined tongue model

For a more realistic tongue model that can be used in quantitative comparisons with measurements of tongue movement, the scope of modeling has to be extended to include more functional components of the articulatory system. Further, the representation of the anatomy needs to be refined compared to the initial model. One new method of combining anatomical drawings with MRI data will be used for establishing a three-dimensional "anatomical gauge" for the design of the new finite element model, and a method that proved successful in designing the geometry of the current FE model based on a geometrically simple "topological" model will be extended.

6.1.1   Integration of MRI and anatomy

The integration of MRI data and anatomical drawings in application to the anatomy of the tongue is based on an the assumption of anatomical similarity in the sense that two different anatomies are related by a smooth continuous mapping. In order to find the mapping between two anatomies (metamorphosis), several corresponding landmarks have to be labeled in both representations and a mapping function has to be found which maps the marked points of one specimen on the corresponding points (homologues) of the other. Among the possible mappings which do this, one tries to find one that fullfills a maximum smoothness criterion. For two-dimensional mappings such methods are known as thin-spline mapping, Meinguet [Mei79], and Bookstein [Boo91]. An extension which includes mapping of edge directions (edgels) at some or all landmarks (edgels) is described in Bookstein and Green [BG93]. The original thin-spline mapping method is easily extendible to three dimensions. [1]

---

[1] In fact, in the formulae (2) in [BG93], page 233, one only has to add an additional column with the z-coordinates of the points where the mapping is evaluated, the mapping function is extended by an additional term $a_z z$ in formula (4) (page 233 in [BG93]), and the rest follows easily.

In a preliminary experiment the two-dimensional mapping method was implemented to make its use clear for the purpose of integrating anatomical drawings with MRI data. It can be used for both mapping of polygon data or for deformation of pixel images, see the figures 10 and 11. A detailed set of tongue section drawings will be used as the data base for the anatomical representations, see Miyawaki [Miy74].

Part I. Matching of MRI data and anatomical drawings

Several sets of MRI scans of human heads and vocal tracts can be used in this study (Kiyoshi Honda, ATR, personal communication). They typically were assessed as 32 slices with 256×256 pixels and with a voxel volume of approximately $1 \times 1 \times 3mm^3$. The purpose of these MRI scans, among others, has been for estimating the area function of the vocal tract during vowel production. Therefore, the tongue was mostly held in constant articulation position for a vowel during the scanning time.

MRI data provide the outer shape of the tongue, palate and other parts of the articulatory apparatus. Anatomical drawings provide the intrinsic structure. In addition some hints about the intrinsic structure can be made visible in some of the MRI sections. The two aspects need to be mapped into one in order to obtain an approximate quantified 3-dimensional structure of the human tongue. The purpose of this work is to obtain a quantitative anatomical model of the tongue and related structures that will serve as gauge for adapting the initial geometry of a finite element model. The word gauge is used here to refere to a data representation in the computer that allows various views and overlapping its view with that of the finite element model (described below) to fit the geometry of finite element model to the anatomy. To obtain the gauge, the following steps will be undertaken:

(a) Computer scans of Miyawaki's tongue sketches will be reproduced as handdrawn polygons using simple Matlab procedures (partially already implemented). The polygons are labeled so that they include classification.

(b) The various muscle regions and the projected fiber directions of the muscles are marked. Miyawaki's tongue sketches consist of three directions of cutting two tongues. By translating, rotating and deforming the two-dimensional figures, they are approximately brought to a match for three-dimensional display. This part of the work will result in a geometric model of the intrinsic three-dimensional structure of a human tongue in some state of deformation.

(c) Based on MRI image display, tongue surfaces, and hard palate shapes are outlined (hand drawn) and stored as polygnomial data. It is noted here that automatic procedures may become available for part of the work. However, in the case of the anatomical drawings the results depend on proper interpretation of the drawings and no automatic procedures (e.g. edge detection) can be used.

(d) In both the polygon data from MRI and the polgon data from drawings, several clearly corresponding anatomical landmarks are labeled and stored. (These landmarks are used
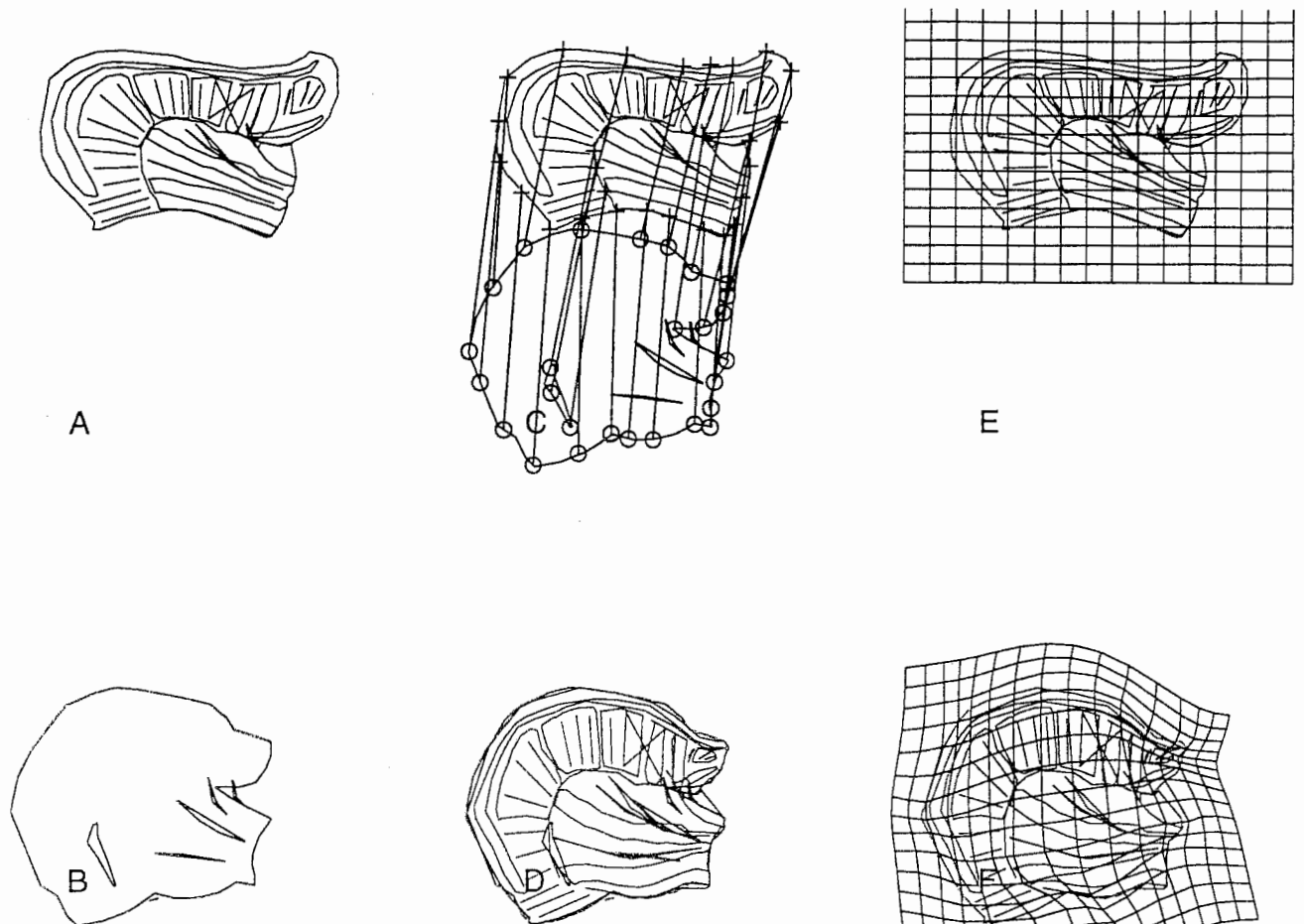
Figure 10: *Demonstration of the mapping with two-dimensional thin-plate splines.* **Hand-drawn polygons were used in this example to show the concept..** *(A) A typical sketch of a tongue section as in Miyawaki's tongue drawings. (B) Outline of tongue as could be obtained from MRI. (C) Specification of corresponding landmarks (here 27 landmark pairs). (D) Figure A mapped onto figure B with thin-plate spline. (E) – (F) Demonstration of the mapping by using a grid. This technique can be extended straight forward to three dimensions.*
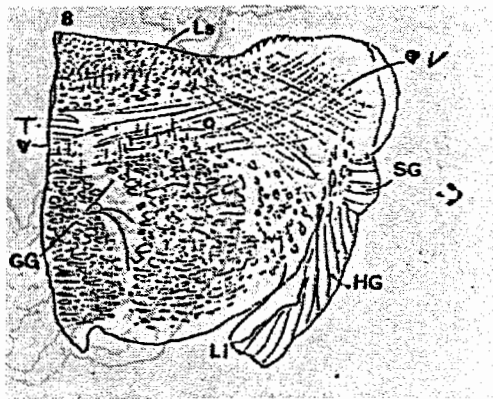
A: Drawing
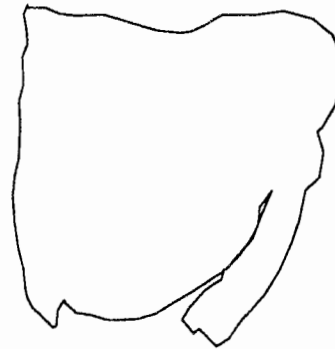
B: Outline
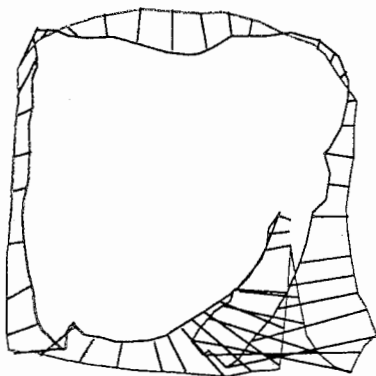
C: Homologue point pairs
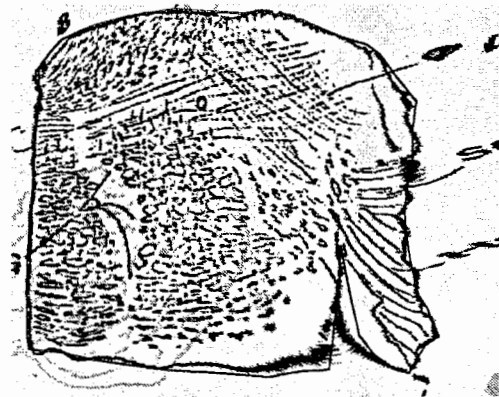
D: Mapped image

Figure 11: *Deformation of anatomical drawings and mapping onto shape targets. Upper left: Scan of a drawing by Miyawaki of a coronal section of one half of a human tongue. Upper right: outline of the drawing. Lower left: Landmarks and their homologues on an assumed (arbitrarily sketched) outline of a similar section. Lower right: The mapped and deformed drawing with the target outline*
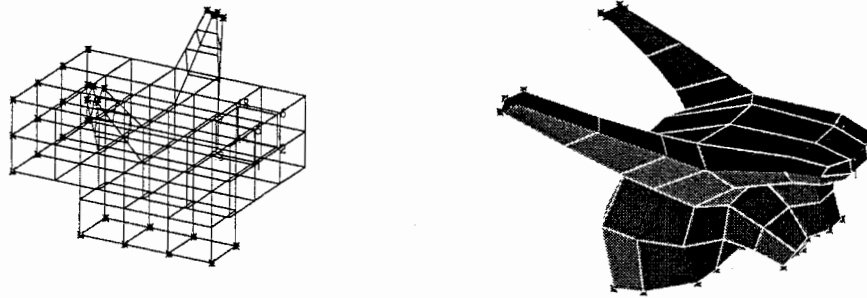
Figure 12: *On the left the topologically equivalent model is shown. By means of a three-variate Bézièr-polynomial mapping, this is mapped onto the figure to the right, which shows the initial geometry of the preliminary tongue model.*

to calibrate the mapping with thin-plate splines in three dimensions. The mapping function interpolates exactly the landmarks and fullfills a minimum bending energy constraint (minimizing the total integral of the second metric tensor of the mapping over the manifold).

(e) The resulting mapping is checked for reasonability. For example, structures inside the tongue should be mapped inside, etc. If needed, additional homologue landmark pairs have to be specified to make the mapping more accurate. (There is no principle limit on the number of landmark pairs, but smoother mappings are usually obtained with fewer mapping landmarks.)

Part II. Adaptation of a new FE model to the anatomical model

The adaptation of a finite element description to the anatomical data happens in one or several stages of a mapping process from a simple topologically equivalent model. This model (sometimes simply called the topological model) has the same connectivity as the final model but is of maximal simplicity in its geometrical specification. The initial geometry of the finite element model and the topological equivalent are related by a one-to-one mapping that has to be found.

A technique with Bézièr mappings was used in the design of the preliminary tongue model (see figure 12). Bézièr control points were moved with a mouse to specify the behavior of a free-form deformation mapping which determines the model geometry. This method will be modified for the new model design, in that the Bézièr mapping is replaced by a three-dimensional thin-spline mapping.[2] In the anatomical "gauge" as described above, several

---

[2]The expression thin-spline mapping is actually only used for the two-dimensional mapping; it is used

landmarks are paired with points in the topological model and the topological model is mapped onto the gauge.

The specification of the topological model is done in part manually, or by adhoc grid generating algorithms that need only work for the most simple geometric volumes, namely for bricks prisms and tetrahedra. The new model will consist of a hexahedral, tetrahedral, and prismatic isoparametric elements, whereas in the current model only hexahedral (8-node) elements have been used.

As part of the geometric design, the fiber directions for each element and muscle have to be specified. For most tongue muscles, the fiber direction can be roughly estimated given the outer shape of the muscle and anatomical knowledge. The anatomical drawings by Myawaki give three different views of the fiber directions. This will allow to specify the fiber direction with sufficient accuracy.[3]

As was done in the design of the first tongue model, the fiber directions will be specified in a coordinate system that is associated with the topological model. The actual fiber direction field is related to this by a multiplication with the Jacobian of the mapping. This makes it possible to update the fiber directions computationally if the geometry of the reference model is modified by changing the mapping.

6.2 A new muscle model

In the present tongue model a simple nonlinear model of muscle stress production is used. It is a three factor model which computes the stress by computing the product of three functions: The externally specified activation as a function of time, the strain rate to stress relation, and the strain to stress relation.

A more physiologically oriented muscle model should replace the existing one for two reasons: (a) The activation parameters that are driving it do not reflect higher level physiological function. EMG is both load and length dependent. (b) In order to combine the model with a recently built seven-muscle model of jaw and hyoid movement (Ostry and Laboissière, pers. communication) it is attempted to find a common ground for future work on an integrated jaw and tongue model and an integrated control model for these speech articulators.

The proposed muscle model is adopted from an existing model of physiological macroscopic

---

here for the three-dimensional generalization of the method.

[3]By inspection of two rather complete but in parts too distorted microtome slides of tongue muscles from two fetuses, we observed that for most tongue muscles the general fiber direction is parallel to the main length direction of the muscle. However, for the intrinsic tongue muscles transversalis and verticalis, this does not hold. If we succeed to obtain a high precision scan of a cadaver tongue (planned work in cooperation with the MRI facilities of the Ohio State University Hospitals) we might obtain additional information about instrinsic structure of the tongue.

muscle modeling which is known as the λ-model in the literature, see Flanagan, Feldman and Ostry [FFO92]. This model is one of at several models that are based on an equilibrium point hypothesis which states that the nervous system only needs to specify direction and rates of changes of equilibrium positions in multimuscle systems, see Feldman [Fel86]. The λ in the λ-model represents an α motor neuron membrane exitability shift as an externally controlled parameter. There have been some critiques addressing this model, partially from researchers who favor the equilibrium point hypothesis but explain the α-motor activity as a direct consequence rather than indirect consequence of CNS activity (Bizzi et. al. [BHMIG92], and McIntyre and Bizzi [MB93]). Also, neurophysiological findings (Rudomin [Rud90]) indicate that the assumptions of the λ-model may not be valid in some motion control. The findings point at selectable control of muscle length or muscle tension.

Nevertheless, using the λ it was possible to model arm reaching movements and recently it has been applied in a 7-muscle model for the jaw and the hyoid bone. (D. J. Ostry and R. Laboissière, personal communication).

For the implementation into the tongue model, the original λ-model needs modifications. This is partially necessary because in the case of a continuum mechanical model the kinematic state of a muscle is not represented by only two variables, namely length and shortening rate, but by many variables, namely a field of length ratios and length ratio rates.

The λ-model for muscle control in its current form consists of the following parts (see figure 13). The control input variable λ in the model reflects a variable threshold length at which the muscle motorneurons will begin to be recruited and generate muscle forces.

In the currently used implementation of the model for a seven-muscle jaw model (Ostry and Laboissière, personal communication), the kinematic state of the muscle, namely the muscle length and its speed of contraction or elongation is time delayed in order to model the delay of afferent information going to the brain stem.

The level of activation associated with the recruitment of the motorneurons and their firing depends on the difference between the muscle's actual length (l) and λ. This difference is modified in addition by a velocity dependent reflex damping mechanism which has a stabilizing function. The activation A is computed as the following function of time:

$$A(t) = max \left[l(t-d) - \lambda(t) + \mu(t)\dot{l}(t-d) \, , \, 0 \right] \tag{79}$$

where $l(t)$ and $\dot{l}(t)$ are the muscle length at time t and the lengthening velocity of the muscle, d is a reflex delay, and μ is the reflex damping. The coefficient μ is positive, and since $\dot{l}(t)$ is negative for contracting muscle, a fast contracting muscle will result in a lowering of the activation $A(t)$. This is the simplest form of implementing a reflex damping. μ is in principle time dependent since if may be centrally controlled.

The complete relation between the activation and the generated muscle force is by means of
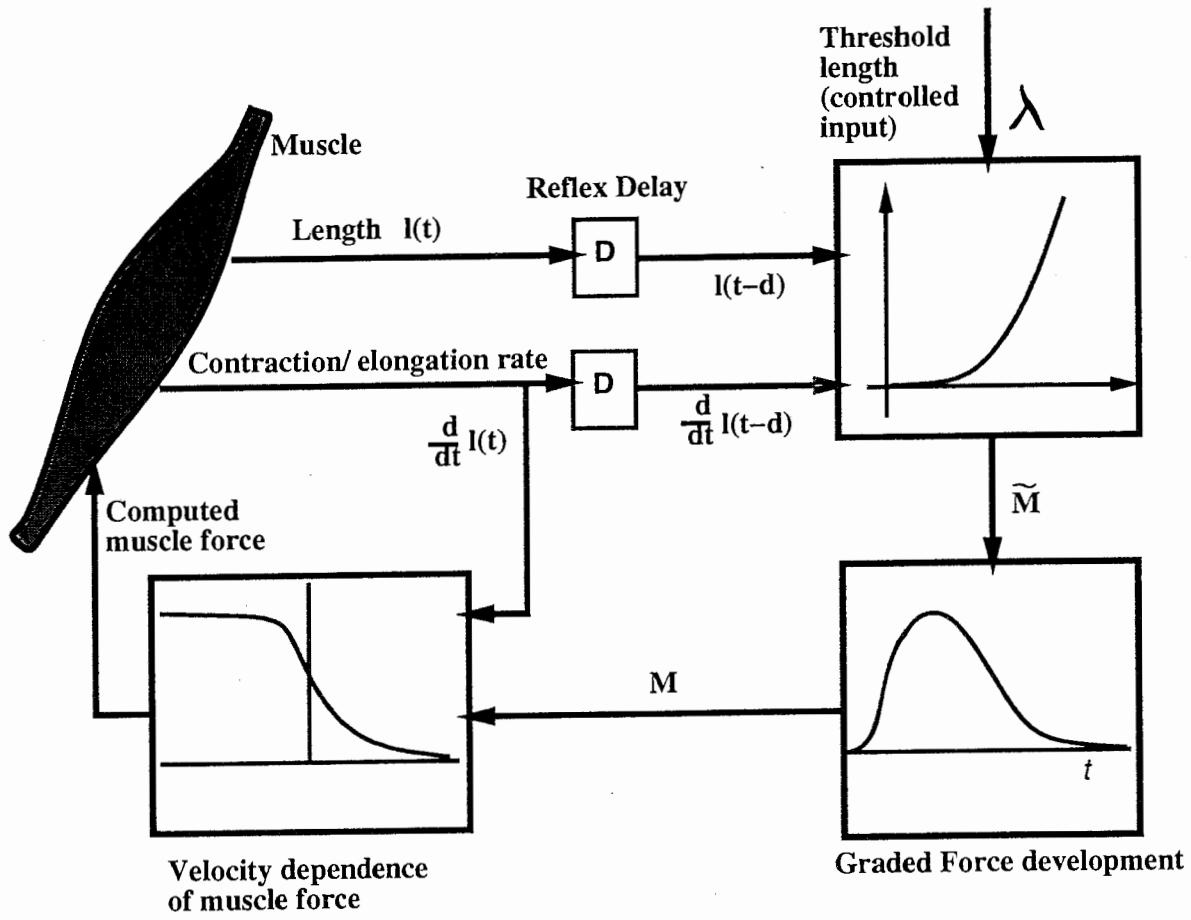
Figure 13: *The muscle control structure of the λ-model.*

a the following system.

$$A(t) = max \left[l(t - d) - \lambda(t) + \mu(t)\dot{l}(t - d) , 0 \right] \tag{80}$$

$$\tilde{M}(t) = \rho \left[\exp\left(cA(t) \right) - 1 \right] \tag{81}$$

$$\tau^2 \ddot{M}(t) + 2\tau \dot{M}(t) + M(t) = \tilde{M}(t) \tag{82}$$

$$M_*(t) = M(t) V(\dot{l}(t)) \tag{83}$$

An exponential function computes a recruitement of muscle force $\tilde{M}$ from the activation $A(t)$. The nonlinearity of this function represents the property of muscle systems where with increasing activation, an increasing number of motor neurons are recruited which represent higher fiber strengths. This is important for the model since it results in more force for increasing threshold input than a linear relation would. A graded force development in response to a sudden increase of the recruitement, as found in real musculature, is modeled by a lowpass filter, which is a second order critically damped system. The output of the lowpass filter is $M(t)$ which is obtained by integrating the shown 2nd order differential equation. The actual force output takes the force-velocity relation of the muscle into account, which is modeled by the function $V(l)$. Note that the input to the function is the instantaneous muscle contraction velocity and not the delayed one. The funciton V has a value of 1 for zero velocity, it increases with negative velocity (muscle is elongating), and decreases with positive velocity (muscle is shortening).

The proposed muscle model for the continuum mechanical case is designed partially as an extension and partially in deviation of the current λ model:

(i) For the continuous muscle tissue, the model needs to differentiate between variables which describe a muscle as a whole, and others which characterize the local muscle tissue. (ii) The model explicitly differentiates between the recruitement of motorneurons and the actual stress production in the muscle tissue. The significance of this change is that in the stress production the instantaneous length of the muscle fibers is taken into account whereas in the above λ model the stress has no dependence of the instantaneous fiber length (at time t) but only of the delayed fiber length (at time $t - d$). The complete model for active stress is described in the following system:

$$l(t) = Ave_{\Omega}[\epsilon(\boldsymbol{X}, t)] \tag{84}$$

$$\dot{l}(t) = Ave_{\Omega}[\dot{\epsilon}(\boldsymbol{X}, t)] \tag{85}$$

$$A(t) = max \left[l(t - d) - \lambda(t) + \mu(t)\dot{l}(t - d) , 0 \right] \tag{86}$$

$$\tilde{\Pi}(t) = R(A(t)) \tag{87}$$

$$\tau^2 \ddot{\Pi}(t) + 2\tau \dot{\Pi}(t) + \Pi(t) = \tilde{\Pi}(t) \tag{88}$$

$$S_*(\boldsymbol{X}, t) = \Pi(t) S_{max} V(\dot{\epsilon}(\boldsymbol{X}, t)) S(\epsilon(\boldsymbol{X}, t)) \tag{89}$$
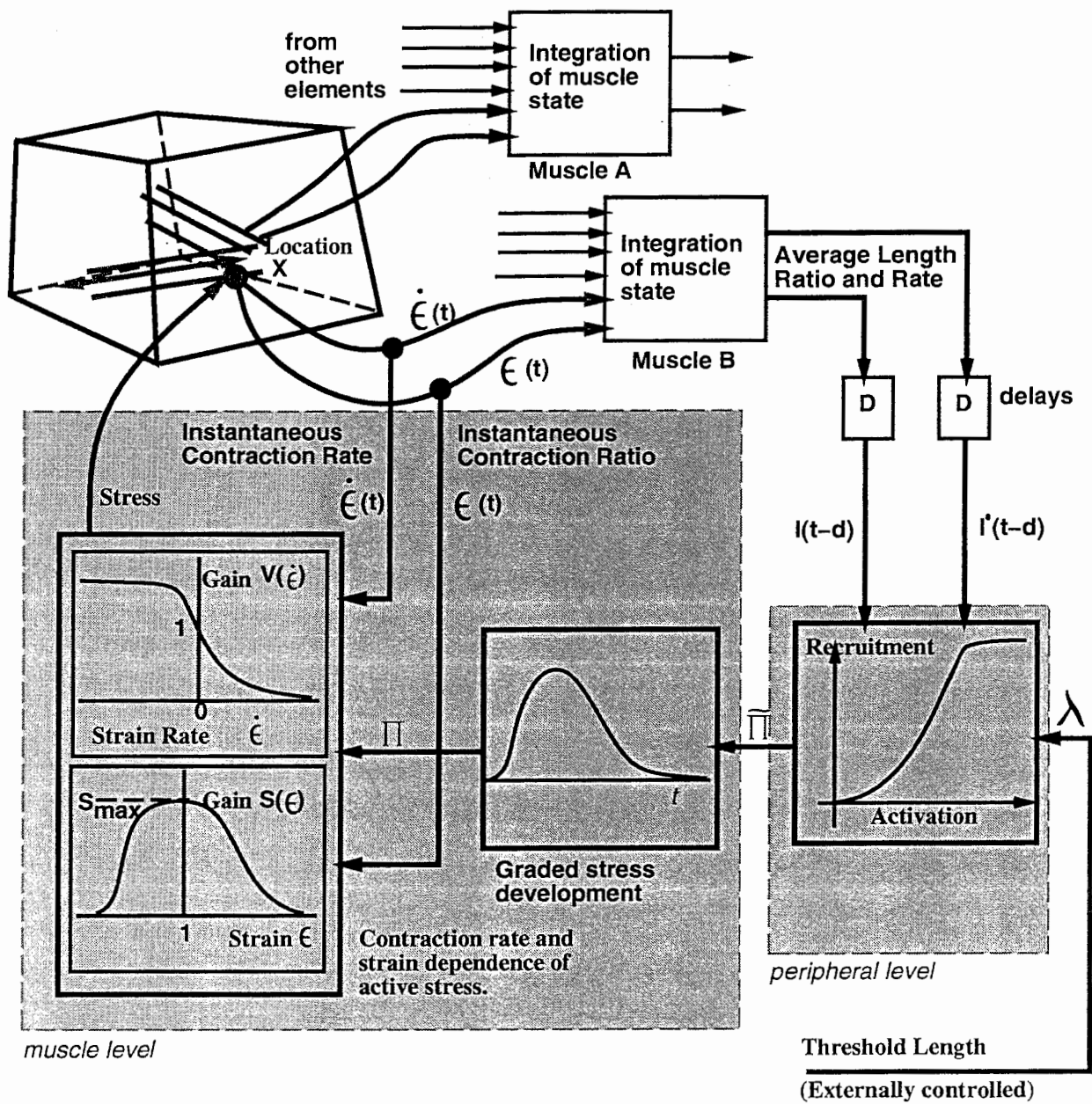
Figure 14: *Outline of the proposed physiological muscle model showing the generation of active stress in one type of muscle. Based on the state information in each element, the instantaneous state of the muscle fiber field is evaluated at the Gauss-Legendre points of the element. Local states of the muscle in all elements are assembled to a global state of the muscle, comprising the current length ratio of the muscle. Using the λ model, a recruitement level for the whole muscle is computed. This variable is filtered by a finite impulse response filter which represents what is known as graded stress development. The boxes labeled "Gain" represent the characteristics of the muscle tissue which generates stress in accordance to the recruitment and the instantaneous strain and strain rate. See text for detailed description.*

The variables $l(t)$ and $\dot{l}(t)$ are now interpreted as average normalized length of the muscle and the corresponding rate of $l(t)$. They are obtained by averaging the lengthening ratio of the muscle fibers $\epsilon(\boldsymbol{X}, t)$ and its rate $\dot{\epsilon}(\boldsymbol{X}, t)$ ($\boldsymbol{X}$ denotes location) over the domain Ω of the muscle[4] which is symbolically represented in (84) and (85).

The differential equation (88) models the recruitment dynamics which is characterised by a graded development of the recruitment of contractile elements. Contractile elements are assumed to be continously distributed in the muscle. Thus, $\Pi(t)$, the result of integrating the second order system (88) reflects the biochemical change in the muscle tissue and is understood as density of activation, corresponding to the percentage of activated contratile elements. The ouput of the box which models the recruitment of motor neurons, $\tilde{\Pi}$ and its lowpass-filtered version Π are thus not interpreted as forces.

The actual stress production at a location $\boldsymbol{X}$, $S_*(\boldsymbol{X}, t)$, in the muscle is further a function of the local kinematic state of the muscle tissue. This relationship is represented by two dimensionless gain functions $V(\dot{\epsilon})$ and $S(\epsilon)$. The constant S_{max} is a scaling factor and has units of stress (N/m^2). The function $V(\dot{\epsilon})$ has a similar meaning as in the original λ-model, namely relating the muscle stress (or force) to the rate of change of the muscle fiber length. The function $S(\epsilon(\boldsymbol{X}, t))$ has a maximum of 1 at for the extension ratio $\epsilon = 1$, corresponding to the length of the muscle fibers at which the stress production is maximal, and falls down to zero for both smaller values of ϵ (e.g. $\epsilon < 0.6$) and larger values (e.g. $\epsilon > 1.5$). This reflects the property that muscle fibers can only generate stress within a limited length range.

In this model, the relation between muscle length and muscle force is contained in the product of the recruitment function $R(A)$ and the stress gain function $S(\epsilon)$: If we take for simplicity a uniform muscle in a steady state, where one can identify the global and the local strain and strain rate variables ($l = \epsilon$ and $\dot{l} = \dot{\epsilon}$), and have small or zero muscle length changes ($\dot{l} = \dot{\epsilon} = 0$), the output stress of the model is $S_* = S_{max} S(l) \cdot R(l - \lambda)$.

The additional assumption of using a saturated recruitment function rather than an exponential (as indicated in figure reffig:musclefeedback) compatible with the λ-model and physiolocially more realistic. Veltik et al (Veltink et. al. [VCCB92]) could estimate such recruitment functions from an animal model, using a very similar three factor approach for the stress production as in formula (89).

---

[4]The averaging is obtained as the integral of the variables over the total spatial domain of the muscle, divided by the volume of the muscle. This is implemented numerically by applying the Gauss-Legendre integration method in each finite element where the muscle has fibers.

7   Acknowledgements

A   Appendix

A.1   Incompressible isoparametric element

An example of an isoparametric element is the brick element with 8 or 20 nodes. At a point of the element the deformation gradient can be written by two ways:

$$\boldsymbol{F} = \boldsymbol{I} + \sum_{K=1}^{\mathcal{N}} \boldsymbol{U}^K \, \nabla \mathcal{N}_K \quad = \quad \sum_{K=1}^{\mathcal{N}} \boldsymbol{x}^K \, \nabla \mathcal{N}_K \quad , \tag{90}$$

where $\boldsymbol{U}^K$ are the node displacements, and $\boldsymbol{x}^K = \boldsymbol{X}^K + \boldsymbol{U}^K$ are the current positions of the nodes when in the deformed configuration.

The total volume of an element with domain Ω in the reference configuration is:

$$A = \int_{\Omega} \text{Det} \boldsymbol{F} \, d\Omega \tag{91}$$

This integral is the constraint function for the element which needs to stay constant.

The deformation tensor $\boldsymbol{F}$ is in components:

$$\boldsymbol{F}_{ij} = \sum_{K=1}^{N_N} \boldsymbol{x}_i^K \mathcal{N}_{K,j} \tag{92}$$

For the integration over an element domain the node coordinates $\boldsymbol{x}_i^K$ are constants, therefore differentiation can be exchanged with integration. It can be seen that:

$$\frac{\partial \det \boldsymbol{F}}{\partial \boldsymbol{F}_{ij}} = \boldsymbol{F}_{ij}^* = \frac{1}{2} \varepsilon_{ipq} \varepsilon_{jrs} \boldsymbol{F}_{pr} \boldsymbol{F}_{qs} = \frac{1}{2} \varepsilon_{ipq} (\boldsymbol{F}_p \wedge \boldsymbol{F}_q)_j \quad , \tag{93}$$

where ε_{ipq} represents the completely assymetric 3-rd order tensor. The expression

$$F_p = \sum_{K=1}^{N_N} x_p^K \nabla \mathcal{N}_K \tag{94}$$

represents the p-th line of the deformation tensor, and F^* is the adjunct of F. We need to compute the differentials:

$$\frac{\partial \det F}{\partial U_l^M} = \frac{\partial \det F}{\partial F_{ij}} \frac{\partial F_{ij}}{\partial U_l^M} = F_{ij}^* \frac{\partial F_{ij}}{\partial U_l^M} \tag{95}$$

For the computation below, the vector triple product is written as a bracket: $[x, y, z] = (x \wedge y) \cdot z$. Step by step the following is obtained:

$$
\begin{aligned}
F_{ij}^* & \frac{\partial F_{ij}}{\partial U_l^M} \\
&= \frac{1}{2} \varepsilon_{ipq} \varepsilon_{jrs} F_{pr} F_{qs} \mathcal{N}_{M,j} \delta_{il} \\
&= \frac{1}{2} \varepsilon_{lpq} \varepsilon_{jrs} F_{pr} F_{qs} \mathcal{N}_{M,j} \\
&= \frac{1}{2} \varepsilon_{lpq} (F_p \wedge F_q)_j \mathcal{N}_{M,j} \\
&= \frac{1}{2} \varepsilon_{lpq} \left(\sum_{K=1}^{N_N} x_p^K \nabla \mathcal{N}_K \right) \wedge \left(\sum_{L=1}^{N_N} x_q^L \nabla \mathcal{N}_L \right) \cdot \nabla \mathcal{N}_M \\
&= \frac{1}{2} \sum_{K=1}^{N_N} \sum_{L=1}^{N_N} \varepsilon_{lpq} x_p^K x_q^L (\nabla \mathcal{N}_K \wedge \nabla \mathcal{N}_L) \cdot \nabla \mathcal{N}_M \\
&= \frac{1}{2} \sum_{K=1}^{N_N} \sum_{L=1}^{N_N} (x^K \wedge x^L)_l [\nabla \mathcal{N}_K, \nabla \mathcal{N}_L, \nabla \mathcal{N}_M] \\
&= \sum_{K=1}^{N_N} \sum_{L=K+1}^{N_N} (x^K \wedge x^L)_l [\nabla \mathcal{N}_K, \nabla \mathcal{N}_L, \nabla \mathcal{N}_M]
\end{aligned}
$$

To obtain the differentials of the constraint function with respect to node displacements, one has to intergrate this expression over the domain of an element. This results in:

$$\int_\Omega \frac{\partial \mathrm{Det} F}{\partial U^M} \, d\Omega = \sum_{K=1}^{N_N} \sum_{L=K+1}^{N_N} \left(x^K \wedge x^L \right) \kappa_{KLM} \tag{96}$$

Where the coefficients κ_{KLM} which are defined as:

$$\kappa_{MKL} = \int_\Omega \nabla \mathcal{N}_M \left(\nabla \mathcal{N}_K \wedge \nabla \mathcal{N}_L \right) d\Omega \quad \text{(invariant u. cycl. permut. of indices)}, \qquad (97)$$

are independent of the node displacements, and need to be computed only once. For the 8 node brick element, the κ_{KLM} coefficients are all multiples of $\frac{1}{12}$. Here are two tables with coefficients different from zero. The first part has positive coefficients, and the second part has negative coefficients:

$$\kappa_{KLM} = \frac{1}{12} \quad \text{for} \quad \left\{ \begin{array}{rcccccccccccc} K & = & 1 & 1 & 1 & 2 & 2 & 3 & 3 & 4 & 5 & 5 & 5 & 6 \\ L & = & 2 & 2 & 5 & 3 & 3 & 4 & 4 & 5 & 6 & 6 & 7 & 7 \\ M & = & 5 & 6 & 8 & 6 & 7 & 7 & 8 & 8 & 7 & 8 & 8 & 8 \end{array} \right\} \qquad (98)$$

and

$$\kappa_{KLM} = -\frac{1}{12} \quad \text{for} \quad \left\{ \begin{array}{rcccccccccccc} K & = & 1 & 1 & 1 & 1 & 1 & 1 & 2 & 2 & 2 & 3 & 3 & 4 \\ L & = & 2 & 2 & 3 & 4 & 4 & 5 & 3 & 5 & 6 & 6 & 7 & 7 \\ M & = & 3 & 4 & 4 & 5 & 8 & 6 & 4 & 6 & 7 & 7 & 8 & 8 \end{array} \right\} \qquad (99)$$

The second derivative can be evaluated, starting at integrals of the above differential quotients, as follows:

$$\frac{\partial^2 \int_\Omega \det \boldsymbol{F} \, d\Omega}{\partial U_j^N \, \partial U_l^M}$$

$$= \frac{1}{2} \sum_{K=1}^{N_N} \sum_{L=1}^{N_N} \frac{\partial}{\partial U_j^N} \left(\boldsymbol{x}^K \wedge \boldsymbol{x}^L \right)_l \kappa_{KLM}$$

$$= \frac{1}{2} \sum_{K=1}^{N_N} \sum_{L=1}^{N_N} \frac{\partial}{\partial U_j^N} \varepsilon_{lrs} \boldsymbol{x}_r^K \boldsymbol{x}_s^L \kappa_{KLM}$$

$$= \frac{1}{2} \sum_{K=1}^{N_N} \sum_{L=1}^{N_N} \varepsilon_{lrs} \delta_{jr} \delta_{NK} \boldsymbol{x}_s^L \kappa_{KLM} + \frac{1}{2} \sum_{K=1}^{N_N} \sum_{L=1}^{N_N} \varepsilon_{lrs} \delta_{js} \delta_{NL} \boldsymbol{x}_r^K \kappa_{KLM}$$

$$= \frac{1}{2} \sum_{L=1}^{N_N} \varepsilon_{ljs} \boldsymbol{x}_s^L \kappa_{NLM} + \frac{1}{2} \sum_{K=1}^{N_N} \varepsilon_{lrj} \boldsymbol{x}_r^K \kappa_{KNM}$$

$$= \frac{1}{2} \sum_{K=1}^{N_N} \varepsilon_{ljs} \boldsymbol{x}_s^K \kappa_{NKM} + \frac{1}{2} \sum_{K=1}^{N_N} \varepsilon_{lrj} \boldsymbol{x}_r^K \kappa_{KNM}$$

$$= \sum_{K=1}^{N_N} \frac{1}{2} \left(\varepsilon_{ljs} \boldsymbol{x}_s^K \kappa_{NKM} + \varepsilon_{lrj} \boldsymbol{x}_r^K \kappa_{KNM} \right)$$

$$= \sum_{K=1}^{N_N} \frac{1}{2} \left(\varepsilon_{jls} \boldsymbol{x}_s^K \, \kappa_{KNM} \; + \; \varepsilon_{lrj} \boldsymbol{x}_r^K \, \kappa_{KNM} \right)$$

$$= \sum_{K=1}^{N_N} \frac{1}{2} \left(\varepsilon_{jls} \boldsymbol{x}_s^K \, \kappa_{KNM} \; + \; \varepsilon_{jlr} \boldsymbol{x}_r^K \, \kappa_{KNM} \right) \;\; = \sum_{K=1}^{N_N} \varepsilon_{jls} \boldsymbol{x}_s^K \, \kappa_{KNM} \;\; =: \sum_{K=1}^{N_N} W_{jl}^K \, \kappa_{KNM}$$

In the last line a matrix W_{jl}^K is used. It is defined as follows:

$$W_{jl}^K = \mathbf{W} \left(\boldsymbol{x}^K \right)_{jl} = \begin{pmatrix} 0 & x_3^K & -x_2^K \\ -x_3^K & 0 & x_1^K \\ x_2^K & -x_1^K & 0 \end{pmatrix} \tag{100}$$

So we obtain for the second derivative:

$$\boldsymbol{H}_{jl}^{NM} = \sum_{K=1}^{N_N} \begin{pmatrix} 0 & x_3^K & -x_2^K \\ -x_3^K & 0 & x_1^K \\ x_2^K & -x_1^K & 0 \end{pmatrix}_{jl} \kappa_{KNM} \quad , \tag{101}$$

References

[BAH+92]   P. H. M. Bovendeerd, T. Arts, J. M. Huyghe, D. H. van Campen, and R. S. Reneman. Dependence of local left ventricular wall mechanics of myocardial fiber orientation: A model study. *J. Biomechanics*, 25(10):1129–1140, 1992.

[BG93]   Fred J. Bookstein and William D.K. Green. A feature space for edgels in images with landmarks. *Jounal of Mathematical Imaging and Vision*, 3:231–261, 1993.

[BHMIG92] E. Bizzi, N. Hogan, F. A. Mussa-Ivaldi, and S. Giszter. Does the nervous system use equilibrium-point control to guide singe and multiple joint movements? *Behavioral and Brain Sciences*, 15(4):603–613, December 1992.

[Boo91]   F. L. Bookstein. *Morphometric Tools for Landmark Data*. Cambridge University Press, New York, 1991.

[Fel86]   A. G. Feldman. Once more on the equilibrium-point hypothesis (λ model) for motor control. *Journal of Motor Behavior*, 18:17–54, 1986.

[FFO92]   J. Randall Flanagan, Anatol G. Feldman, and David J. Ostry. Equilibrium trajectories underlying rapid target-directed arm movements. In G.E. stelmach and J. Requin, editors, *Totorials in Motor Behavior*, pages 661–675. Elsevier Science Publishers B. V., 1992.

[Fuj90]   Osamu Fujimura. Methods and goals of speech production research. *Language and Speech*, 33(3):195–258, 1990.

[Fun81]   Yuan-Cheng Fung. *Biomechanics, Mechanical Properties of Living Tissues*. Springer Verlag, New York, 1981.

[Fun90]   Yuan-Cheng Fung. *Biomechanics, Motion, Flow, Stress, and Growth*. Springer Verlag, New York, 1990.

[Gur81]   Morton E. Gurtin. *An Introduction to Continuum Mechanics*. Academic Press, New York, 1981.

[GZ60]   A.E. Green and W. Zerna. *Theoretical Elasticity*. Clarendon Press, Oxford, 1960.

[HLY+88]   A. Horowitz, Y. Lanir, F.C.P. Yin, I. Sheinman, R.P. Strumpf, M. Perl, and S. Sideman. Structural three-dimensional constitutive law for the passive myocardium. *ASME Journal of Biomechanical Engineering*, 110:200–207, 1988.

[HS86]   Kiyoshi Hashimoto and Shinsuke Suga. Estimation of the muscular tensions of the human tongue by using a three-dimensional model of the tongue. *J. Acoust. Soc. Japan*, (E) 7,1:39–46, 1986.

[HSL88a] A. Horowitz, I. Sheinman, and Y. Lanir. Nonlinear incompressible finite element for simulating loading of cardiac tissue – part ii: Three dimensional formulations for thick ventricular wall segments. *J. Biomechanical Engineering*, 110:62–68, 1988.

[HSL+88b] A. Horowitz, I. Sheinman, Y. Lanir, M. Perl, and S. Sideman. Nonlinear incompressible finite element for simulating loading of cardiac tissue – part i: Two dimensional formulation for thin myocardial strips. *J. Biomechanical Engineering*, 110:57–61, 1988.

[HY89] J. D. Humphrey and F. C. P. Yin. Biaxial mechanical properties of passive myocardium. In A. L. Yettram, editor, *Material properties and stress analysis in biomechanics*, pages 25–43. Manchester University Press, 1989.

[KFH85] Y. Kakita, O. Fujimura, and K. Honda. Computation of mapping from muscular contraction patterns to formant patterns in vowel space. In Victoria A. Fromkin, editor, *Phonetic Linguistics*. Academic Press, 1985. Essays in Honor of Peter Ladefoged.

[KMFM76] S. Kiritani, K. Miyawaki, O. Fujimura, and J.E. Miller. A computational model of the tongue. *Ann. Bul. Research Institute of Logopedics and Phoniatrics, Univ. Tokyo*, 10:243–251, 1976.

[KNNH92] Masanobu Kumada, Mamoru Niitsu, Seiji Niimi, and Hajime Hirose. A study of the inner structure of the tongue in the production of the 5 japanese vowels by tagging snapshot mri. *Ann. Bul. Research Institute of Logopedics and Phoniatrics, Univ. Tokyo*, 26:1–11, 1992.

[MB93] J. McIntyre and E. Bizzi. Servo hypotheses for the biological control of movement. *Journal of Motor Behavior*, 25(3):193–202, September 1993.

[Mei79] J. Meinguet. Multivariate interpolation at arbitrary points made simple. *Z. Angew. Math. Phys.*, 30:292–304, 1979.

[Miy74] Kuniko Miyawaki. A study of the musculature of the human tongue. *Ann. Bul. Research Institute of Logopedics and Phoniatrics, Univ. Tokyo*, 8:23–50, 1974.

[NAF87] R.D. Nadler, J.H. Abbs, and O. Fujimura. Speech movement research using the new x-ray microbeam system. In *Proceedins of the eleventh Congress of Phonetic Sciences*, volume 1, pages 221–224, Tallinn, Estonia, 1987.

[NKNI92] Mamoru Niitsu, Masanobu Kumada, Seiji Niimi, and Yuji Itai. Tongue movement during phonation: A rapid quantitative visualization using tagging snapshot mr imaging. *Ann. Bul. Research Institute of Logopedics and Phoniatrics, Univ. Tokyo*, 26:149–155, 1992.

[Ode72]   J.T. Oden. *Finite Elements of Nonlinear Continua.* McGraw-Hill, 1972.

[Ogd84]   R. W. Ogden. *Non-Linear Elastic Deformations.* John Wiley & Sons, New York, 1984.

[PCS+92]   Joseph S. Perkell, Marc H. Cohen, Mario A. Svirsky, Melanie L. Matthies, Iñaki Garabieta, and Michel T. T. Jackson. Electromagnetic midsagittal articulometer system for transducing speech articulatory movements. *J. Acoust. Soc. Am.*, 92:3078–3096, 1992.

[Per74]   Joe S. Perkell. *A physiologically-oriented model of tongue activity in speech production.* PhD thesis, MIT, 1974.

[Pin87]   J. G. Pinto. A constitutive description of contracting papillary muscle and its implications to the dynamics of the intact heart. *J. Biomechanical Engineering*, 109:181–191, 1987.

[Rud90]   P. Rudomin. Presynaptic inhibition of muscle spindle and tendon organ afferents in the mammalian spinal cord. *Trends in Neuroscience*, 13(12):499–505, 1990.

[SK89]   Kathleen K. Smith and William M. Kier. Trunks, tongues, and tentacles: Moving with skeletons of muscle. *American Scientist*, 77:29–35, 1989.

[Sto90]   M. Stone. A three-dimensional model of tongue movement based on ultrasound and x-ray micro-beam data. *J. Acoust. Soc. Am.*, 87(5), 1990.

[Tru91]   Clifford A. Truesdell. *A First Course in Rational Continuum Mechanics*, volume 1. Academic Press, 1991.

[VCCB92]   Peter H. Veltink, Howard J. Chizeck, Patrick E. Crago, and Ahmed El Bialy. Nonlinear joint angle control for artificially stimulated muscle. *IEEE Transactions on Biomedical Engineering*, 39(4), April 1992.

[WR89]   Kenneth L. Watkin and Jonathan M. Rubin. Pseudo-three-dimensional reconstruction of ultrasonic images of the tongue. *J. Acoust. Soc. Am.*, 85(1):496–499, 1989.

[Yin85]   Frank C. P. Yin. Applications of the finite element method to ventricular mechanics. *Critical Reviews in Biomedical Engineering*, 12(4):311–342, 1985.

[Zaj89]   Felix E. Zajac. Muscle and tendon: Properties, models, scaling, and application to biomechanics and motor control. *Critical Reviews in Biomedical Engineering*, 17(4):359–411, 1989.

[Zie71]   O. C. Zienkiewicz. *The Finite Element Method in Engineering Science.* McGraw-Hill, London, second edition, 1971.
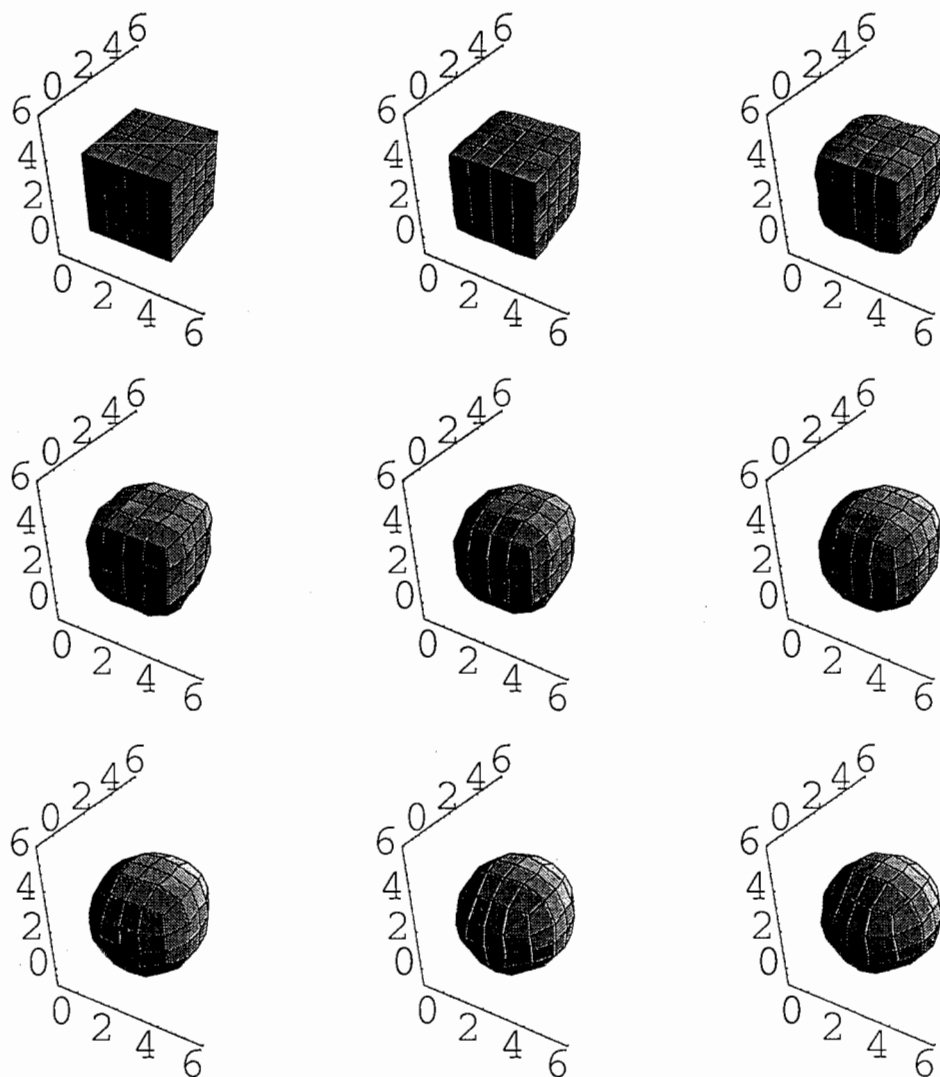
Figure 10: Example of drop forming computed with the C++ finite element code. Only surface tension is acting. The drop consists of 64 elements and is free. The stress computation used viscous stress only. The coefficients are about 1000 times greater than for water because a large volume was used. The computational results were written to file and later displayed using the program Mathematica.

FIGURES
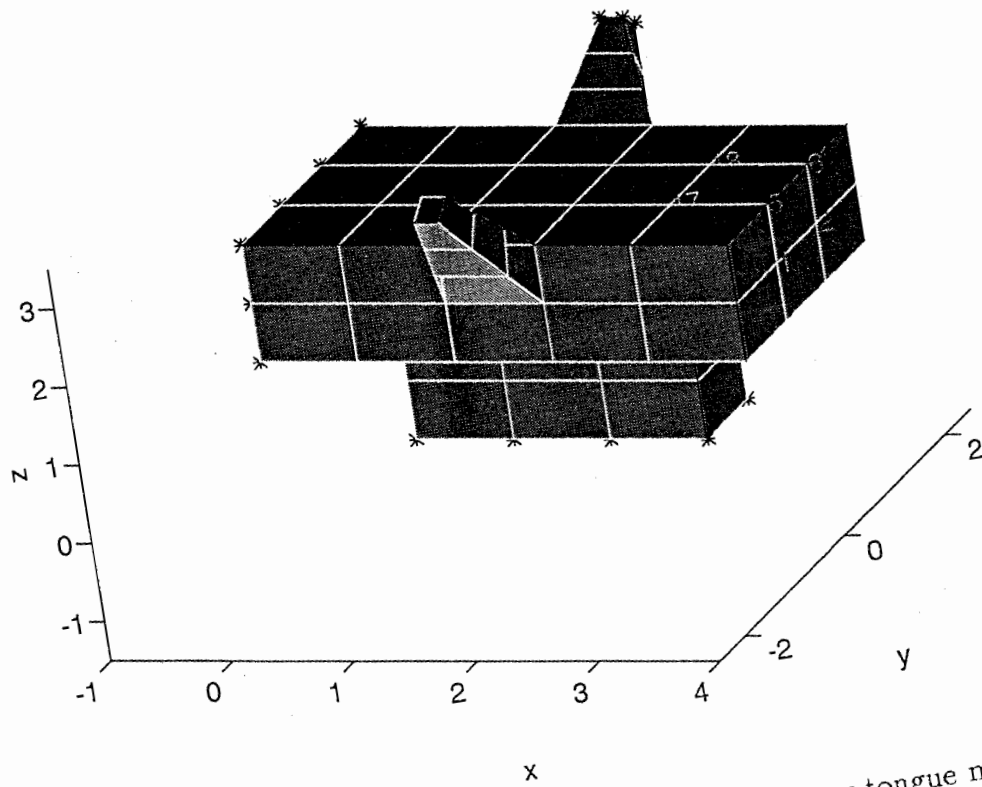
Figure 11: Topological finite element mesh for the preliminary tongue model. Fixed nodes at the Genioglossus, Styloglossus and base of the tongue (left) are marked with stars. The nodenumbers of one of the finite elements are shown.
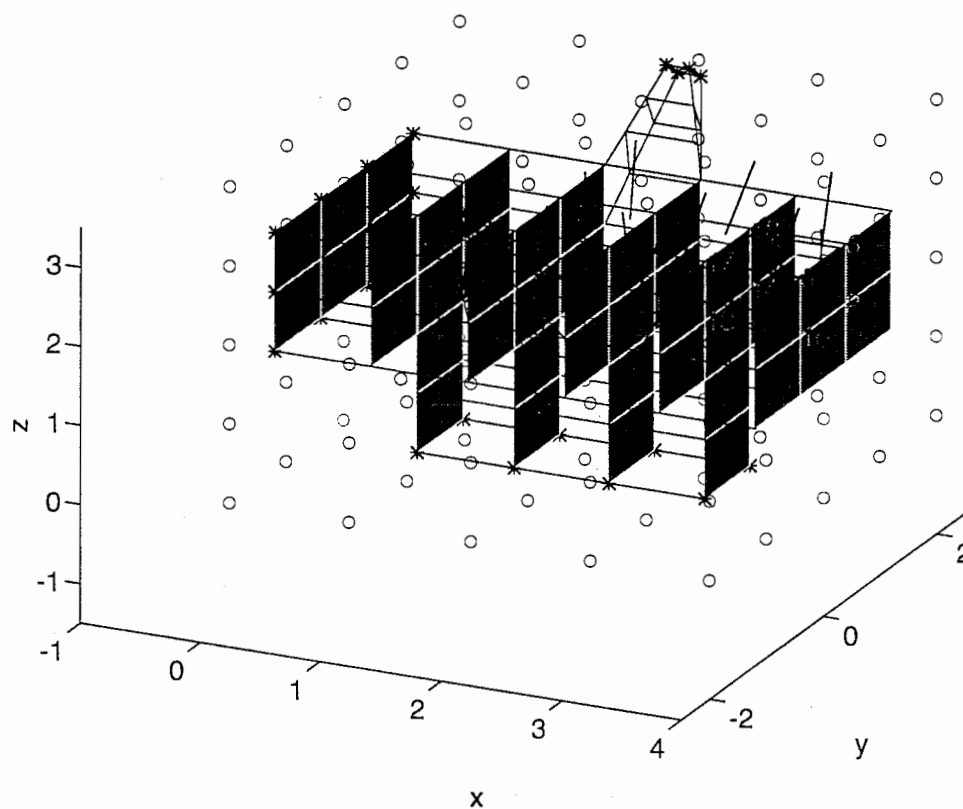
Figure 12: Topological finite element mesh for the preliminary tongue model. The six control planes are shown. All Bézièr controlpoints are in their initial position (many circles). The muscle fiber direction of the Verticalis muscle are displayed in the topological reference model as lines in some of the upper elements.
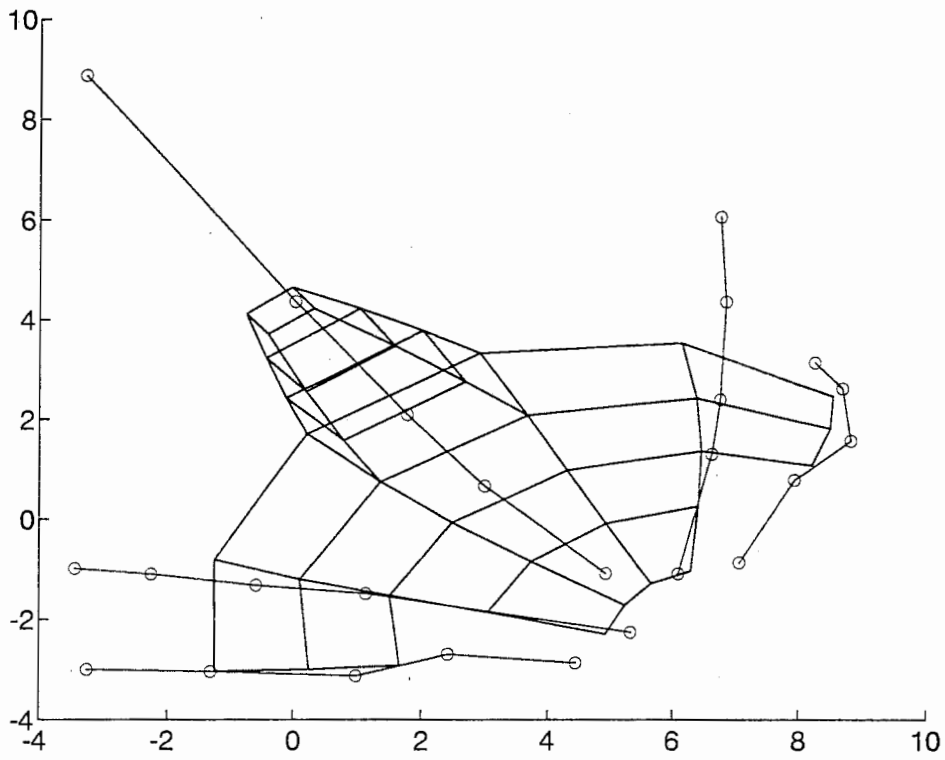
Figure 13: Modeling preliminary tongue in a Bezier solid. All Bezier points are lined up and shown as circles.
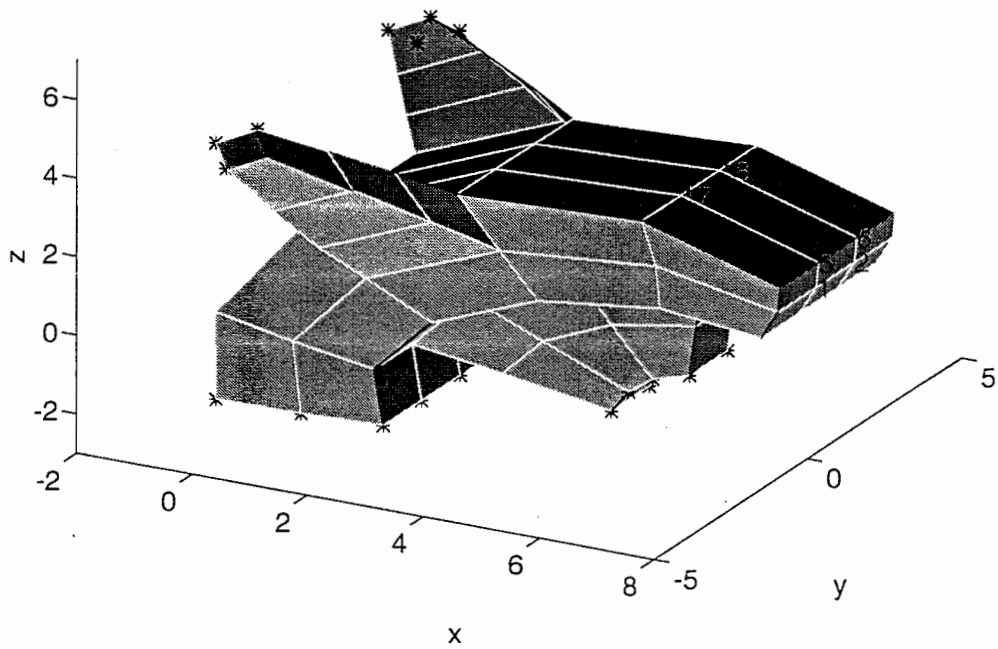
Figure 14: Modeling preliminary tongue in a Bezier solid. The corresponding three-dimensional view obtained from moving Bezier control vertices in the x-z plain.
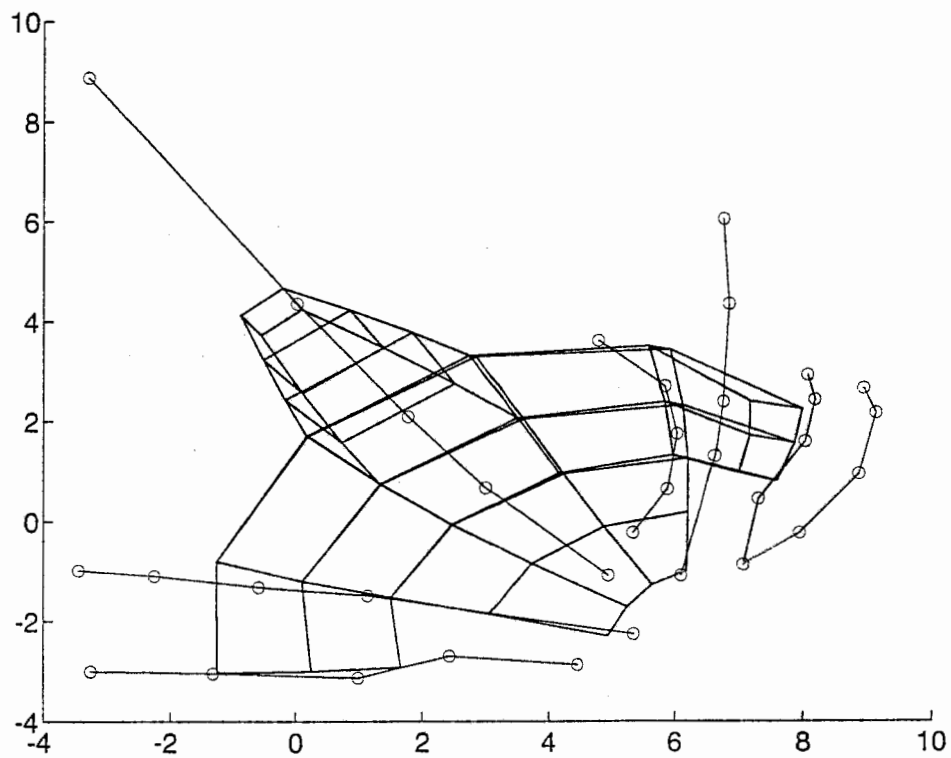
Figure 15: Modeling the tip of the tongue using the Bezier solid method. The Bezier points in three planes are moved in different ways to form the rounding at the tip of the tongue.

B FIGURES
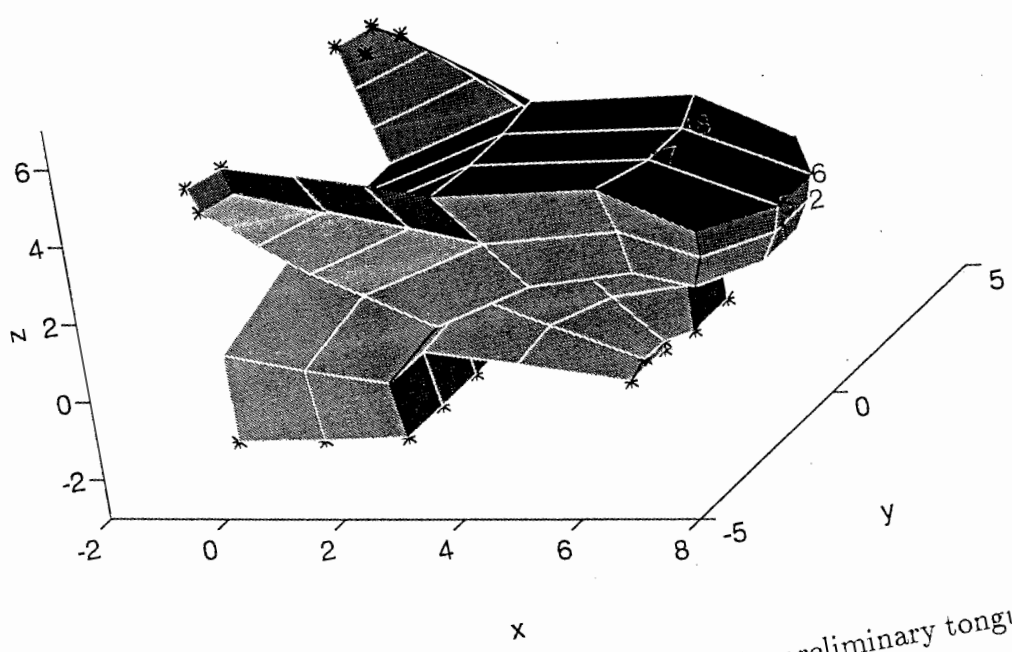
Figure 16: Modeling the tongue tip of the preliminary tongue.
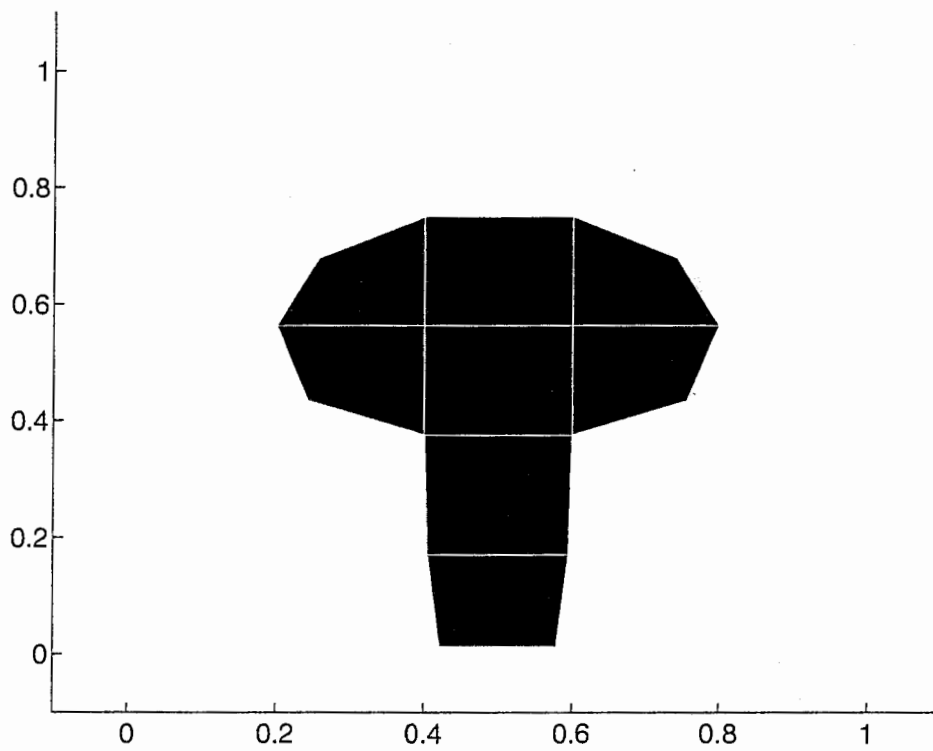
Figure 17: Modification of the rst coordinates of one of the coronal tongue planes.
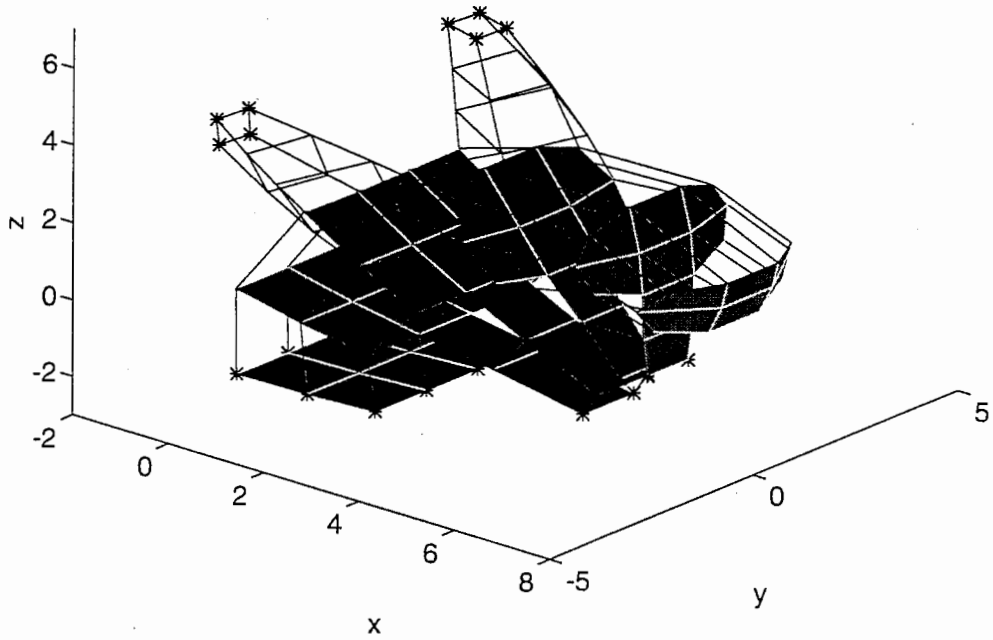
Figure 18: Modeling the round shape of the tongue by modification of individual planes. The first four planes were changed, see previous figure.
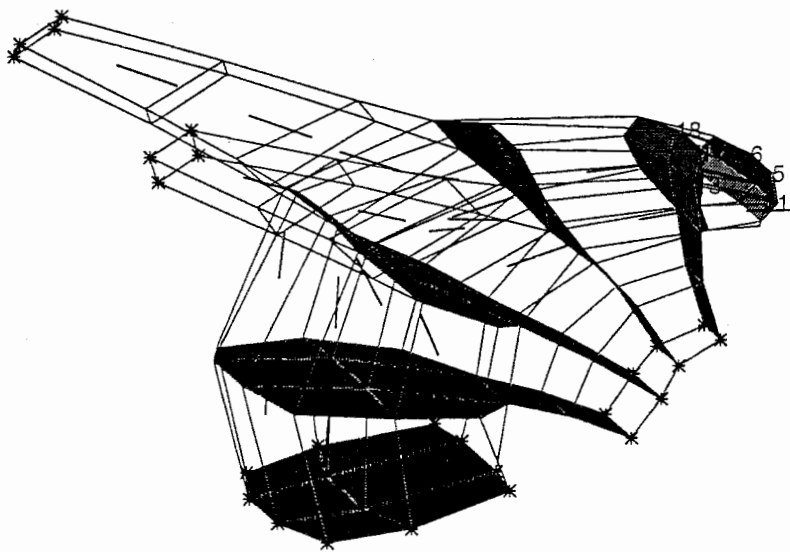
Figure 19: Muscle fiber directions for the styloglossus muscle. The direction of the muscle fibers is in this experimental tongue model assumed to be constant in each element, and is shown at the center of gravity of the elements as short line segments. Fibers are only in the lateral elements.
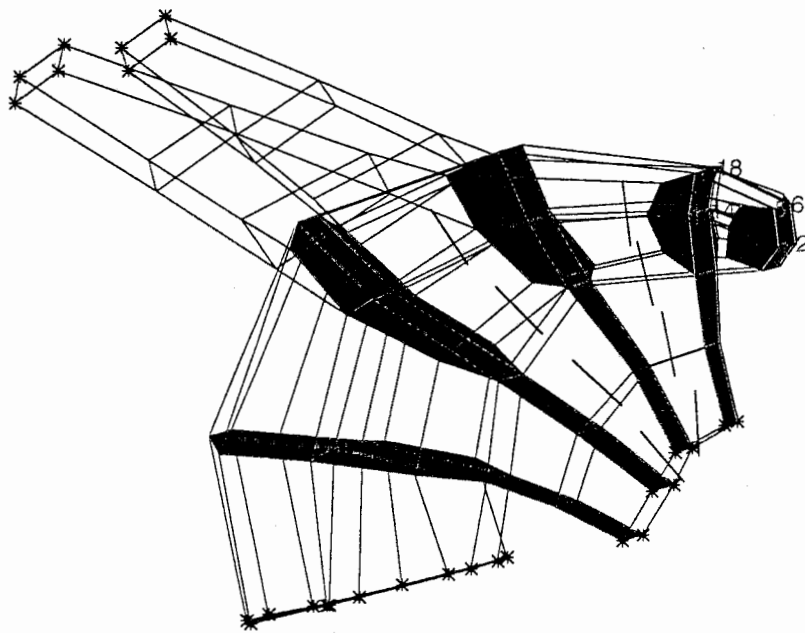
Figure 20: Fiber directions of Genioglossus Anterior, only the central elements.
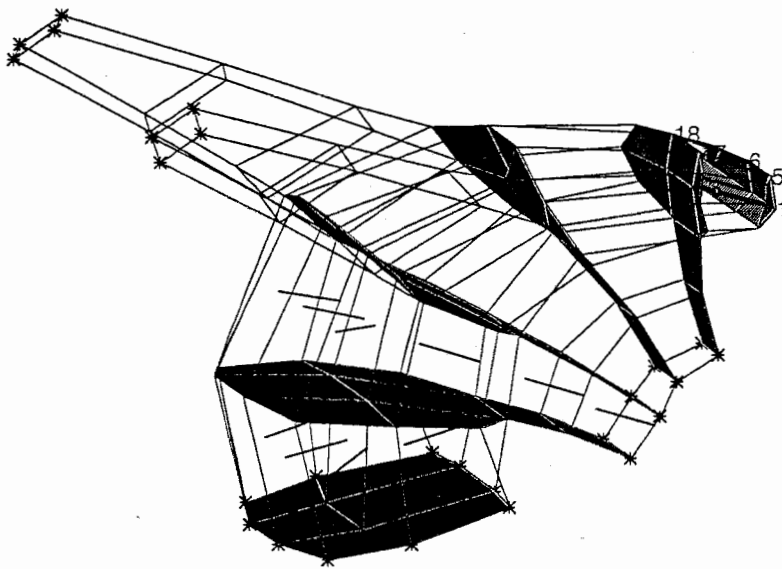
Figure 21: Fiber directions of Genioglossus Posterior.
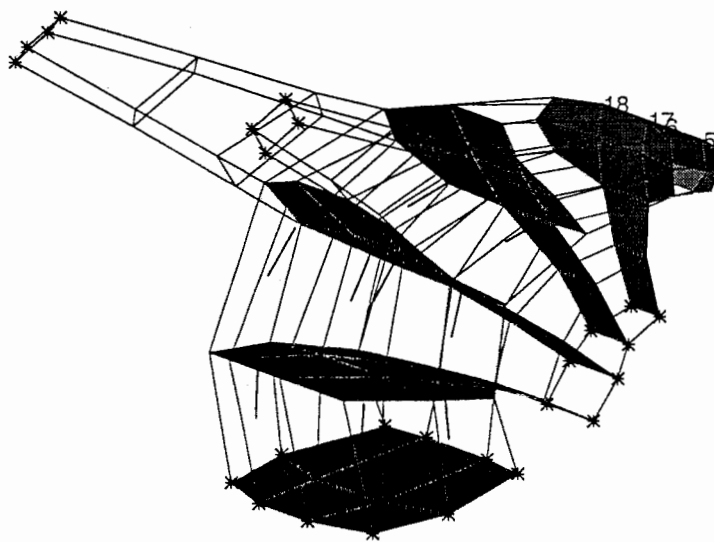
Figure 22: Fiber directions of the Hyoglossus muscle.
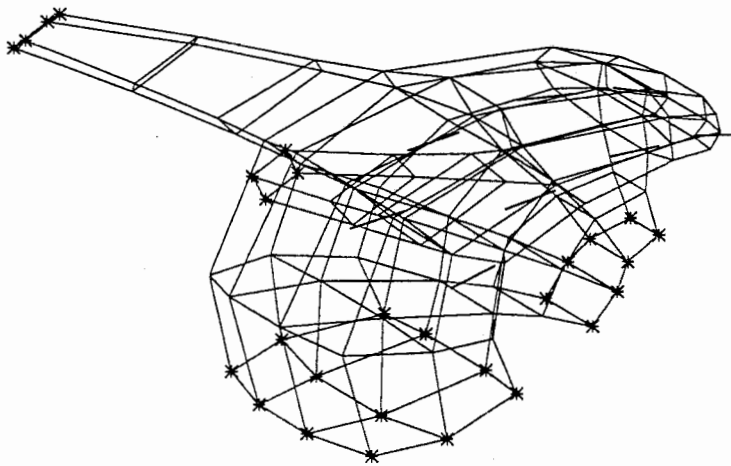
Figure 23: Fiber directions of fibers of the Longitudinalis Inferioris muscle. This muscle has most fibers under the tongue laterally and is not connected with the hyoid bone.
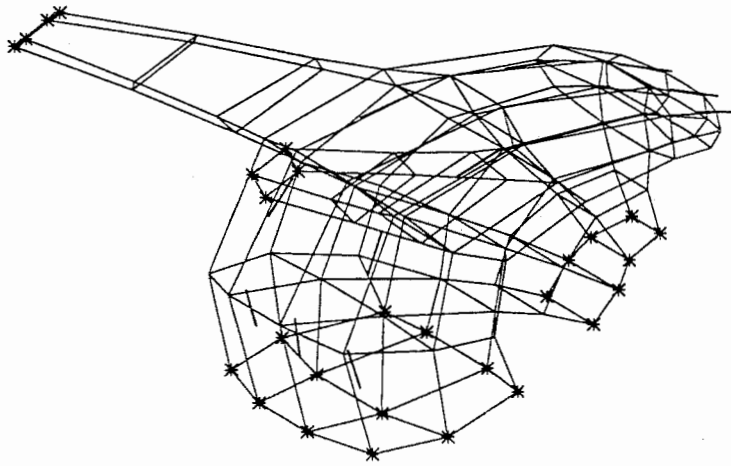
Figure 24: Fiber directions of the fibers of the Longitudinalis Superioris muscle. This muscle has most fibers on the back of the tongue.
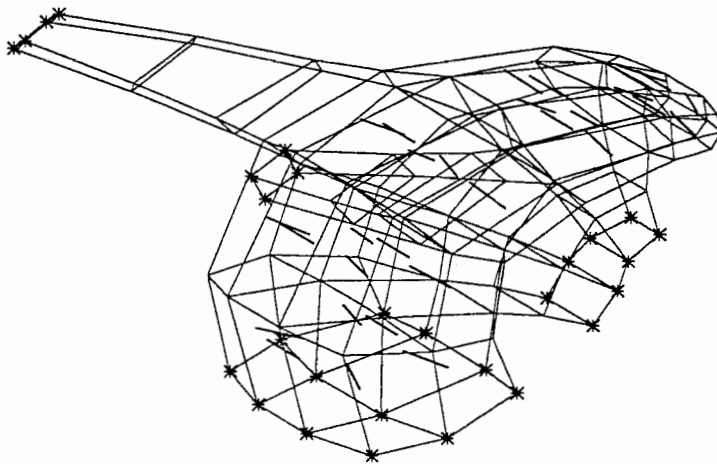
Figure 25: Fiber directions of Transversalis muscle. This muscle has most fibers on the back
of the tongue. In some individuals the upper layer may form an independently controllable
muscle structure.
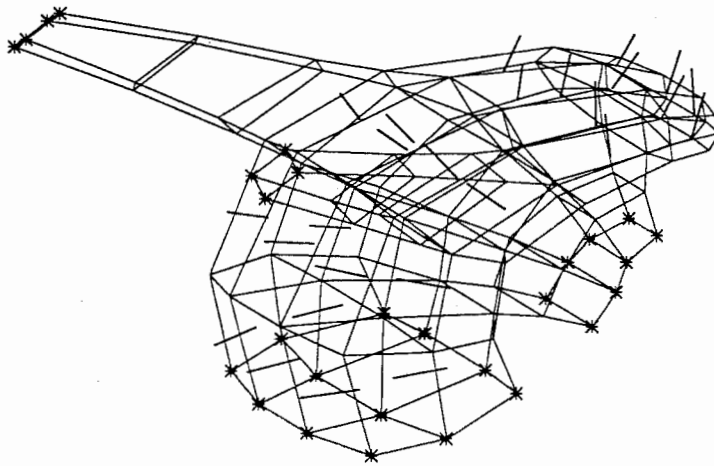
Figure 26: Fiber directions of Verticalis muscle. This muscle has most fibers both sides of the tongue. Transversalis and Verticalis are highly interdigitated and probably cocontract mostly. If they contract both the tongue body extends due to incompressibility, which could also be demonstrated with the simple model.
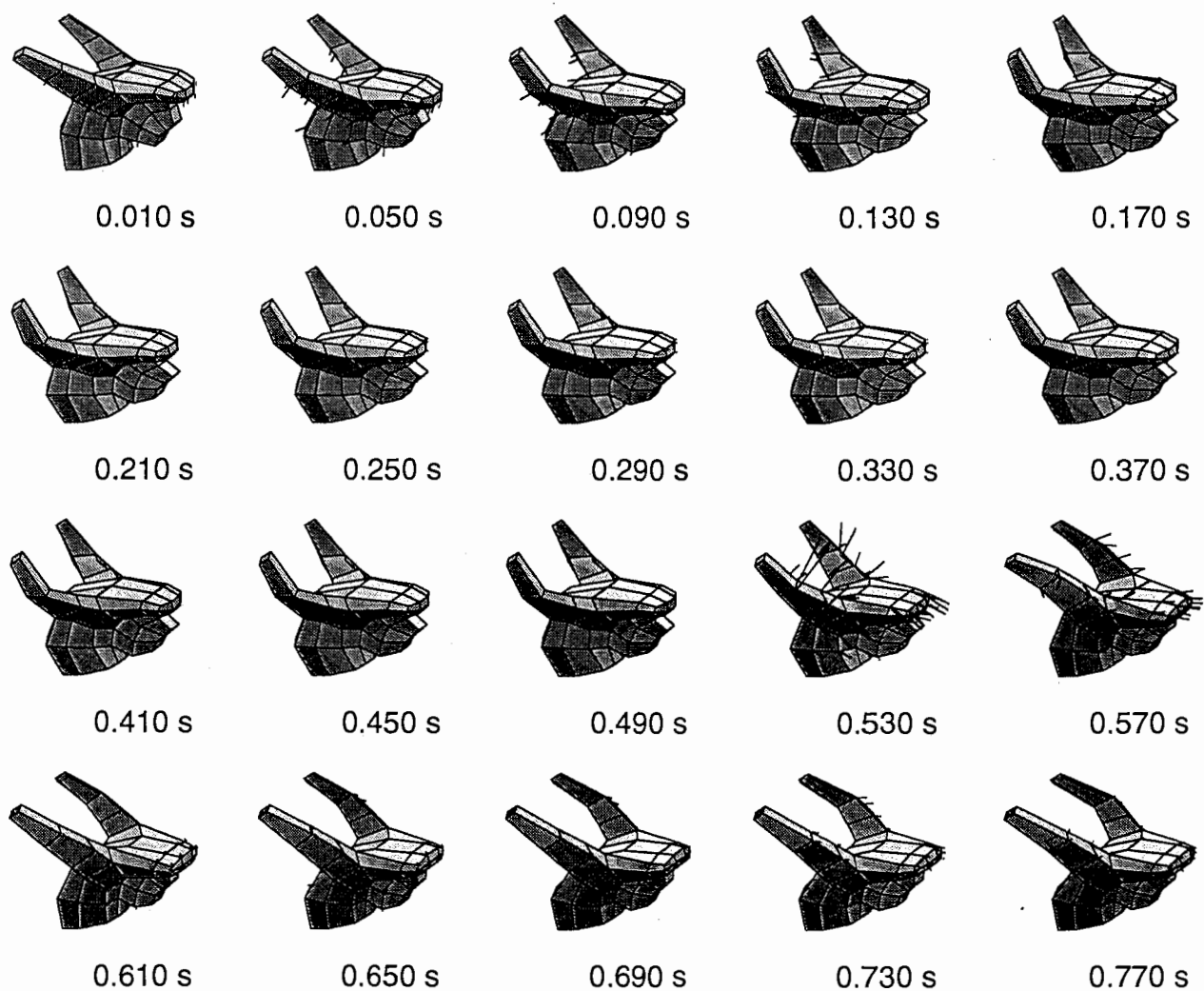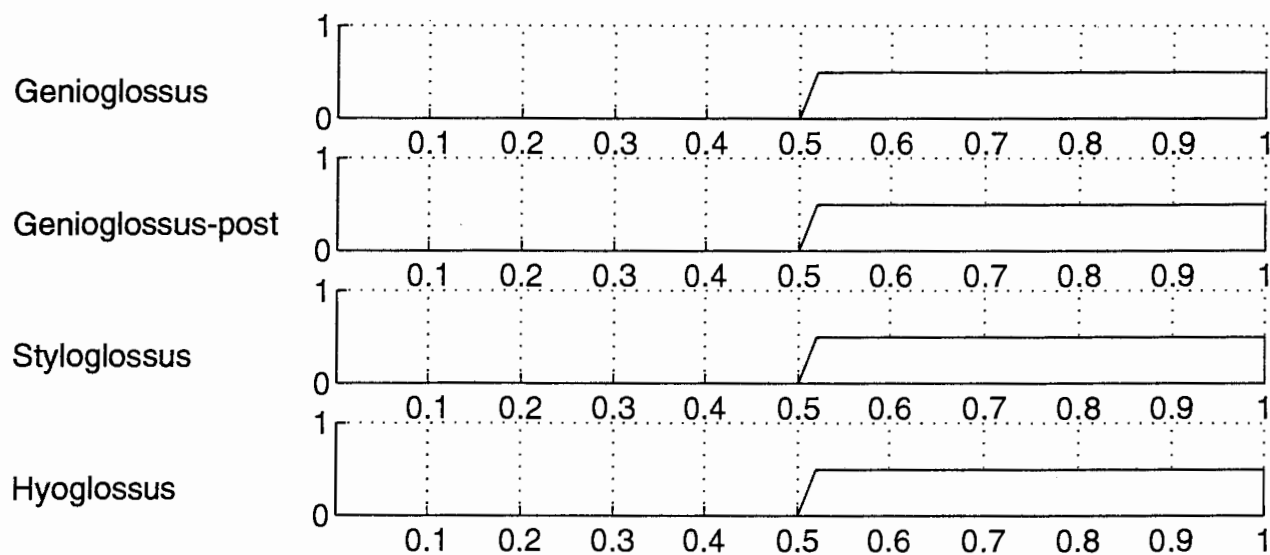
Figure 27: Gravity effects and muscle contraction. For the first 500 ms the model collapses to a rest position starting from its initial condition where no gravity is applied. Then all 8 muscles are activated in the same way as shown for the first 4 muscles, and the tongue jumps into another equilibrium condition.

Genioglossus

Genioglossus-post

Styloglossus

Hyoglossus

Transversalis

Verticalis

Longitudinalis-inf.

Longitudinalis-sup.

t=0.400
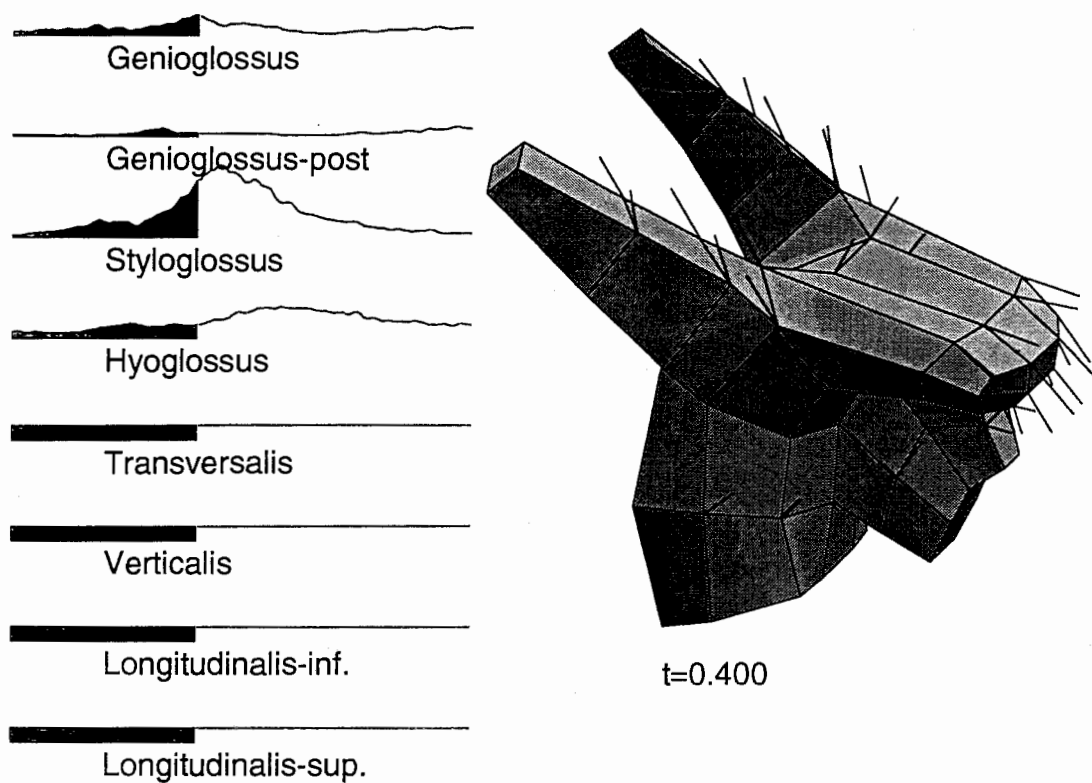
Figure 28: One frame of a movement sequence. The activations are normalized EMG data that had been measured for an utterance /əpɔp/. Constant low activation was assumed for the levels of the not measured intrinsic tongue muscles. The "wiskers" on the tongue model represent node velocities. The frame shows strong contraction of styloglossus.

Genioglossus

Genioglossus-post

Styloglossus

Hyoglossus

Transversalis

Verticalis

Longitudinalis-inf.

Longitudinalis-sup.

t=0.400
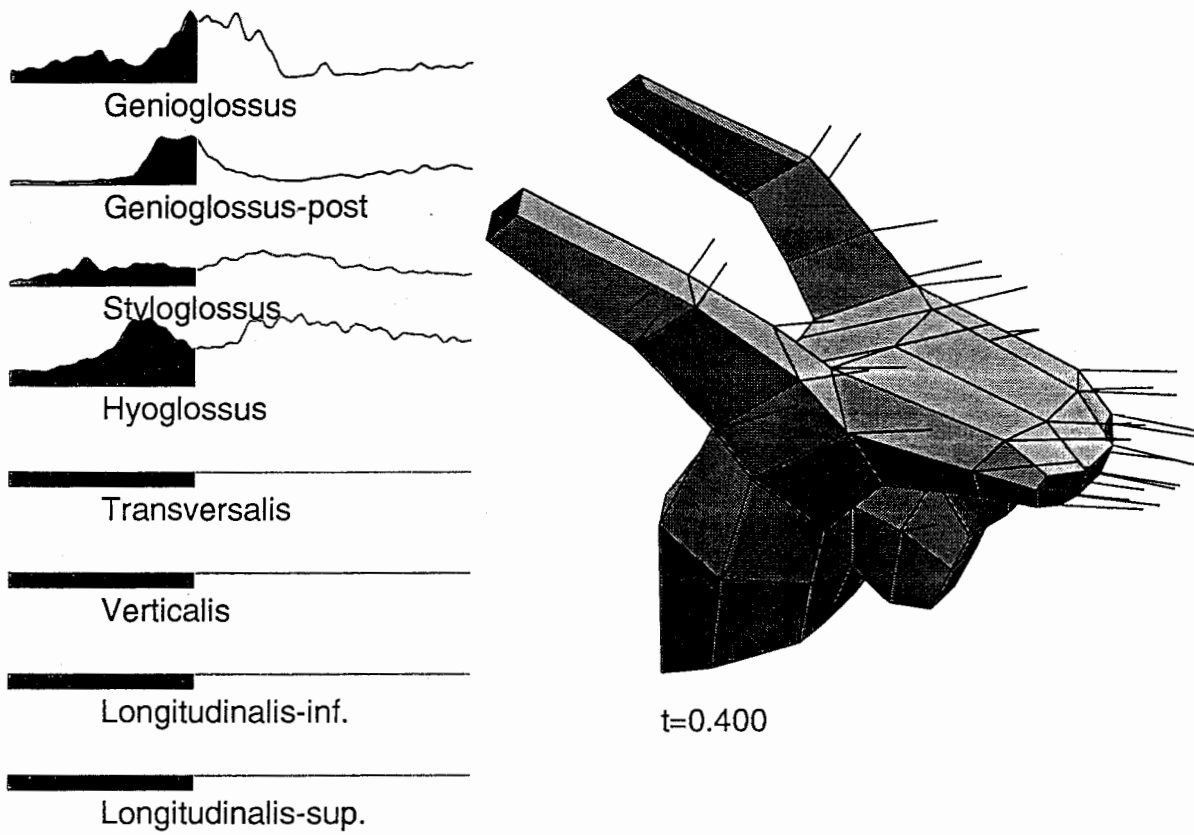
Figure 29: One frame of a movement sequence. The activations are normalized EMG data that had been measured for an utterance /əpɪp/. Constant low activation was assumed for the levels of the not measured intrinsic tongue muscles. Node velocities are displayed as short lines. Strong contraction of both parts of genioglossus and hyoglossus.
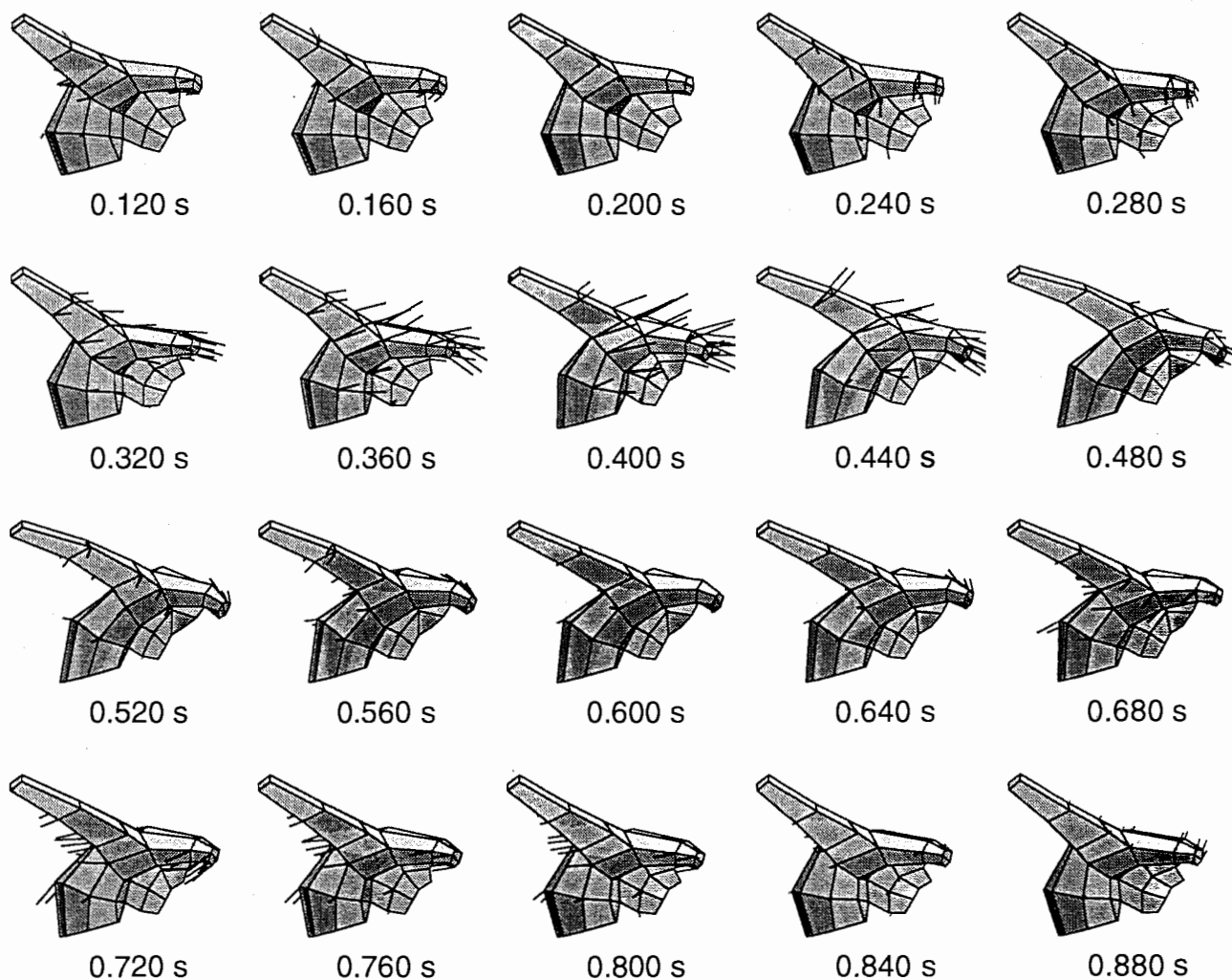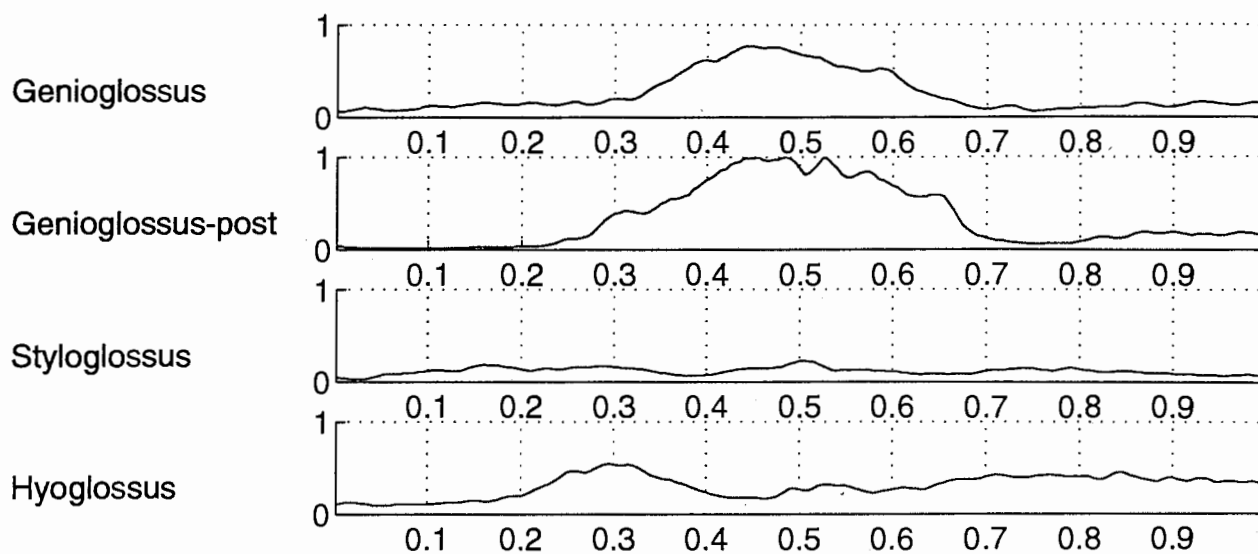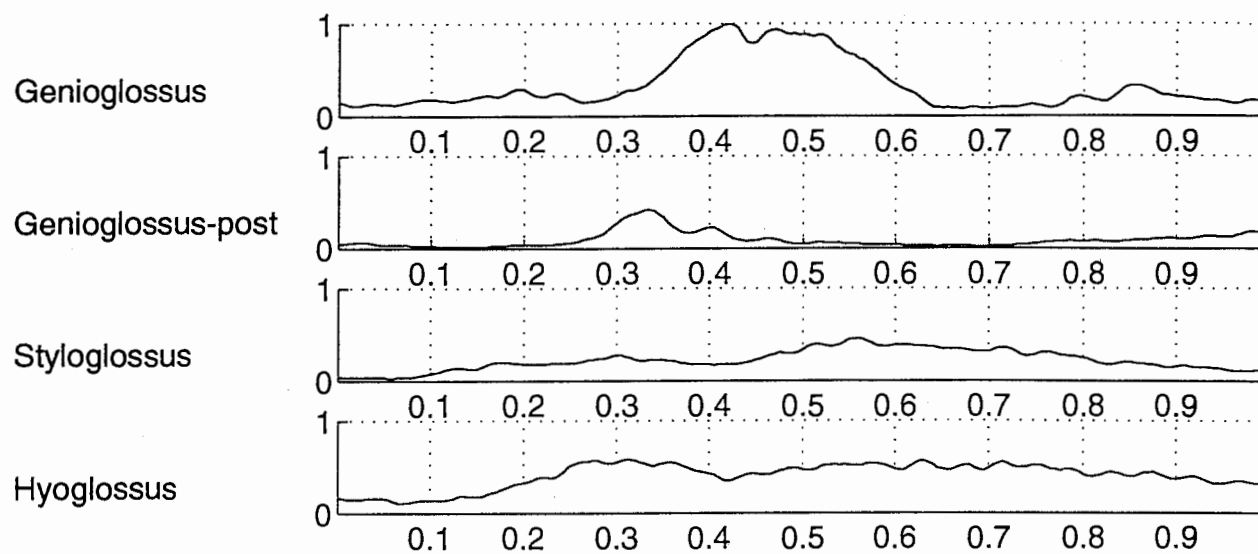
Figure 30: Utterance 1: /əpip/. 20 frames of a simulated tongue movement sequence. The muscle activation levels were normalized EMG records for the four extrinsic muscles. Nodes velocities are shown as short lines.
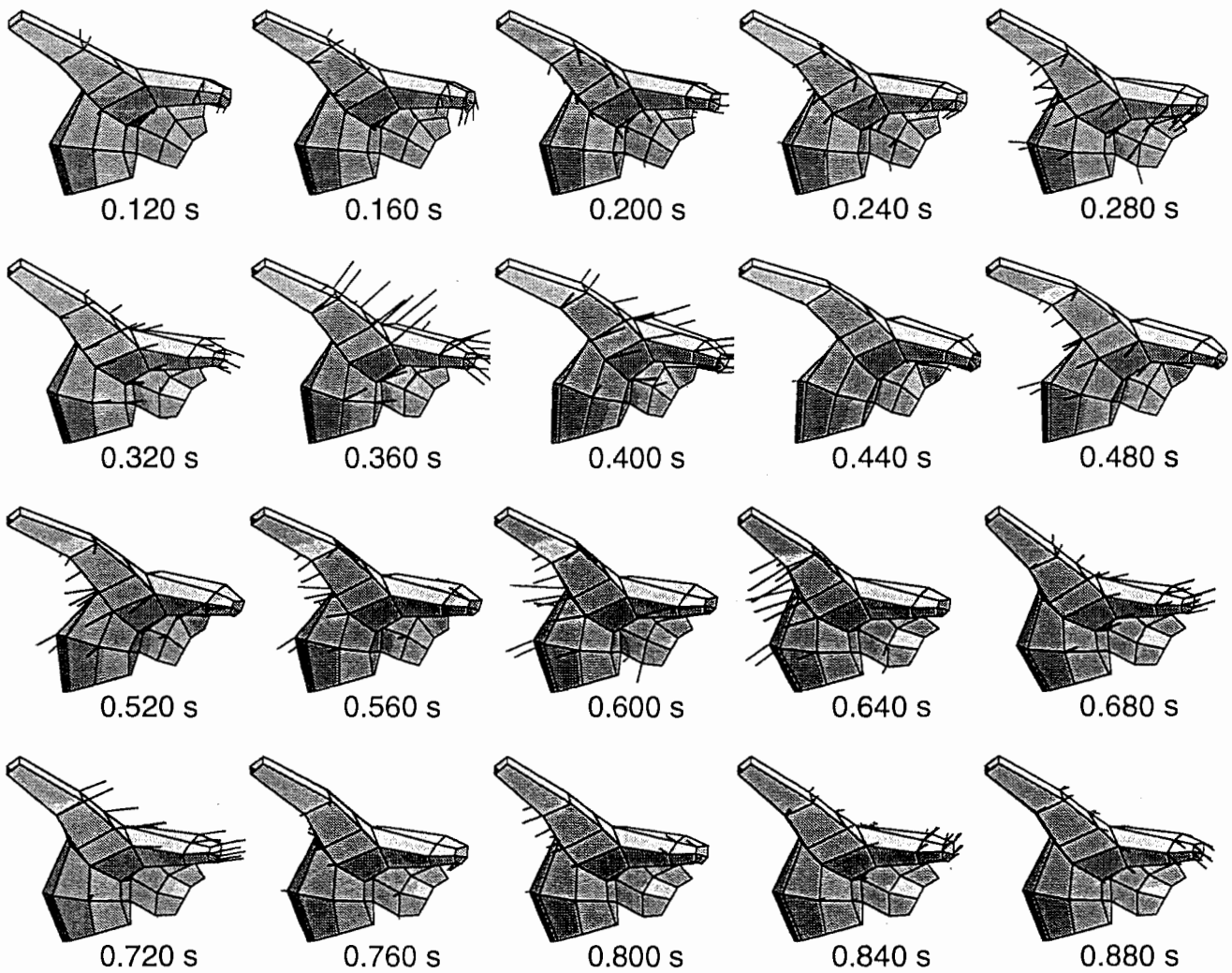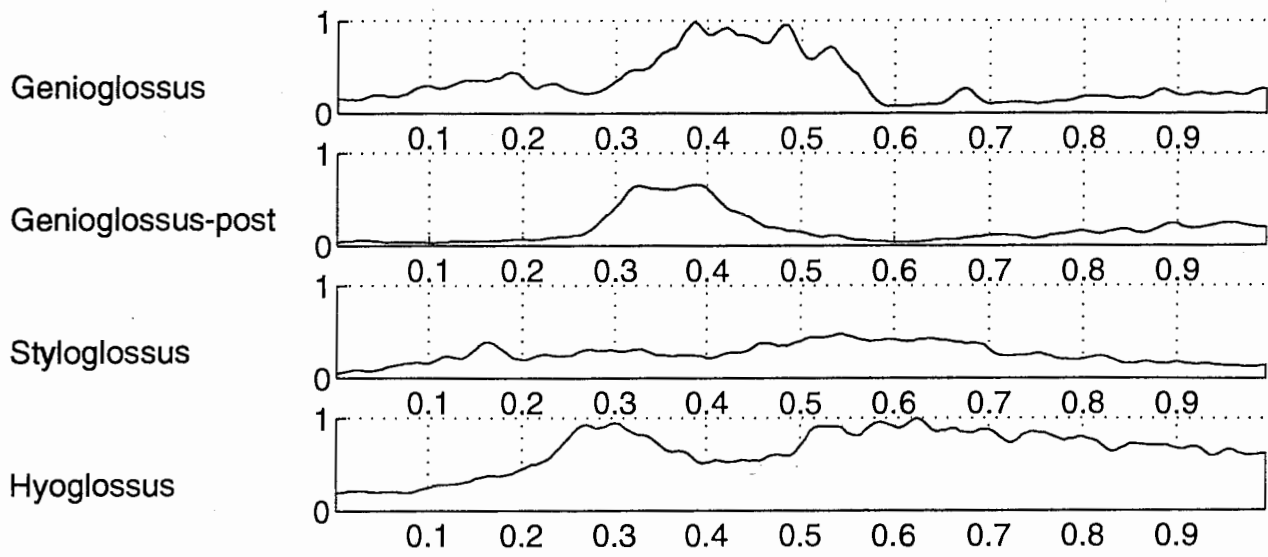
Figure 31: Utterance 2: /əpɪp/. 20 frames of a simulated tongue movement sequence. The muscle activation levels were normalized EMG records for the four extrinsic muscles. The intrinsic muscle activation levels were set to constant 20 % of maximum. Nodes velocities are shown as short lines.
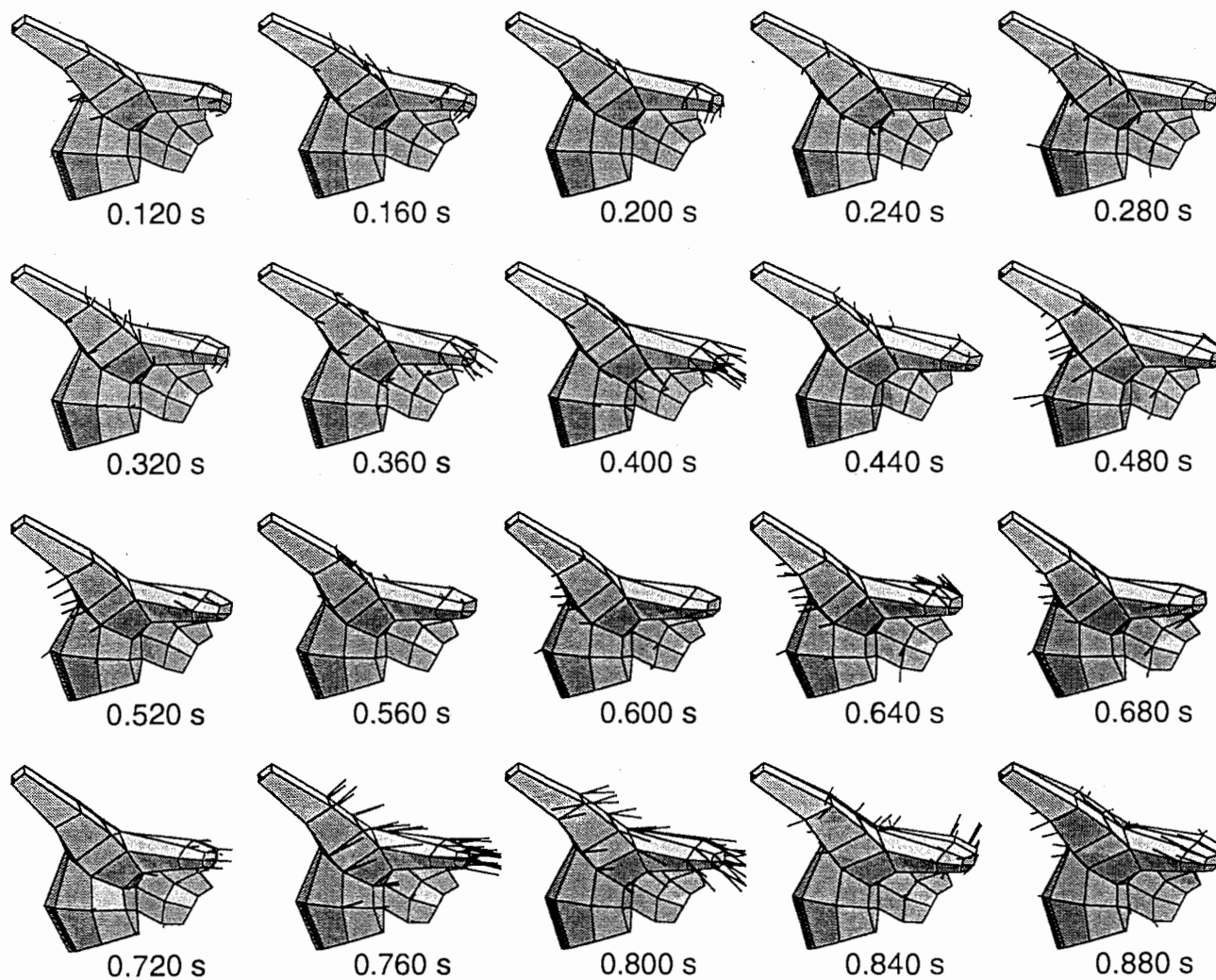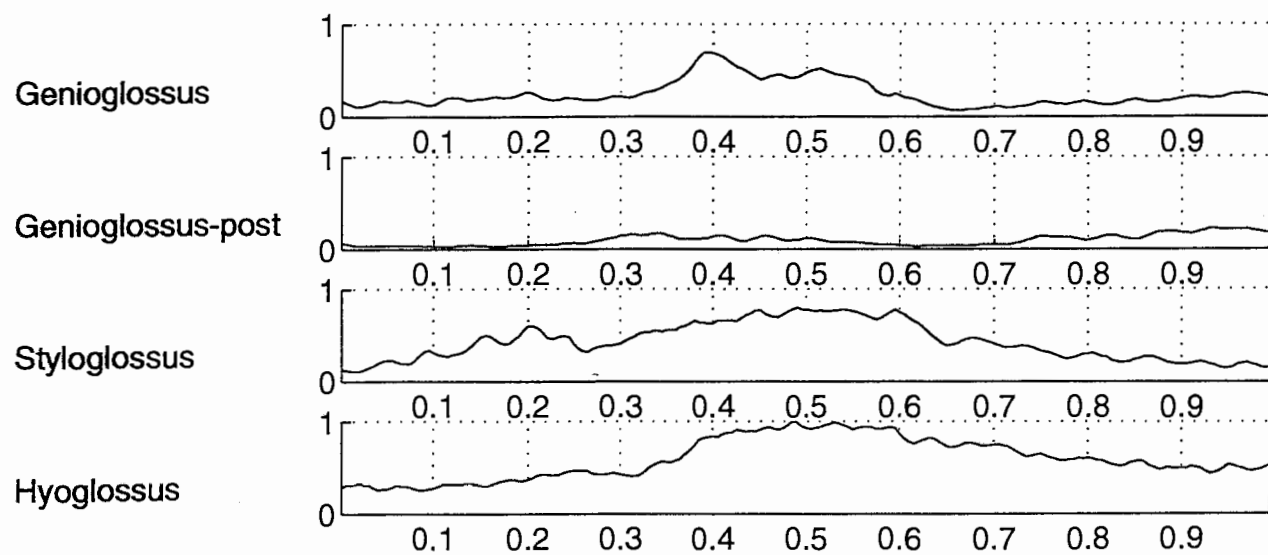
Figure 32: Utterance 3: /əpep/. 20 frames of a simulated tongue movement sequence. The muscle activation levels were normalized EMG records for the four extrinsic muscles. The intrinsic muscle activation levels were set to constant 20 % of maximum. Nodes velocities are shown as short lines.

Genioglossus

Genioglossus-post

Styloglossus

Hyoglossus

0.120 s   0.160 s   0.200 s   0.240 s   0.280 s

0.320 s   0.360 s   0.400 s   0.440 s   0.480 s

0.520 s   0.560 s   0.600 s   0.640 s   0.680 s
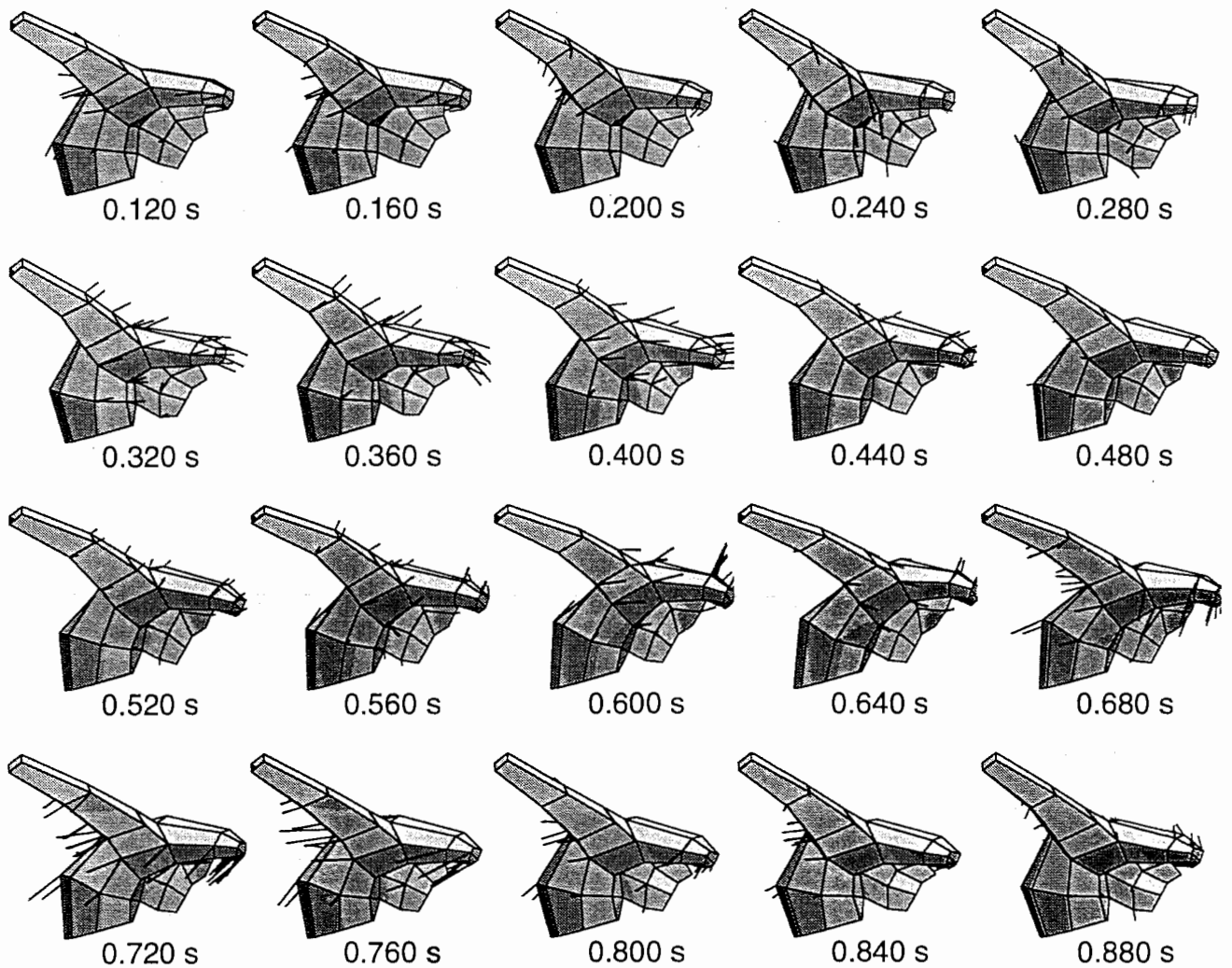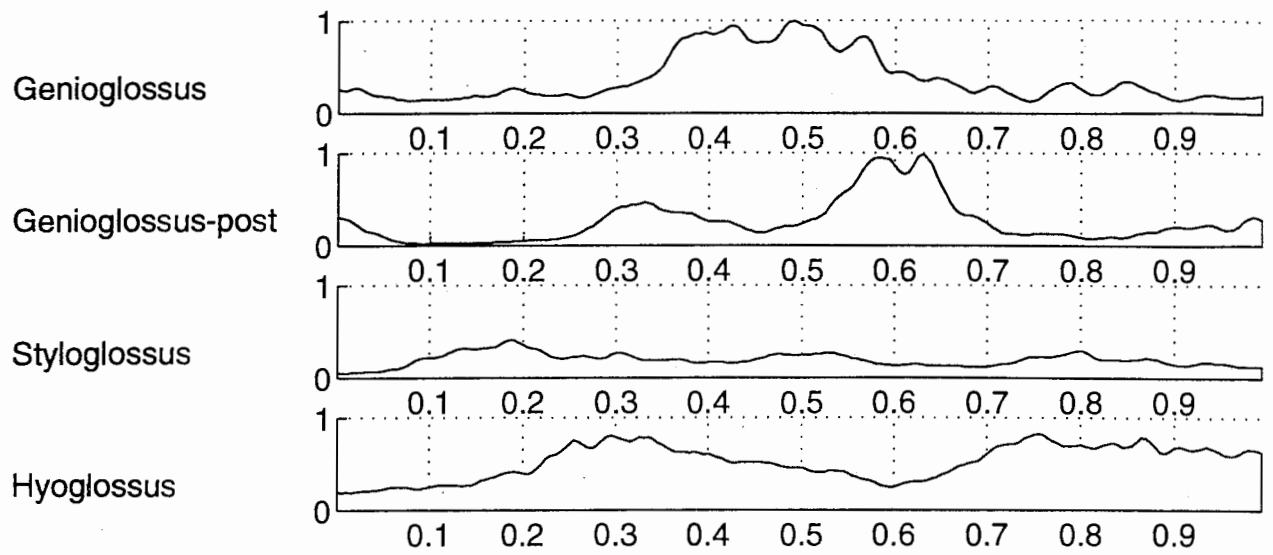
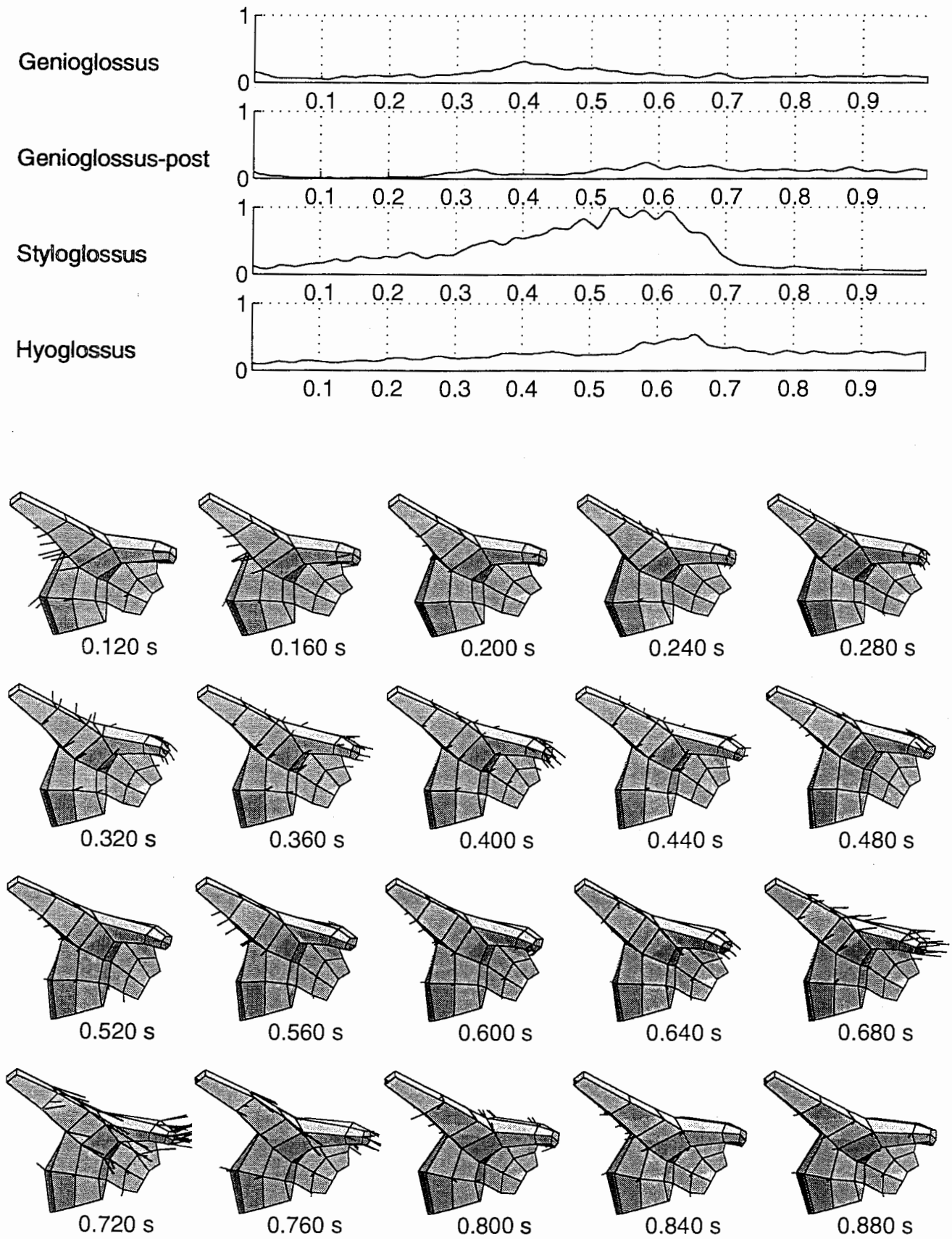0.720 s   0.760 s   0.800 s   0.840 s   0.880 s
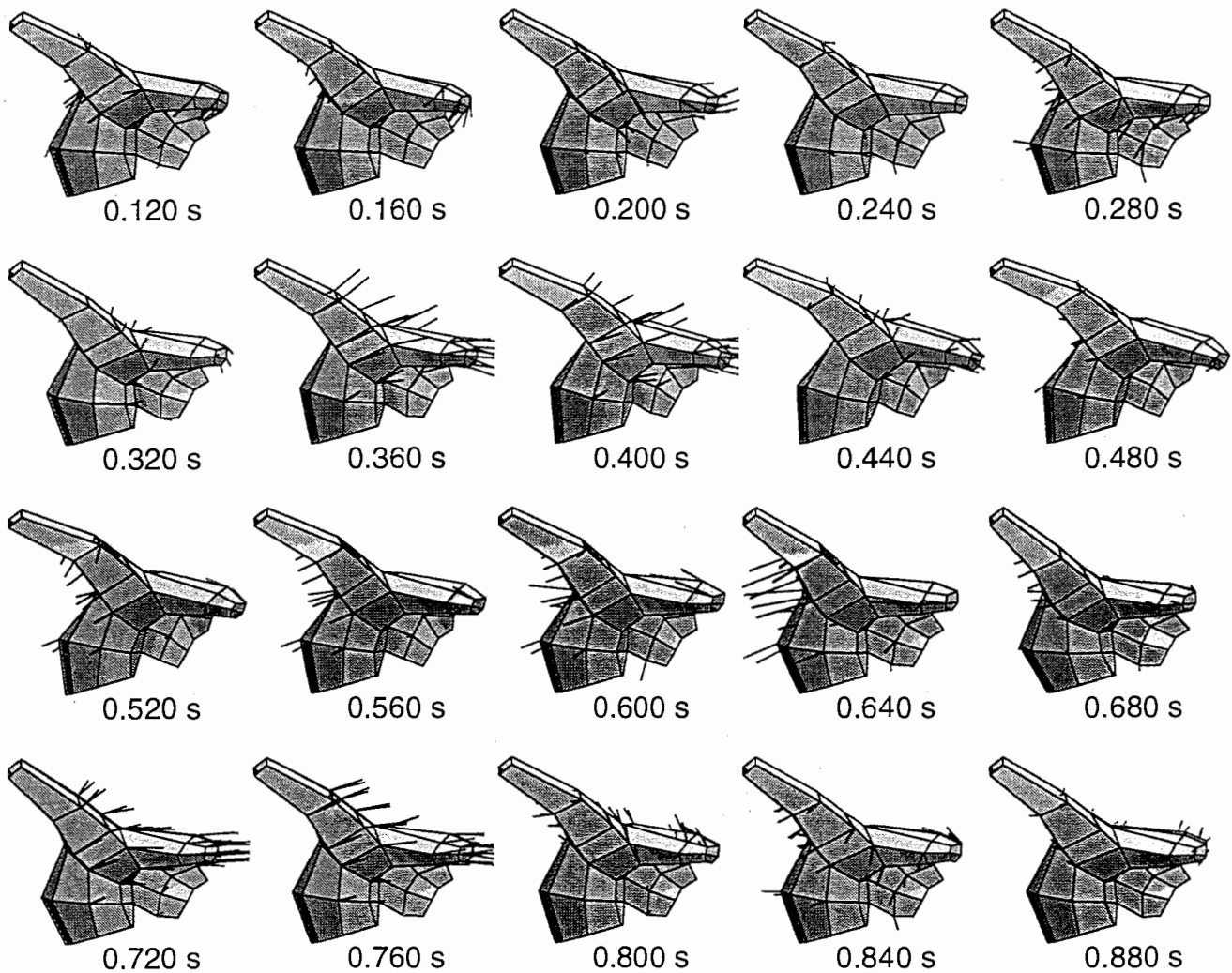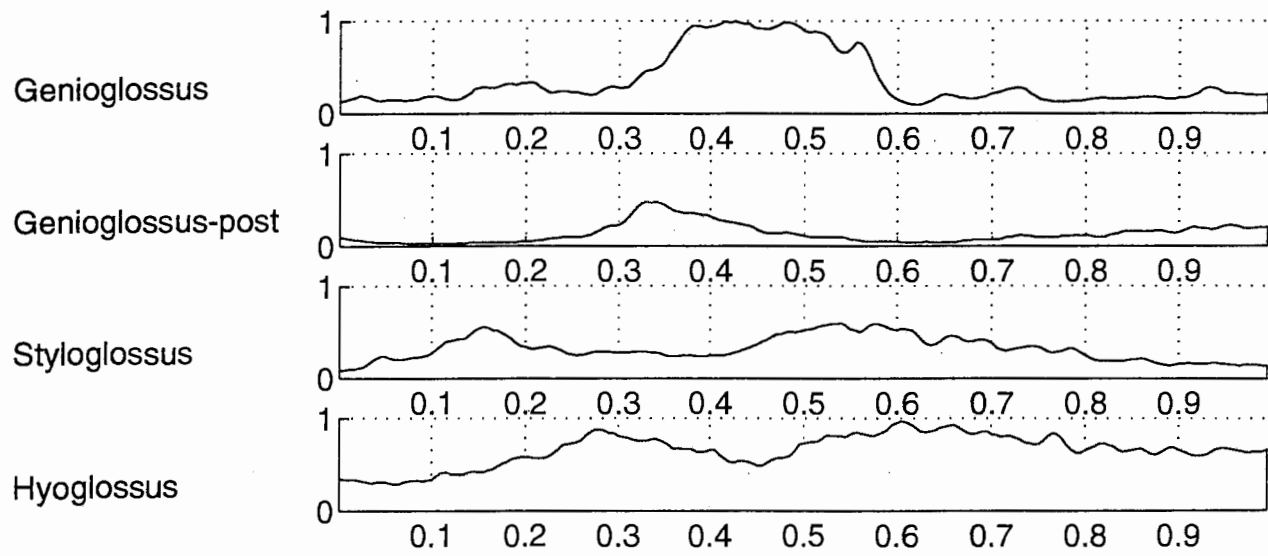
Figure 33: Utterance 4: /əpɛp/. 20 frames of a simulated tongue movement sequence. The muscle activation levels were normalized EMG records for the four extrinsic muscles. The intrinsic muscle activation levels were set to constant 20 % of maximum. Nodes velocities are shown as short lines.
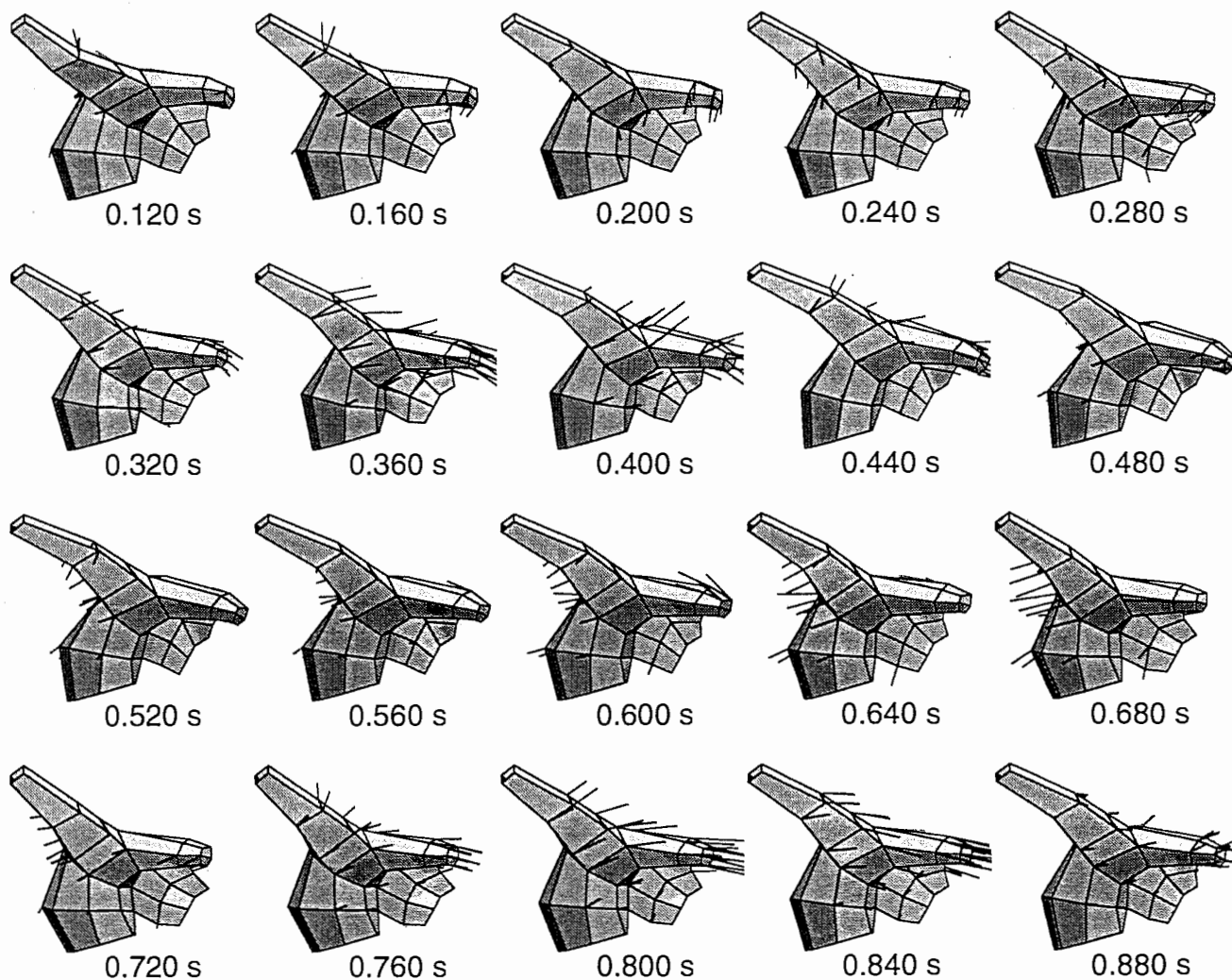
Figure 34: Utterance 5: /əpæp/. 20 frames of a simulated tongue movement sequence. The muscle activation levels were normalized EMG records for the four extrinsic muscles. The intrinsic muscle activation levels were set to constant 20 % of maximum. Nodes velocities are shown as short lines.
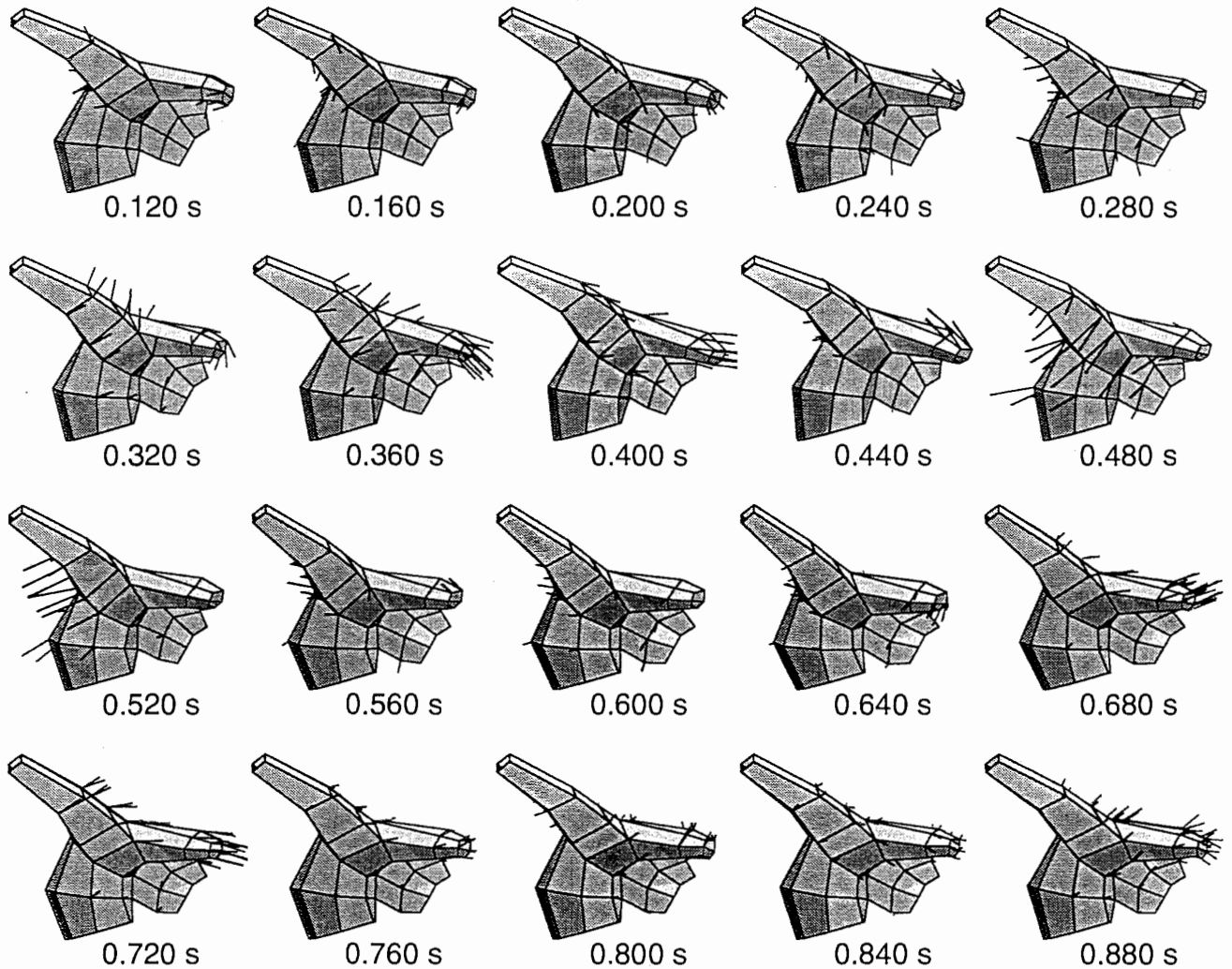
Figure 35: Utterance 6: /əpɑp/. 20 frames of a simulated tongue movement sequence. The muscle activation levels were normalized EMG records for the four extrinsic muscles. The intrinsic muscle activation levels were set to constant 20 % of maximum. Nodes velocities are shown as short lines.
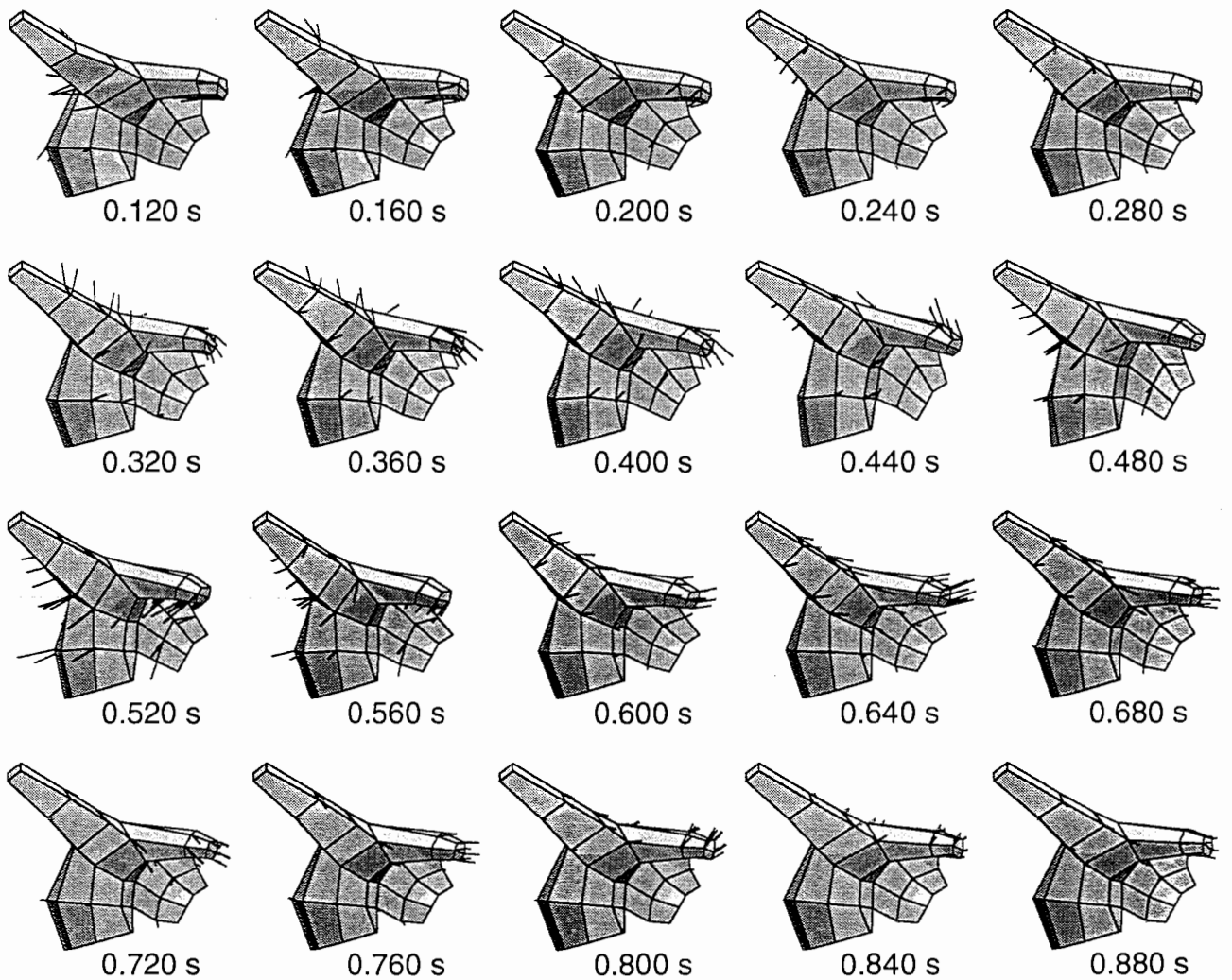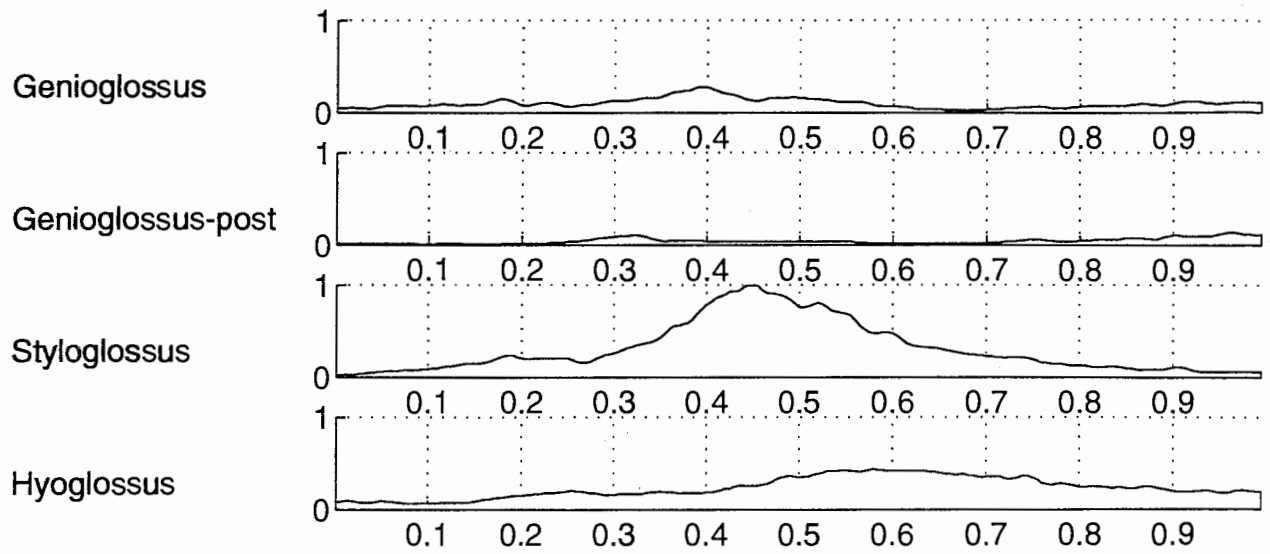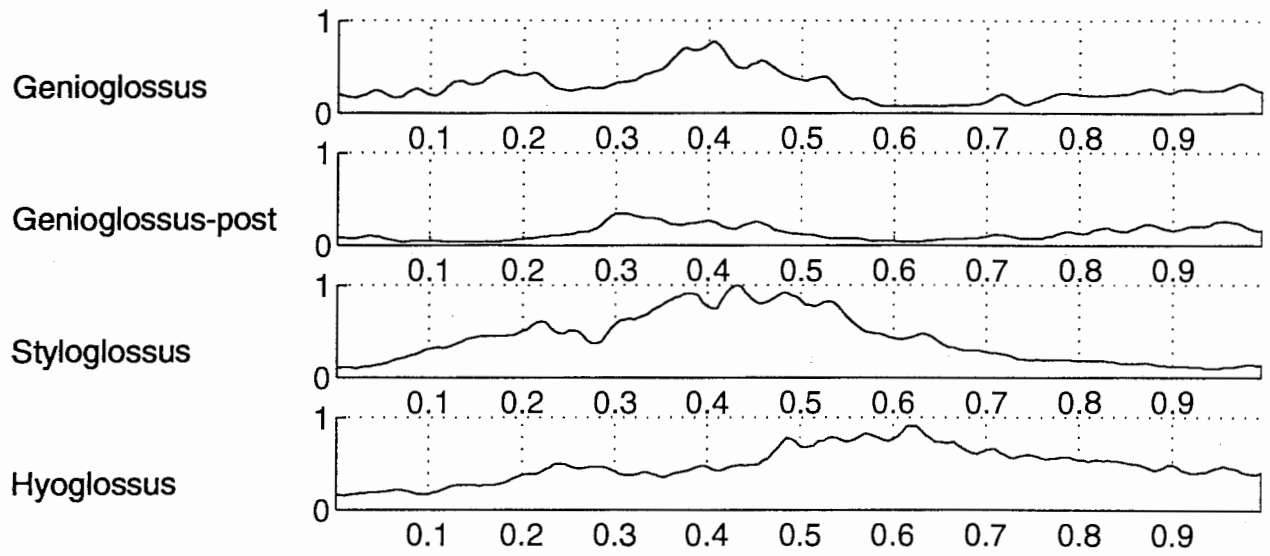
Figure 36: Utterance 7: /əpɔp/. 20 frames of a simulated tongue movement sequence. The muscle activation levels were normalized EMG records for the four extrinsic muscles. Nodes velocities are shown as short lines.

Figure 37: Utterance 8: /əpop/. 20 frames of a simulated tongue movement sequence. The muscle activation levels were normalized EMG records for the four extrinsic muscles. The intrinsic muscle activation levels were set to constant 20 % of maximum. Nodes velocities are shown as short lines.
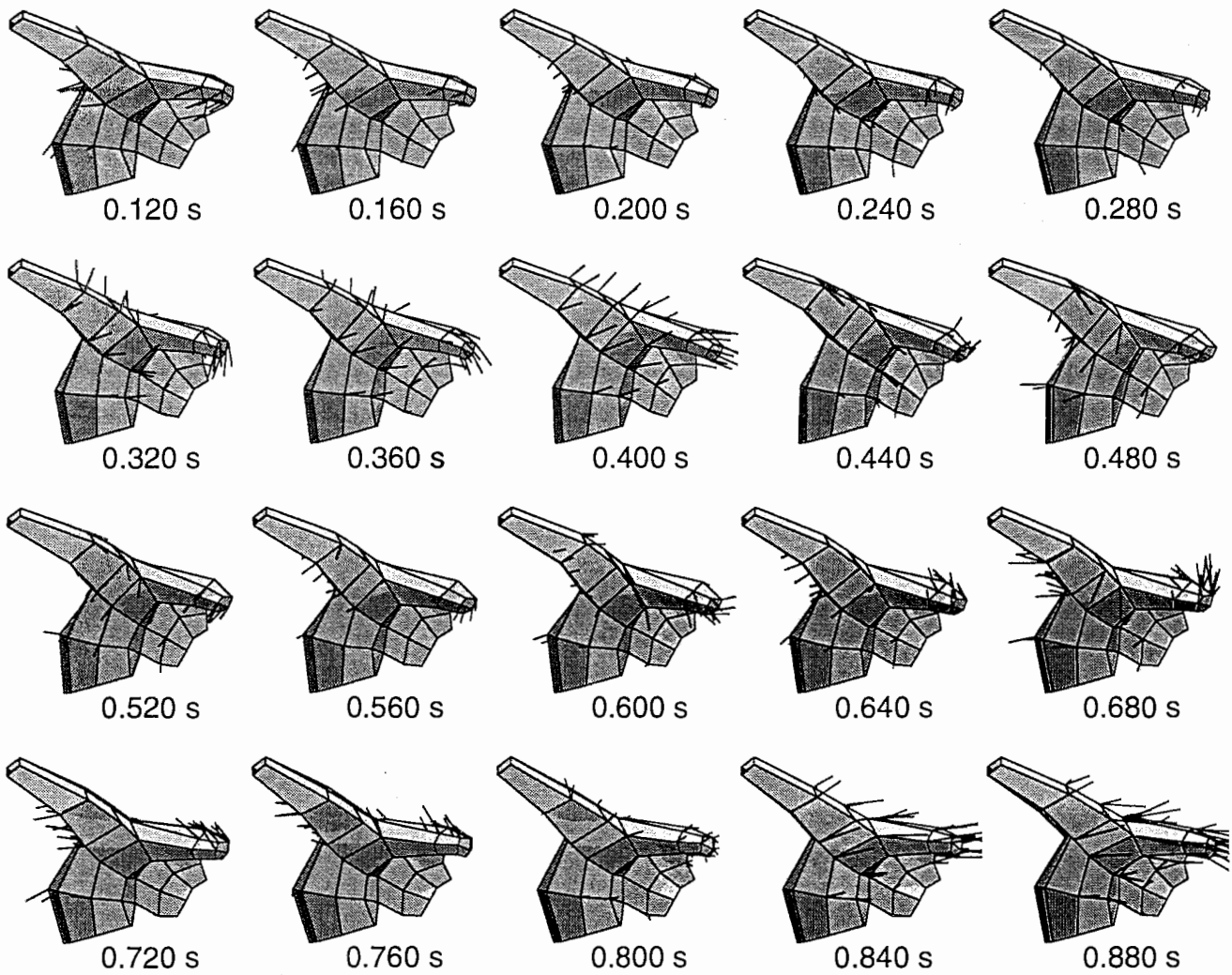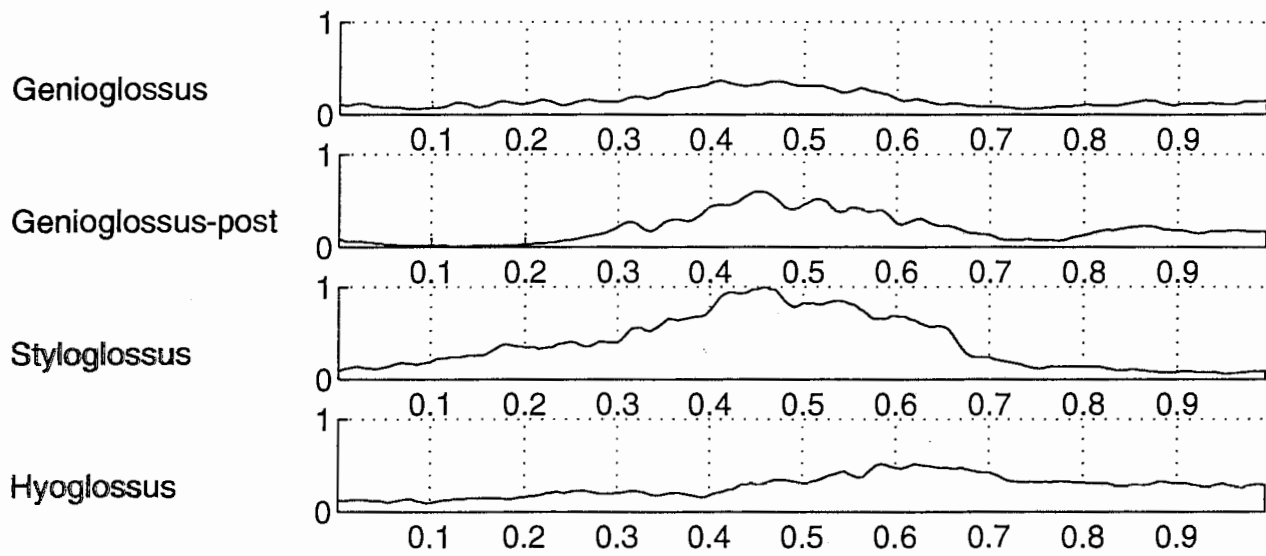
Figure 38: Utterance 9: /əpʊp/. 20 frames of a simulated tongue movement sequence. The muscle activation levels were normalized EMG records for the four extrinsic muscles. The intrinsic muscle activation levels were set to constant 20 % of maximum. Nodes velocities are shown as short lines.

Figure 39: Utterance 10: /əpup/. 20 frames of a simulated tongue movement sequence. The muscle activation levels were normalized EMG records for the four extrinsic muscles. The intrinsic muscle activation levels were set to constant 20 % of maximum. Nodes velocities are shown as short lines.
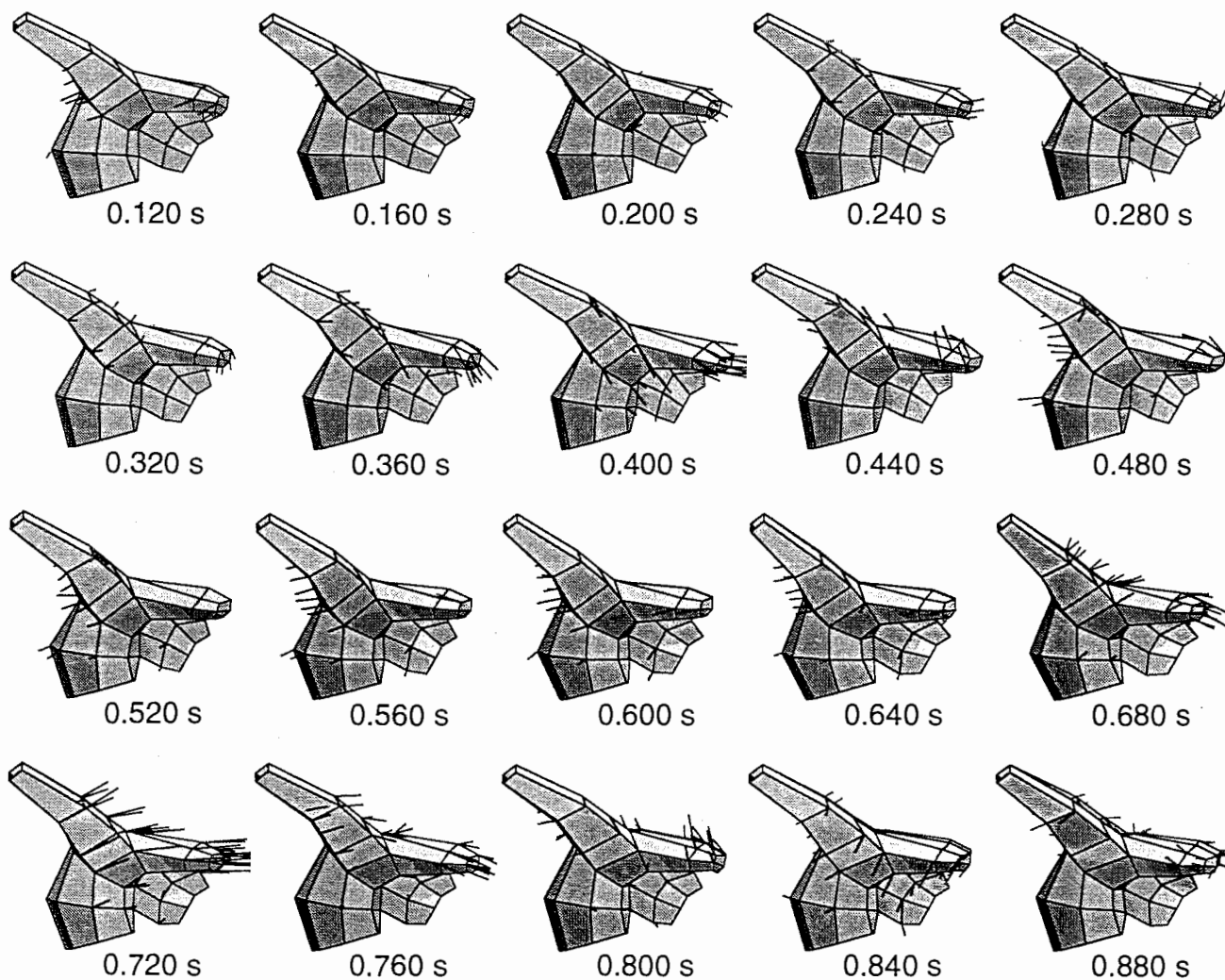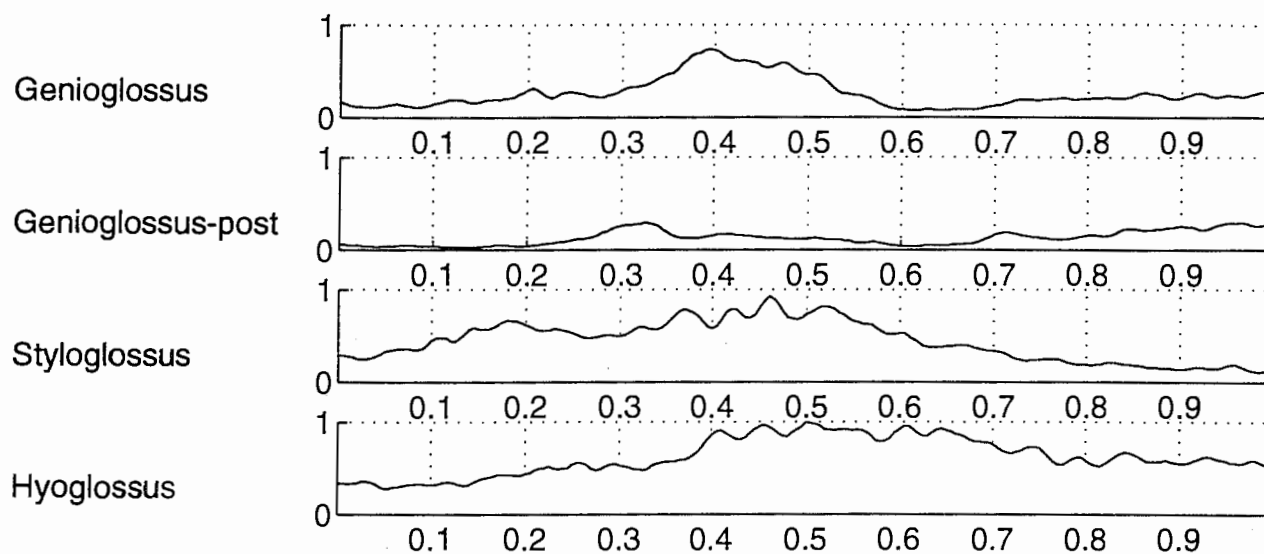
Figure 40: Utterance 11: /əpʌp/. 20 frames of a simulated tongue movement sequence. The muscle activation levels were normalized EMG records for the four extrinsic muscles. The intrinsic muscle activation levels were set to constant 20 % of maximum. Nodes velocities are shown as short lines.